

UNCLASSIFIED

AD NUMBER

AD888383

LIMITATION CHANGES

TO:

Approved for public release; distribution is unlimited.

FROM:

Distribution authorized to U.S. Gov't. agencies only; Test and Evaluation; 01 SEP 1971. Other requests shall be referred to Air Force Weapons Lab., Kirtland AFB, NM.

AUTHORITY

AFWL ltr 29 Apr 1985

THIS PAGE IS UNCLASSIFIED

AFWL-TR-71-54

AFWL-TR-71-54

2 CB

STRESS-STRAIN AND FRACTURE PROPERTIES OF NUGGET SANDSTONE

Wayne S. Brown

Stephen R. Swanson

University of Utah

TECHNICAL REPORT NO. AFWL-TR-71-54

October 1971

AIR FORCE WEAPONS LABORATORY

Air Force Systems Command

Kirtland Air Force Base

New Mexico



DDC
RECEIVED
OCT 18 1971
B

Distribution limited to U.S. Government agencies only because of test and evaluation (1 Sep 71). Other requests for this document must be referred to AFWL (DEV).

4

AD888383



RECEIVED

97

SIGN NO.	
CFTW	DELTE SECTION <input type="checkbox"/>
DOC	DIFF SECTION <input type="checkbox"/>
UNCLASSIFIED	<input type="checkbox"/>
AS: INFORMATION	
BY	
DISTRIBUTION/SECURITY CODE	
DECL.	AVAIL. and/or SPECIAL
B	

AIR FORCE WEAPONS LABORATORY
Air Force Systems Command
Kirtland Air Force Base
New Mexico 87117

When US Government drawings, specifications, or other data are used for any purpose other than a definitely related Government procurement operation, the Government thereby incurs no responsibility nor any obligation whatsoever, and the fact that the Government may have formulated, furnished, or in any way supplied the said drawings, specifications, or other data, is not to be regarded by implication or otherwise, as in any manner licensing the holder or any other person or corporation, or conveying any rights or permission to manufacture, use, or sell any patented invention that may in any way be related thereto.

This report is made available for study with the understanding that proprietary interests in and relating thereto will not be impaired. In case of apparent conflict or any other questions between the Government's rights and those of others, notify the Judge Advocate, Air Force Systems Command, Andrews Air Force Base, Washington, DC 20331.

DO NOT RETURN THIS COPY. RETAIN OR DESTROY.

STRESS-STRAIN AND FRACTURE
PROPERTIES OF NUGGET SANDSTONE

Wayne S. Brown
Stephen R. Swanson
University of Utah

TECHNICAL REPORT NO. AFWL-TR-71-54

Details of illustrations in
this document may be better
studied on microfiche

Distribution limited to U. S. Government agencies
only because of test and evaluation (1 Sep 71).
Other requests for this document must be referred
to AFWL (DEV).

FOREWORD

This report was prepared by the University of Utah, Salt Lake City, Utah, under Contract F29601-68-C-0071. The research was performed under Program Element 61102H, Project 5710, Subtask SB144, and was funded by the Defense Nuclear Agency (DNA).

Inclusive dates of research were November 1968 through July 1971. The report was submitted 3 September 1971 by the Air Force Weapons Laboratory Project Officer, Lieutenant Stoney P. Chisolm (DEV-F). The former project officer was Captain Scott Blouin.

The contractor report number is UTEC ME 71-058.

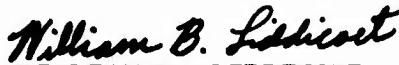
This technical report has been reviewed and is approved.



STONEY P. CHISOLM
Lieutenant, USAF
Project Officer



GERALD G. LEIGH
Major, USAF
Chief, Facilities Survivability
Branch



WILLIAM B. LIDDICOET
Colonel, USAF
Chief, Civil Engineering Research
Division

ABSTRACT

Experimental measurements of the stress-strain and fracture properties of laboratory specimens of Nugget sandstone are described. A servo-controlled triaxial compression testing apparatus was employed which permitted simultaneous control of the lateral and axial stresses. Results are given for a variety of stress path conditions including: unconfined compression and tension, constant confining pressure, proportional stress, constant mean stress, one-dimensional strain, and proportional strain tests. In general, Nugget sandstone was found to be reasonably isotropic and to exhibit considerable inelastic behavior including hysteresis and dilatancy. A plasticity model was formulated which is capable of representing the stress-strain characteristics of the sandstone reasonably well over a variety of stress path conditions.

(Distribution Limitation Statement B)

CONTENTS

<u>Section</u>		<u>Page</u>
I	INTRODUCTION	1
II	EXPERIMENTAL SECTION	2
III	DISCUSSION OF RESULTS	4
IV	MATHEMATICAL REPRESENTATION	8
V	SUMMARY AND CONCLUSIONS	14
	REFERENCES	85

ILLUSTRATIONS

Figure	Title	Page
1	Photomicrographs of Nugget sandstone, thin sections	26
2	Typical instrumented rock specimens	27
3	High pressure laboratory apparatus	28
4	Fracture stress for Nugget sandstone in triaxial compression	29
5	Loading paths for triaxial tests of intact Nugget sandstone	30
6	Principal stress-strain curves for Nugget sandstone Specimen No. 19 in unconfined compression	31
7	Principal stress-strain curves for Nugget sandstone Specimen No. 1, constant confining pressure, $P = 5$ ksi	32
8	Principal stress-strain curves for Nugget sandstone Specimen No. 2, $P = 10$ ksi	33
9	Principal stress-strain curves for Nugget sandstone Specimen No. 3, constant confining pressure, $P = 5$ ksi	34
10	Principal stress-strain curves for Nugget sandstone Specimen No. 4, constant confining pressure, $P = 41$ ksi	35
11	Principal stress-strain curves for Nugget sandstone Specimen No. 5, constant confining pressure, $P = 60$ ksi	36
12	Principal stress-strain curves for Nugget sandstone Specimen No. 41, constant confining pressure, $P = 80$ ksi	37
13	Principal stress-strain curves for Nugget sandstone Specimen No. 6 in proportional loading, $\sigma_3/\sigma_1 = 0.056$.	38
14	Principal stress-strain curves for Nugget sandstone specimen No. 7 in proportional loading, $\sigma_3/\sigma_1 = 0.084$	39

ILLUSTRATIONS (continued)

Figure	Title	Page
15	Principal stress-strain curves for Nugget sandstone specimen No. 34 in proportional loading $\sigma_3/\sigma_1 = 0.142$	40
16	Principal stress-strain curves for Nugget sandstone specimen No. 9 in proportional loading, $\sigma_3/\sigma_1 = 0.177$	41
17	Principal stress-strain curves for Nugget sandstone specimen No. 40 in proportional loading, $\sigma_3/\sigma_1 = 0.190$	42
18	Comparison of axial and lateral strains in hydrostatic pressure loading of Nugget sandstone	43
19	Pressure-volume strain curves in hydrostatic pressure loading of five Nugget sandstone specimens	44
20	Hysteresis in Nugget sandstone under hydrostatic compression loading	45
21	Shear stress-strain curves of Nugget sandstone in constant confining pressure tests	46
22	Dilatation stress-strain curves for Nugget sandstone in constant confining pressure tests	47
23	Shear stress-strain curves of Nugget sandstone in proportional loading tests	48
24	Dilatation stress-strain curves of Nugget sandstone in proportional loading tests	49
25	Shear stress-strain curves for Nugget sandstone in constant J_1 tests	50
26	Dilatation stress-strain curves of Nugget sandstone in constant J_1 tests	51
27	Loading path of one-dimensional strain test of Nugget sandstone specimen No. 42	52
28	Shear stress-strain curves of Nugget sandstone specimen No. 42 in one-dimensional strain test	53
29	Dilatation stress-strain curve of Nugget sandstone specimen No. 42 in one-dimensional strain test	54
30	Loading path of Nugget sandstone specimen No. 31 under constant strain ratio loading $\epsilon_3/\epsilon_1 = -0.249$	55
31	Shear stress-strain curves of Nugget sandstone in proportional strain, $\epsilon_3/\epsilon_1 = -0.249$	56

ILLUSTRATIONS (continued)

Figure	Title	Page
32	Dilatation stress-strain curves of Nugget sandstone in proportional strain, $\epsilon_3/\epsilon_1 = -0.249$	57
33	Stress-strain curves in hydrostatic pressure loading of Nugget sandstone specimen No. 31, before and after proportional strain test	58
34	Principal stress-strain curve for tension test of Nugget sandstone specimens	59
35	Shear stress-strain curves in unconfined tension tests of Nugget sandstone	60
36	Dilatation stress-strain curves in unconfined tension tests of Nugget sandstone	61
37	Comparison of principal stress-strain curves of Nugget sandstone in unconfined tension and compression	62
38	Shear stress-strain curves for constant stress ratio tests of Nugget sandstone specimen No. 11 (cycled) and specimen No. 7	63
39	Dilatation stress-strain curves for constant stress ratio tests of Nugget sandstone specimen No. 11 (cycled) and specimen No. 7	64
40	Shear stress-strain curves for constant stress ratio tests of Nugget sandstone specimen No. 13 (cycled) and specimen No. 7	65
41	Dilatation stress-strain curves for constant stress ratio test of Nugget sandstone specimen No. 13 (cycled) and specimen No. 7	66
42	Effect of loading path on shear stress-strain response for Nugget sandstone	67
43	Effect of loading path on dilatational stress-strain response for Nugget sandstone	68
44	Effect of loading path on shear stress-strain response for Nugget sandstone	69
45	Effect of loading path on dilatational stress-strain	70
46	Effect of loading path on shear stress-strain response for Nugget sandstone	71

ILLUSTRATIONS (continued)

Figure	Title	Page
47	Effect of loading path on dilatational stress-strain response for Nugget sandstone	72
48	Comparison of model and experiment; constant confining pressure tests of Nugget sandstone	73
49	Comparison of model and experiment; constant confining pressure of Nugget sandstone	74
50	Comparison of model and experiment; proportional stress loading of Nugget sandstone	75
51	Comparison of model and experiment; proportional stress loading of Nugget sandstone	76
52	Comparison of model and experiment; constant J_1 loading of Nugget sandstone	77
53	Comparison of model and experiment; constant J_1 loading of Nugget sandstone	78
54	Comparison of model and experiment; one-dimensional strain loading of Nugget sandstone	79
55	Comparison of model and experiment; one-dimensional strain loading of Nugget sandstone	80
56	Comparison of model and experiment; one-dimensional strain loading of Nugget sandstone	81
57	Comparison of model and experiment; proportional strain ($\epsilon_3/\epsilon_1 = -0.249$) loading of Nugget sandstone	82
58	Comparison of model and experiment; proportional strain ($\epsilon_3/\epsilon_1 = -0.249$) loading of Nugget sandstone	83
59	Comparison of model and experiment; proportional strain ($\epsilon_3/\epsilon_1 = -0.249$) loading of Nugget sandstone	84

SECTION I

INTRODUCTION

Stress-strain properties of Nugget sandstone measured in triaxial compression laboratory experiments are presented. From these data a mathematical representation is formulated that is suitable for use in computer codes used to calculate the motion of rock masses subjected to stress wave loadings.

The calculation of the response of rock masses to applied stress necessitates a knowledge of the stress-strain properties and fracture characteristics of the rock media. The in-situ rock mass differs from the usual laboratory specimens in that the in-situ rock may contain joints or faults that in some cases may strongly influence the rock response. Thus, for some problems the results of laboratory tests on intact rock specimens may not be directly applicable to the in-situ rock mass. However, the in-situ response undoubtedly does depend to some degree on the properties of the intact rock. Thus, laboratory tests of the type described herein are essential and from an economic viewpoint are the first logical step in the characterization of the rock behavior.

Previous work on Westerly granite and Cedar City tonalite [1,2] has shown the triaxial compression test to be a convenient experimental tool for investigating rock stress-strain behavior if the test apparatus is capable of applying loads along a number of different stress loading paths. In the present study, a large number of test conditions were employed to generate data, furnishing a detailed examination of the stress-strain response of Nugget sandstone. These data are analyzed in detail in this report and a mathematical representation of the model is described.

SECTION II

EXPERIMENTAL SECTION

The rock used in this study was Nugget sandstone, collected near Salt Lake City, Utah. The intact rock is a strong, fine-grained, silica-cemented, pure quartzitic sandstone, with a measured porosity of 4% by volume. The composition, determined by thin section analysis, is predominantly quartz with minor chert and hematite. This rock is very isotropic without any discernible fabric. Failure undoubtedly occurs primarily across grain boundaries. The density is 2.52 gm/cc and the porosity is 4% by volume. A photomicrograph of a thin section is shown in Figure 1. The rock has a faint visual indication of layering. The sandstone has also been used in dynamic tests and in prefractured compression tests [3].

The rock specimens used in this study were right circular cylinders with a length to diameter ratio of two and diameters of either one or 3/4 inch. The specimens were all cored from a large block in a direction transverse to the layering marks unless otherwise noted. The specimens were ground on all surfaces and strain gages bonded to the axial center of the specimens in axial and transverse directions. The specimens were then covered with laboratory plastic tubing and sealed. A typical instrumented specimen is shown in Figure 3.

An overall view of the test apparatus is shown in Figure 2. This apparatus has been described in detail previously [1]; it consists of a 7kb confining pressure vessel and intensifier actuated by two load frames. These load frames are electro-hydraulic with closed loop servo-control and are slaved together with a two-channel servo-controller. In this way the confining pressure and the axial stress difference can be controlled independently so as to produce various loading paths in stress space.

The specimen axial force and confining pressure are measured internal to the pressure vessel, using a steel cylinder load cell instrumented with bonded foil strain gages, and a Manganin pressure coil, as described previously [1]. The force, pressure, and specimen strain readings were all recorded continuously on a multichannel

Offner pen type recorder. Tests were carried out at an axial strain rate of approximately 10^{-4} /sec. A discussion of the loading paths used in this study will be given in the next section along with the test results.

SECTION III

DISCUSSION OF RESULTS

A large number of triaxial tests were performed, utilizing a variety of stress loading paths. The axial stress difference at fracture is shown as a function of the confining pressure in Figure 4. Brittle fracture was produced at all confining pressure levels used in this study. The paths utilized to load the specimens are illustrated in Figure 5. It can be seen that the failure locus is independent of the loading path as observed previously for tonalite and granite [1,2,4]. The loading paths shown in Figure 5 are of two general types: stress controlled and strain controlled. Included in the former are tests at constant confining pressure, proportional loading, constant mean stress (constant J_1), and a two-step loading consisting of proportional loading followed by a decrease in confining pressure with the axial stress difference held constant. The strain controlled tests include the one-dimensional strain test and proportional straining tests. Specimen fracture was not produced in any of the strain controlled tests. These tests will be discussed later in more detail.

Typical plots of the principal stress-strain curves obtained from these tests are shown in Figures 6 to 12 for constant confining pressure tests and Figures 13 to 17 for proportional loading. These results follow a trend previously observed for Cedar City tonalite and Westerly granite [1,2], in that the lateral stress-strain curves are much more nonlinear than the axial stress-strain curves.

The results of strain measurements in hydrostatic compression tests are shown in Figures 18 to 20. The linear strains from two typical specimens are shown in Figure 18. The difference in the strains in the two principal material directions was seen to be not significant and it is therefore concluded that Nugget sandstone exhibits essentially isotropic stress-strain response, even though the rock had faint visual layering. The amount of scatter exhibited by tests of different specimens is shown in Figure 19. The results of unloading and reloading in the

hydrostatic test are shown in Figure 20. It appears as though a small amount of permanent compaction takes place; but, in general, the hysteresis is quite small and may not be experimentally significant.

The results of constant confining pressure tests are shown in Figures 21 and 22. The stresses and strains have been decomposed into shearing and volumetric components. The data are seen to form consistent curves that point up the effects of confining pressure on both the fracture and stress-strain behavior. The initial shear response is seen in Figure 21 to be more dependent on the confining pressure level than seen previously for tonalite and granite [1,2]. The volumetric curves shown in Figures 22 all exhibit dilatancy as observed previously for other rocks [1,2, 5]. The results of the proportional loading tests are plotted in a similar fashion in Figures 23 and 24 for different ratios of the principal stresses. The curves are qualitatively similar to the constant confining pressure test results.

The results of two constant J_1 or mean stress tests are shown in Figures 25 and 26 for the shearing and volumetric components, respectively. This test condition is achieved by loading the specimen hydrostatically to a given pressure level and then simultaneously decreasing the pressure as the axial stress difference is increased so as to keep the sum of the three principal stresses constant.

The one-dimensional strain test results are shown in Figures 27 to 29. The stress-loading path is determined by the condition of the two lateral strains being zero. This has been shown before in Figure 5, but it is repeated in Figure 27. The shearing and volumetric stress-strain curves are shown in Figures 28 and 29, respectively. A new type of strain-controlled test was developed in this program in which the ratio of the axial and lateral strains was held constant. The results from two specimens tested at a strain ratio of $\epsilon_3/\epsilon_1 = -0.249$ are shown in Figures 30 to 32. Actually the strain ratio during the initial portion of the test is less than the stated value. The specimen is loaded in unconfined compression during the initial portion of the test. Once the principal strains do reach the ratio of -0.249 at the stress indicated in the figures, the confining

pressure is servo-controlled to keep the strains in this ratio. The stress loading path established during the test is shown in Figure 30. It can be seen that the loading path rises sharply at first and then curves so as to stay just within the failure locus. Shearing and volumetric strains from these tests are shown in Figures 31 and 32, respectively. An interesting result also obtained from this test is shown in a hydrostatic loading of a specimen before and after the proportional strain test (Fig. 33). The behavior before the test is nearly isotropic while after the proportional strain test the anisotropy is very evident. As suggested by Walsh [6] this anisotropy could be produced by directional microcracking in the specimen during the proportional strain test.

Strain-controlled tests, such as the one-dimensional strain and proportional strain described above, differ in various fundamental respects from the stress-controlled tests. Primarily, the strain-controlled tests furnish a particular loading path in stress space, determined by the strain conditions as well as stress-strain response.

The loading paths shown in Figures 27 and 30 reflect the basically non-linear response of this sandstone. A comparison of these two figures indicates that changing the strain ratio ϵ_3/ϵ_1 from 0 to -0.249 causes the loading path to tend toward the fracture locus. It is believed that as long as the rock exhibits dilatancy before brittle fracture, further decreases in the strain ratio will not produce fracture. Rather the expected result would be to cause the stress loading path to more closely approximate the fracture locus. While these ideas must be regarded as conjectural at the present time, further tests at various constant strain ratios could be employed to check this hypothesis. It appears that the strain-controlled tests can provide significant information about the rock behavior.

A number of unconfined tension tests were performed on the Nugget sandstone and some typical results are shown in Figures 34 to 36. These tests were run with three-inch long by one-inch diameter specimens. The specimens were end-bonded to steel-end caps with epoxy and a small epoxy fillet (approximately 1/16 inch) placed at the end to minimize end-

bond failure. A special fixture with flexible alignment joints was constructed for the tension tests. The specimen fractures appeared to occur randomly throughout the central part of the specimen and were always aligned normal to the specimen axis. Strain gages were placed on the axial midpoint of the specimens and aligned in both axial and transverse directions. The principal stress-strain curves are shown in Figure 34. The fracture stress is approximately 1300 psi. This is about 1/28 of the unconfined compressive strength. It can be seen in this figure that the response is nonlinear. The lateral strain behavior has two interesting aspects. First, the magnitude of the lateral strain is very small. Second, the lateral strain is initially in compression, but changes direction during the test and goes into tension. This result was confirmed on four different specimens. It should be noted that this corresponds to a negative Poisson effect. Clearly, the behavior in tension is as complex as it is in compression and inelastic effects are marked. More evidences of inelastic effects are seen in the tension load-unload cycles shown in Figures 35 and 36. A significant amount of permanent strain is observed in these tests unloaded before fracture. Previous cycled tension tests have been reported by Wawersik [7] with results similar to those given here. A comparison of unconfined tension and compression stress-strain curves is shown in Figure 37. It can be seen that the initial modulus in tension appears to be higher than in compression. This result seems suspicious as a smooth curve passing through the origin would be expected. A further check of these results was not made, however.

A number of load cycling tests were run with proportional stresses in compression. Some typical results are given in Figures 38 through 41. Figures 38 and 40 show the shearing stress-strain response for two different specimens while Figures 39 and 41 show the dilatational response. Permanent set is a characteristic feature in unloading. Also shown in these figures are the stress-strain curves for specimens loaded to fracture at the same stress ratio.

SECTION IV

MATHEMATICAL REPRESENTATION

In this section a mathematical representation of the stress-strain behavior of Nugget sandstone will be developed. Despite recent investigations of the mechanisms involved in rock deformation [6,8,9,10] it is not presently possible to formulate a constitutive equation for rock without recourse to experimental data. This latter procedure, essentially an empirical one, will be followed here.

In previous work on stress-strain models for rock [2], it has been shown that many features of rock behavior can be represented by the use of a plasticity model with strain hardening. In particular, the permanent set observed in unloading tests, the nonlinearity of the shearing stress-strain curves, and the dilatancy effect seen in the volume strain response can all be incorporated into a plasticity constitutive relation. Previous to this the use of plasticity equations for modelling rock behavior has been criticized [11] on the grounds that the deformation mechanisms were not similar in nature to the mechanisms controlling plastic deformation in metals. If one takes the position that the plasticity model is only a conceptual means of aiding the writing of constitutive equations, then the objection appears to be unfounded. However, because of the presumed difference in deformation mechanism, it may be important to carefully verify the applicability of all of the features of plasticity models to the deformation of rock.

In a recent study [12] an assessment of certain features of plasticity models and their application to the stress-strain behavior of brittle rock has been carried out. Two features were studied in particular: the lack of a clearly defined yield point and the effect of the loading path on stress-strain behavior. It was shown that certain changes in the use of conventional strain hardening plasticity models could improve the accuracy of the material representation. For completeness these two developments will be reviewed here.

The lack of a definite yield point can be seen in the shearing curves of Figures 21, 23, 38, and 40. Permanent set can be seen in the unloading curves of Figures 38 and 40 but the effect appears to be a gradual one and no noticeable discontinuity occurs. Thus, a definite elastic limit seems arbitrary and artificial. It was shown in Ref. [12] that the objection could be circumvented by the use of a distributed yield function which can be derived by analogy with some simple spring and friction element models. This technique also appears to be capable of modeling the unloading behavior more accurately than has been done with the strain-hardening model although this has not been carried out to date.

The second point studied in Ref. [12] is concerned with the effects of load path on the stress-strain response. It is difficult to ascertain the effect of load path merely by looking at the stress-strain curves from different tests as in most cases the state of stress is changed as well by the change in the path. To separate the effects of stress state from those of the loading path, per se, a number of parametric plots were constructed so as to vary the loading path but keep the state of stress constant. These were developed and shown previously [12], but will be repeated here for clarity. Consider the loading paths shown in Figure 5. At each intersection of two loading paths a point is reached where the stress state is identical in two different tests but has been reached by different paths. A comparison of the state of strain at the point in question will then reveal whether loading path is an important variable in the deformation. This comparison has been made in Ref. [12] in three different ways. First, the strains along different constant confining pressure loading paths were plotted. The constant confining pressure tests themselves form a continuous curve and at each intersection with another type of test a strain value from that test is plotted. This procedure was repeated for constant J_1 loading paths and the one-dimensional strain loading path. The results from Ref. [12] are shown in Figures 42 through 47. As evidenced by the agreement in the strain at a stress point reached by different load paths, the path dependency of the strain response is minimal.

If unloading as well as loading is considered, then path effects can be observed in the stress-strain response. This can be seen in Figures 38 through 41. Clearly the strain at a given stress point depends on whether or not the point is reached by loading or unloading.

In Ref. [12] a plasticity model was developed that combines the ideas of path independence of the strains for loading conditions and permanent set and, therefore, path dependence if unloading is considered. The model is based on the associated flow rule.

$$d\epsilon_{ij}^P = \frac{\partial G}{\partial \sigma_{ij}} d\lambda \quad (1)$$

where the scalar multiplier $d\lambda$ is given by

$$d\lambda = \frac{dG}{\left(\frac{\partial \sqrt{I_2^P}}{\partial \epsilon_{mn}} \right) \left(\frac{\partial G}{\partial \sigma_{mn}} \right)} \quad \text{if } dG > 0 \quad (2)$$

$$d\lambda = 0 \quad \text{if } dG \leq 0$$

The function $G(\sigma_{ij})$ is taken so that during monotonic loading states only

$$\sqrt{I_2^P} = G(\sigma_{ij}) \quad (3)$$

where $\sqrt{I_2^P}$ is the second invariant of the plastic deviator strain given by

$$\sqrt{I_2^P} = \left\{ \frac{1}{6} \left[(\sigma_1 - \sigma_2)^2 + (\sigma_2 - \sigma_3)^2 + (\sigma_3 - \sigma_1)^2 \right] \right\}^{1/2} \quad (4)$$

If the associated flow rule (1) is applied to monotonic loading states, then the function (3) will be satisfied making the deviatoric strains a function of the stress-state only. This can be simply shown by differentiating (3) and then substituting in from (1) and (2). It should be noted that the flow rule (1) makes only the deviatoric strains path independent.

The total strain increments are divided into elastic and plastic components in the usual fashion as

$$d\epsilon_{ij} = d\epsilon_{ij}^e + d\epsilon_{ij}^p \quad (5)$$

The application of this model to the specific Nugget sandstone data given in this report requires the formulation of laws governing the elastic response and identification of the function G . This involves identifying specific functions for representation and curve-fitting to obtain the necessary constants. The number of constants required depends on how carefully the functions are selected and on how carefully the specific material is being modeled. Since the point of the present work is to demonstrate a new model, an effort was made to match the material behavior quite well. Consequently, the resulting equations are fairly complex. It should be understood that in application to calculations, these equations would be simplified if necessary.

The elastic response was separated into deviatoric and dilatational components as follows:

$$\epsilon_v^e = 10^{-4}[1.95\sigma_m + 45][1 - \exp(-\sigma_m/7)] \quad (6)$$

where ϵ_v^e is the elastic volume strain, equal to the sum of the three linear strain components and σ_m is the mean stress in ksi. The elastic shearing strain was found to depend on the mean stress as well as the shearing stress and also nonlinearly related to the stress. The elastic shearing strains are given by

$$\epsilon_{ij}^e = C_1 \sigma_{ij} + C_2 \left(\frac{\sigma_{ij}}{C_3} \right)^3 \quad i \neq j \quad (7)$$

where

$$C_1 = \frac{0.01}{18.5 + 40[1 - \exp(-\sigma_m/30)]} \quad (8)$$

$$C_2 = 0.006 [1 - \exp(-\sigma_m/80)] \quad (9)$$

$$C_3 = [0.66 \sigma_m + 27.8][1 - \exp(-\sigma_m/17)] \quad (10)$$

The plastic strain function G of Equation (3) was taken as

$$G = C_2 \left(\frac{J_2'}{C_3} \right)^9 \quad (11)$$

where C_2 and C_3 are given above. The fit of these equations to the experimental data is shown in Figures 48 through 59. The shear and volume stress-strain curves for constant confining pressure tests are shown compared with experiment in Figures 48 and 49 respectively. A similar comparison for proportional stress loading is shown in Figures 50 and 51 and for constant J_1 tests in Figures 52 and 53. It can be seen from these figures that good agreement between model and experiment is obtained.

A further comparison between model and experiment is shown in Figures 54 through 56 for the one-dimensional strain test and Figures 57 through 59 for a proportional strain test. Comparisons between model and experiment of the stress loading paths obtained in these strain-controlled tests are shown in Figures 54 and 57. The stress-strain comparisons are shown in Figures 55, 56, 58, and 59. In general, there is more discrepancy between the data and the model for the strain-controlled tests than the stress-controlled tests. This is probably due to the large change in stress which occurs at the onset of dilatancy for relatively small changes in strain. Therefore the model is more sensitive to the strain controlled test. This point deserves further study.

The problem of fitting a generalized model to experimental data is, of course, complicated by having a large amount of data available, particularly data from a variety of types of tests. Each type of test imposes an additional constraint on the model. Clearly it is desirable to test the model under as wide a variety of loading conditions as possible, but it is not surprising that the model does not fit all of the experimental results with the same degree of accuracy. Thus considered, the agreement between the proposed model and the experimental data is good.

As stated above, this model differs from the plasticity models developed previously for Cedar City tonalite and Westerly granite [2] in that in the present model the shearing strains are taken to be path independent under loading conditions. It is difficult to assess whether the present model is applicable to other rocks such as tonalite or Westerly granite without actually going through the detailed curve-fitting process, and this has not been done at the present time. The apparent requirement for the present model resulted from the detailed assessment of the stress-strain response of Nugget sandstone available from the present study. Further insight into the modeling of the stress-strain behavior of rocks could be obtained by applying the present model to the data obtained previously for Cedar City tonalite [1] and Westerly granite [2].

The particular constants appearing in Equations 6 through 11 are significant only in terms of the mathematical expressions chosen. They depend on the choice of expressions used to fit non-linear functions. It is the functions themselves that are significant and reflect the rock behavior. For example, the non-linear hydrostat of Equation 6 could be expressed mathematically in a number of ways, and the resulting constants reflect both the material behavior and the mathematical form. This is in contrast to linear behavior, where a unique representation would result. The underlying basis of the nonlinearity of the hydrostat is attributed to the amount of porosity and void configuration of the rock, but this is not necessarily reflected in the constants of Equation 6.

SECTION V

SUMMARY AND CONCLUSIONS

A large amount of stress-strain data has been obtained from controlled path loading triaxial tests of Nugget sandstone. The tests employed in this study included constant confining pressure, proportional stress, constant J_1 , one dimensional strain, proportional strain, unconfined compression, and unconfined tension. In general, these data are consistent and display a number of interesting features. Nugget sandstone is observed to fracture in a brittle manner over the entire range of confining pressures employed, however, inelastic effects in the stress-strain behavior were observed. These are evidenced by permanent set in unloading tests and dilatancy in the volume strain response.

One of the interesting results from this program was the dilatancy observed in the uniaxial stress tension tests. Repeated tests indicated that as the load was applied the diameter of the specimen first decreased slightly, as would be expected due to the Poisson effect, but that it then began to increase. Since the specimen was simultaneously increasing in length, the increase in diameter resulted in a volumetric increase. It is surmised that micro-cracking may be a possible explanation of this phenomena just as is suspected with the dilatancy associated with compressive states of stress.

The increase in diameter as the specimen is elongated obviously indicates that the "apparent" Poisson's ratio is negative for some states of stress. On the other extreme, the radial strain increases more rapidly than the axial strain just prior to fracture in the triaxial compressive loading experiments. The "apparent" Poisson's ratio for this condition yields values greater than unity. Poisson's ratio for this material therefore varies from a negative value to a value greater than unity depending on the stress conditions employed. This points up the great need to provide more sophisticated models for rocks than the simple elastic models, or variations thereof, that are often utilized in designing structures in rock.

The nature of path dependency of the stress-strain response for Nugget sandstone was reviewed. A plasticity model developed in another study that considers the deviatoric strains in monotonic loading to be independent of the stress path was considered useful. This model was fitted to the experimental results. In general, a good comparison between model and experiment was achieved for all of the experimental tests which included a wide variety of loading paths.

TABLE 1
SUMMARY OF NUGGET SANDSTONE TESTS

Test No.	Date of Testing	Specimen No.	Type of Test	σ_3 Max. ksi	$\sigma_1 - \sigma_3$ Max. ksi	σ_3/σ_1	Specimen Fractured	Comments
1	1/7/70	24	Constant Pressure	5	77.5		X	Not gaged
2	1/16/70	25	Constant Pressure	10	85.8		X	Not gaged
3	1/17/70	26	Constant Pressure	20	122		X	Not gaged
4	1/17/70	1	First Hydrostatic					
5	1/17/70	1	Second Hydrostatic					
6	1/17/70	1	Constant Pressure	5	88.8		X	
7	1/17/70	2	First Hydrostatic					
8	1/17/70	2	Second Hydrostatic					
9	1/17/70	2	Constant Pressure	9.33	108.6		X	
10	1/17/70	3	First Hydrostatic					
11	1/17/70	3	Second Hydrostatic					

TABLE 1

SUMMARY OF NUGGET SANDSTONE TESTS (continued)

Test No.	Date of Testing	Specimen No.	Type of Test	σ_3 Max. ksi	$\sigma_1 - \sigma_3$ Max. ksi	σ_3/σ_1	Specimen Fractured	Comments
12	1/17/70	3	Constant Pressure	19.2	139.1		X	
13	1/27/70	18	Unconfined Compression	0	37.3		X	
14	1/28/70	19	Unconfined Compression	0	37.4		X	
15	1/30/70	4	Hydrostatic					
16	1/31/70	4	Constant Pressure	40	198		X	
17	1/31/70	5	Hydrostatic					
18	2/3/70	5	Constant Pressure	62.6	246		X	
19	2/4/70	6	Hydrostatic					
20	2/4/70	6	Constant Stress Ratio	4.74	79.4	.053	X	
21	2/4/70	7	Hydrostatic					
22	2/4/70	7	Constant Stress Ratio	10.1	108	.085	X	

TABLE 1

SUMMARY OF NUGGET SANDSTONE TESTS (continued)

Test No.	Date of Testing	Specimen No.	Type of Test	σ_3 Max. ksi	$\sigma_1 - \sigma_3$ Max. ksi	σ_3/σ_1	Specimen Fractured	Comments
23	2/7/70	8	Hydrostatic					
24	2/7/70	8	Constant Stress Ratio	25.1	155.2	.132	X	
25	2/7/70	9	Hydrostatic					
26	2/7/70	9	Constant Stress Ratio	48.7	220	.181	X	
27	2/9/70	21	Unconfined Compression	0				Error in Pressure. Test results not used
28	2/14/70	22	Unconfined Compression	0				1/2 cycle
29	2/14/70	22	Unconfined Cycled	0	39.3		X	Full cycle
30	2/14/70	23	Unconfined Cycled	0				1/2 cycle
31	2/14/70	23	Unconfined cycled	0	37.8		X	Full cycle
32	2/14/70	10	Hydrostatic					
33	2/14/70	10	Constant σ_3/σ_1 cycled					1/2 cycle

TABLE 1

SUMMARY OF NUGGET SANDSTONE TESTS (continued)

Test No.	Date of Testing	Specimen No.	Type of Test	σ_3 Max. ksi	$\sigma_1 - \sigma_3$ Max. ksi	σ_3/σ_1	Specimen Fractured	Comments
34	2/14/70	10	Constant σ_3/σ_1 Cycled	9.02	96.2		X	Full cycle
35	2/14/70	11	Hydrostatic					
36	2/14/70	11	Constant σ_3/σ_1 Cycled	5.56	58.4	.087		1/2 cycle
37	2/14/70	11	Constant σ_3/σ_1 Cycled	9.02	96.1	.090	X	Full cycle
38	2/21/70	12	Hydrostatic					
39	2/21/70	12	Constant σ_3/σ_1 Cycled					3/4 cycle
40	2/21/70	12	Constant σ_3/σ_1 Cycled	8.94	95.9	.084	X	Full cycle
41	2/21/70	13	Hydrostatic					
42	2/21/70	13	Hydrostatic					
43	2/21/70	13	Constant σ_3/σ_1 Cycled	7.77	82.2	.087		3/4 cycle

TABLE 1

SUMMARY OF NUGGET SANDSTONE TESTS (continued)

Test No.	Date of Testing	Specimen No.	Type of Test	σ_3 Max. ksi	$\sigma_1 - \sigma_3$ Max. ksi	σ_3/σ_1	Specimen Fractured	Comments
44	2/21/70	13	Constant σ_3/σ_1 cycled	5.6	61.2	0.84		$\frac{1}{2}$ cycle
45	2/21/70	13	Constant σ_3/σ_1 cycled	8.7	100.1	.081	X	Full cycle
46	2/21/70	14	Hydrostatic					Two
47	2/21/70	14	Constant Stress ratio ^d	48.5	215	.193	X	
48	2/28/70	15	Hydrostatic					
49	2/28/70	15	Hydrostatic					
50	2/28/70	15	Constant σ_3/σ_1 cycled	15.1	63.7	.198		$\frac{1}{2}$ cycle
51	2/28/70	15	Constant σ_3/σ_1 cycled	48.6	207.6	.191	X	Full cycle
52	2/28/70	16	Hydrostatic					
53	2/28/70	16	Hydrostatic					
54	2/28/70	16	Constant σ_3/σ_1 cycled	30.3	121.0	.20		$\frac{1}{2}$ cycle

TABLE 1

SUMMARY OF NUGGET SANDSTONE TESTS (continued)

Test No.	Date of Testing	Specimen No.	Type of Test	σ_3 Max. ksi	$\sigma_1 - \sigma_3$ Max. ksi	σ_3/σ_1	Specimen Fractured	Comments
55	2/28/70	16	Constant σ_3/σ_1 cycled	54.8	235.6	0.194	X	Full cycle
56	2/28/70	17	Hydrostatic					
57	2/28/70	17	Constant σ_3/σ_1 cycled	19.0	77.4	0.198		1/4 cycle
58	2/28/70	17	Constant σ_3/σ_1 cycled	43.5	177.3	0.198		3/4 cycle
59	2/28/70	17	Constant σ_3/σ_1 cycled	61.0	260.5	0.191	X	Full cycle
60	3/14/70	40	Hydrostatic					
61	3/14/70	40	Hydrostatic					
62	3/14/70	40	Constant Stress ratio	59.4	244	0.205	X	
63	3/14/70	32	Hydrostatic					
64	3/14/70	32	Two step loading	6.58	90.4		X	
65	3/14/70	39	Hydrostatic					

TABLE 1

SUMMARY OF NUGGET SANDSTONE TESTS (continued)

Test No.	Date of Testing	Specimen No.	Type of Test	σ_3 Max. ksi	$\sigma_1 - \sigma_3$ Max. ksi	σ_3/σ_1	Specimen Fractured	Comments
66	3/14/70	39	Hydrostatic					
67	3/14/70	39	Constant σ_3/σ_1 cycled	46.6	382	.110		3/4 cycle
68	3/14/70	39	Constant σ_3/σ_1 cycled					1/2 cycle
69	3/14/70	39	Constant σ_3/σ_1 cycled					Gage went out
70	3/18/70	42	One-dimensional strain	36.1	198			Fract. after horiz. gage failed.
71	3/18/70	41	Hydrostatic					
72	3/18/70	41	Hydrostatic					
73	3/18/70	41	Constant pressure	80	307		X	
74	3/20/70	20	Hydrostatic					
75	3/20/70	20	Constant ϵ_3/ϵ_1 cycled					No failure. Gage went out.
76	3/20/70	20	Hydrostatic					

TABLE 1

SUMMARY OF NUGGET SANDSTONE TESTS (continued)

Test No.	Date of Testing	Specimen No.	Type of Test	σ_3 Max. ksi	$\sigma_1 - \sigma_3$ Max. ksi	σ_3/σ_1	Specimen Fractured	Comments
77	3/20/70	20	Constant Strain ratio				X	
78	3/20/70	20	Hydrostatic					Horiz. gages working after failure.
79	3/20/70	31	Hydrostatic					
80	3/20/70	31	Constant ϵ_3/ϵ_1 cycled					
81	3/20/70	31	Constant ϵ_3/ϵ_1 cycled					Spec. had num cracks after testing.
82	3/20/70	31	Hydrostatic					
83	3/20/70	33	Hydrostatic					
84	3/20/70	33	Hydrostatic					
85	3/20/70	33	Hydrostatic					
86	3/21/70	33	Two step loading					Equipment failure
87	4/4/70	44	Unconfined tension	0				Error in procedure

TABLE 1

SUMMARY OF NUGGET SANDSTONE TESTS (continued)

Test No.	Date of Testing	Specimen No.	Type of Test	σ_3 Max. ksi	$\sigma_1 - \sigma_3$ Max. ksi	σ_3/σ_1	Specimen Fractured	Comments
88	4/4/70	45	Unconfined tension	0	-1.10		X	Spec. not centered on end cap.
89	4/4/70	46	Unconfined tension	0				1/2 cycle, Spec. not centered.
90	4/4/70	46	Unconfined tension	0				3/4 cycle Transverse grain*
91	4/4/70	46	Unconfined tension	0	-1.07		X	Failed on epoxy bond.
92	4/4/70	47	Unconfined tension	0	-1.31		X	
93	4/4/70	48	Unconfined tension	0				3/4 cycle Transverse grain
94	4/4/70	48	Unconfined tension	0				1/2 cycle
95	4/4/70	48	Unconfined tension	0				3/4 cycle
96	4/4/70	48	Unconfined tension	0	-1.14		X	Full cycle
97	4/4/70	58	Unconfined tension	0	-1.11			Failed on epoxy.
98	4/4/70	59	Unconfined tension	0	-1.27		X	Not centered on end cap.

TABLE 1

SUMMARY OF NUGGET SANDSTONE TESTS (continued)

Test No.	Date of Testing	Specimen No.	Type of Test	σ_3 Max. ksi	$\sigma_1 - \sigma_3$ Max. ksi	σ_3/σ_1	Specimen Fractured	Comments
99	4/4/70	60	Unconfined tension	0	-1.12		X	Failed on epoxy.
100	4/8/70	29	Unconfined tension	0	-.995		X	Data not used.
101	4/22/70	45	Unconfined tension	0				Transverse grain second run.
102	4/22/70	46	Unconfined tension	0				Transverse grain second run.
103	4/25/70	47	Unconfined tension	0				Transverse grain second run.
104	4/25/70	59	Unconfined tension	0				Second run
105	5/9/70	60	Unconfined tension	0				Second run
106	5/9/70	61	Unconfined tension	0				Transverse grain load only measured
107	5/9/70	62	Unconfined tension	0				Transverse grain load only measured

*Grain direction is axial unless noted.

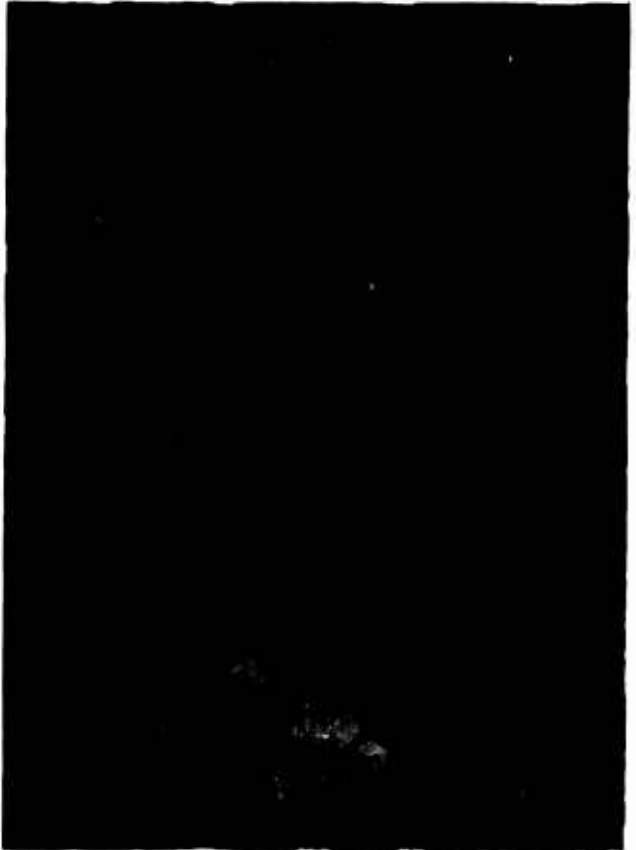
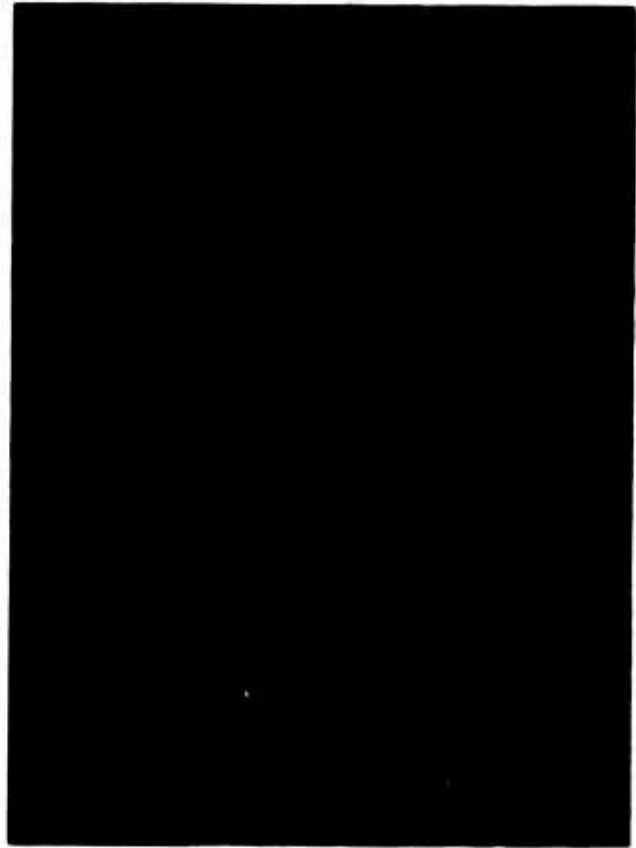
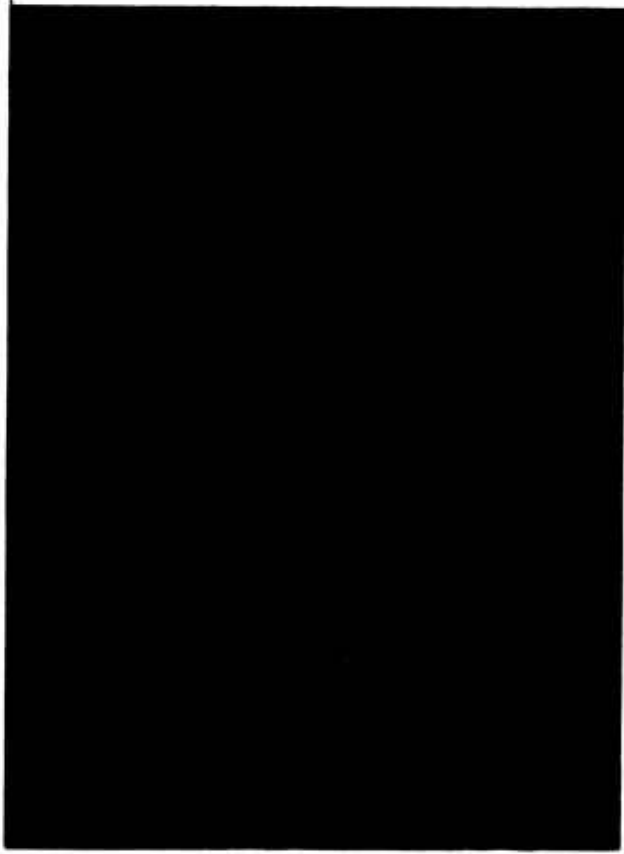


FIGURE 1. Photomicrographs of Nugget Sandstone, Thin Sections at 36 and 120 magnification.



NOT REPRODUCIBLE

FIGURE 2. Typical instrumented rock specimens

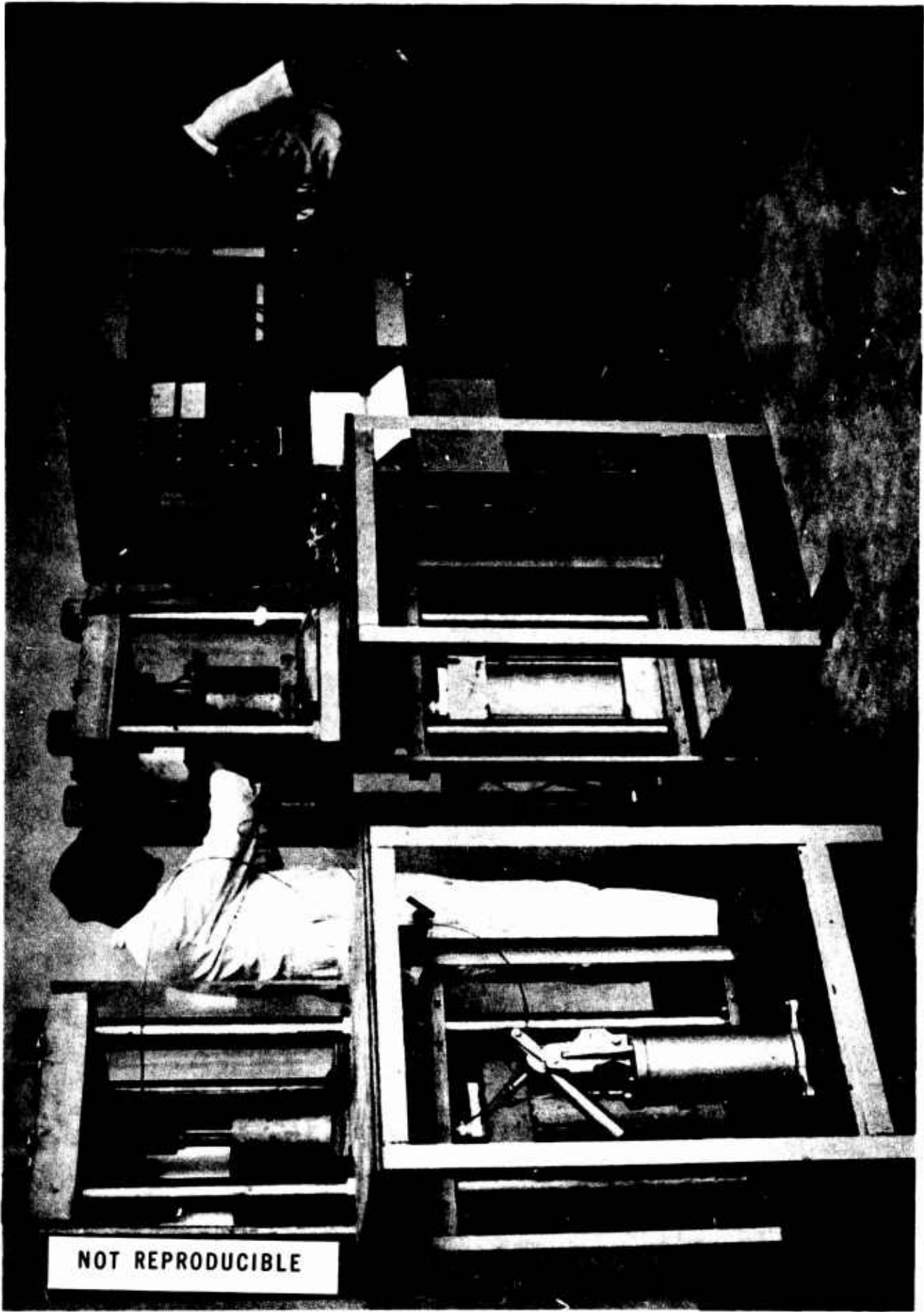


Figure 3. High pressure laboratory apparatus

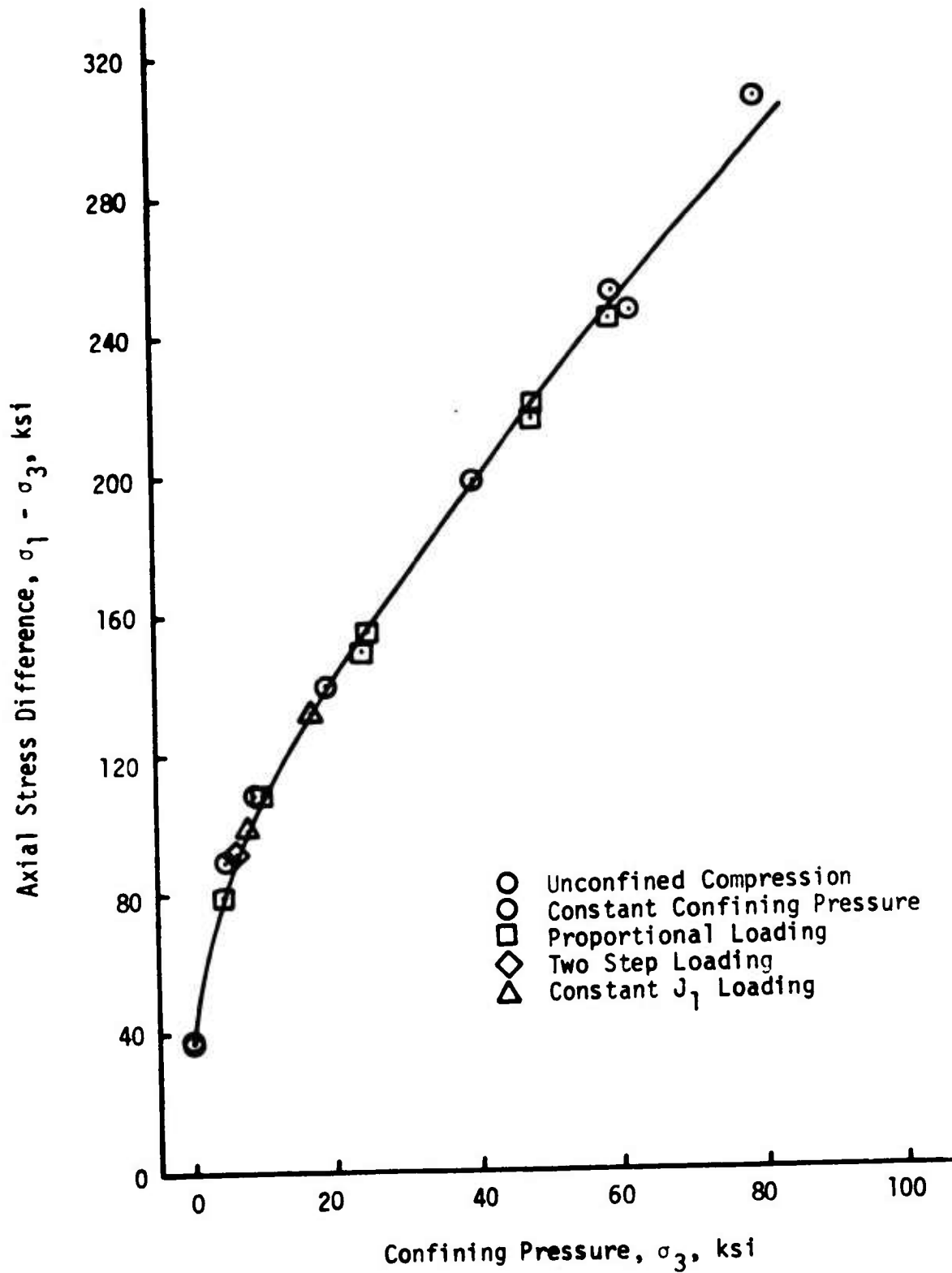


Figure 4. Fracture stress for Nugget sandstone in triaxial compression.

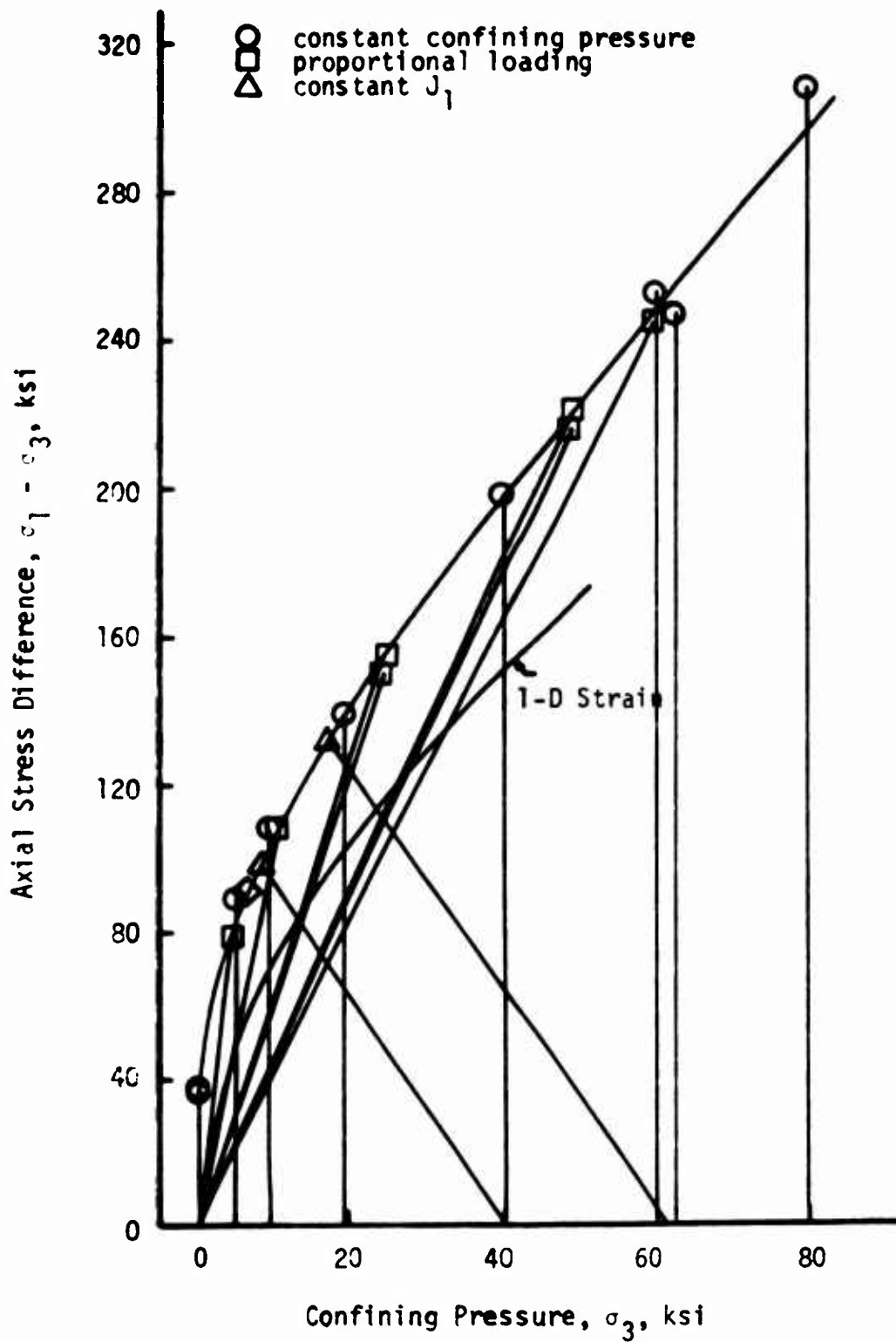


Figure 5. Loading paths for triaxial tests of intact Nugget sandstone

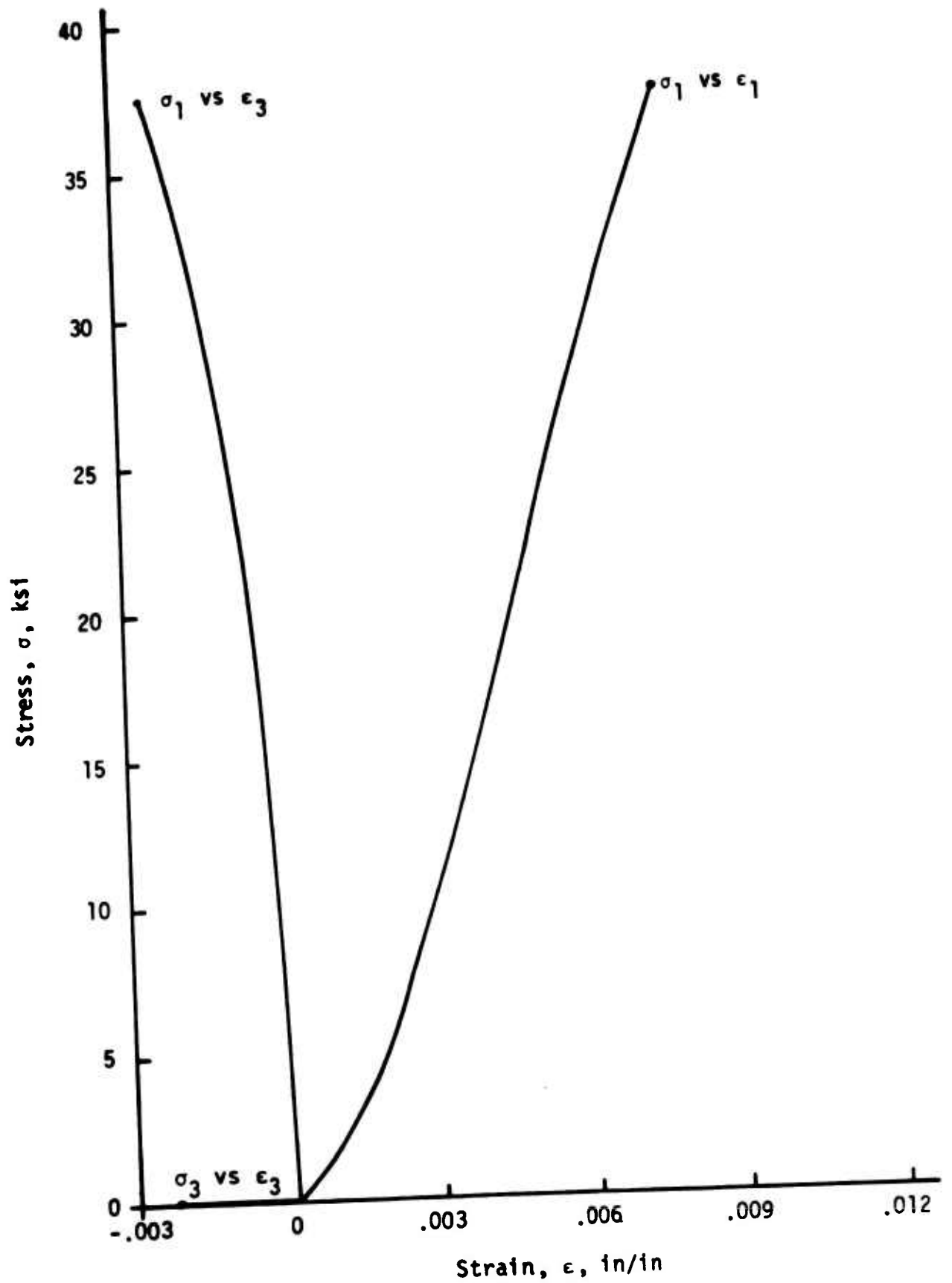


Figure 6. Principal stress-strain curves for Nugget sandstone specimen No. 19 in unconfined compression.

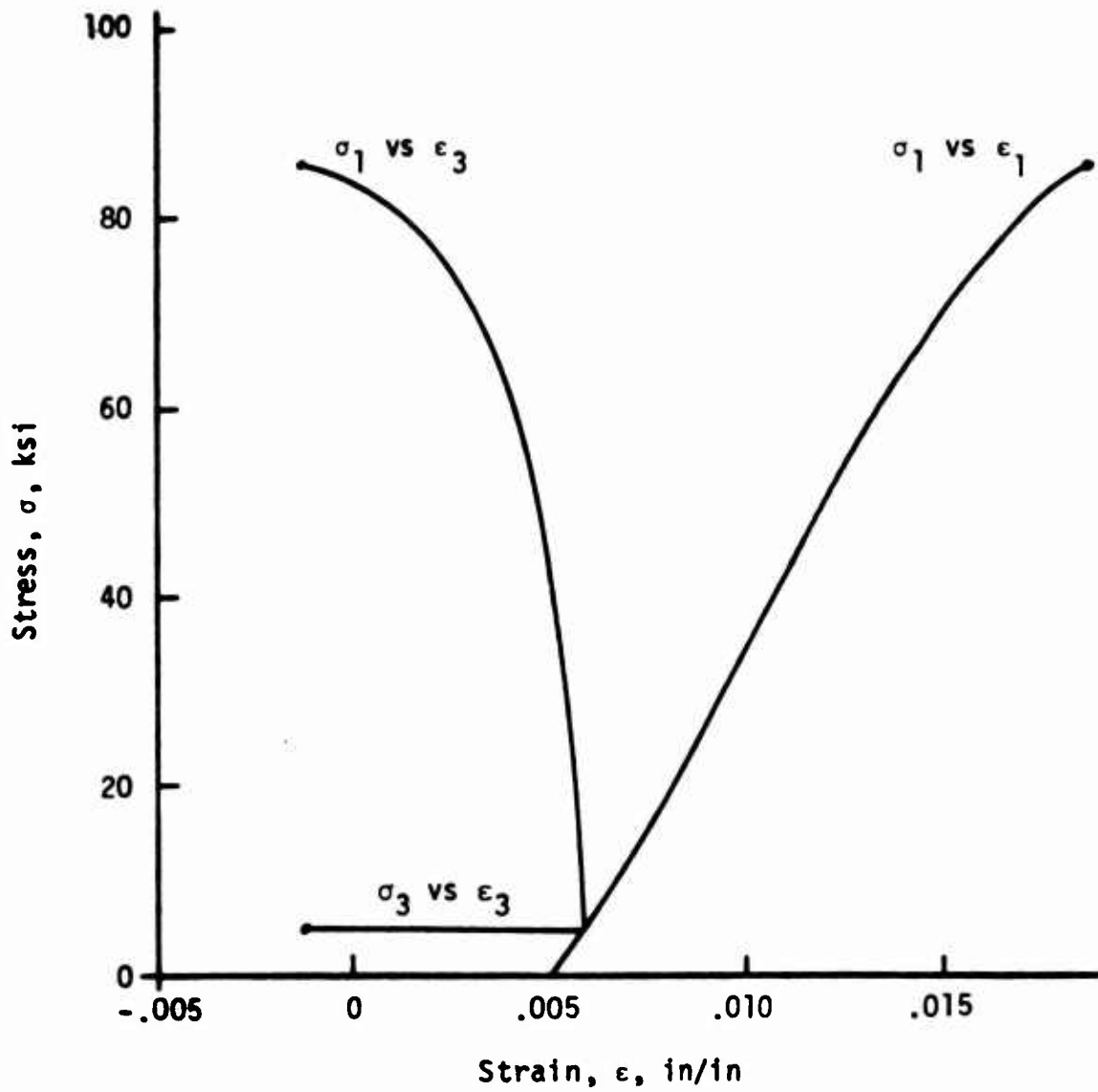


Figure 7. Principal stress-strain curves for Nugget sandstone specimen No. 1, constant confining pressure, $P = 5$ ksi.

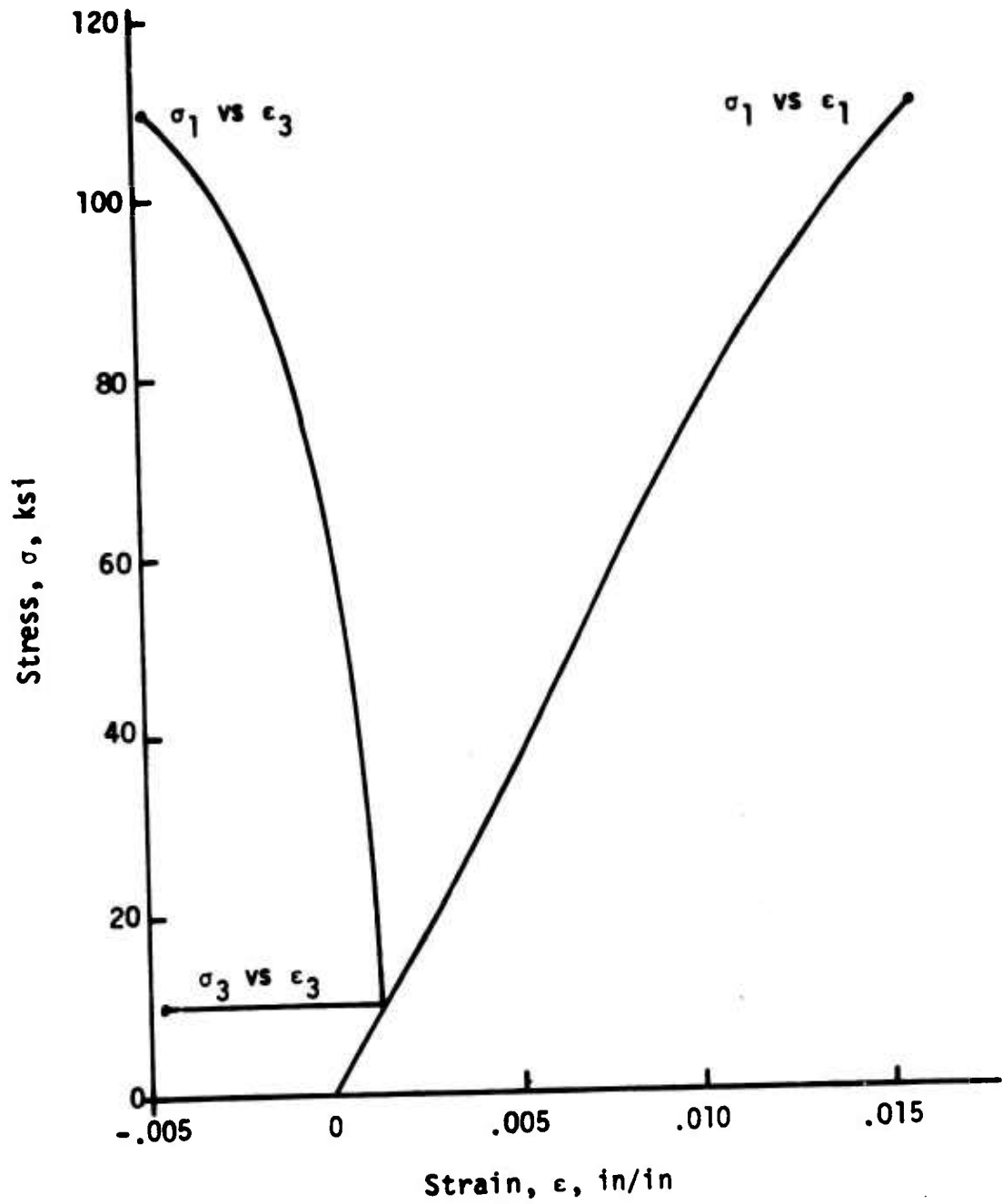


Figure 8. Principal stress-strain curves for Nugget sandstone specimen No. 2, $P = 10$ ksi.

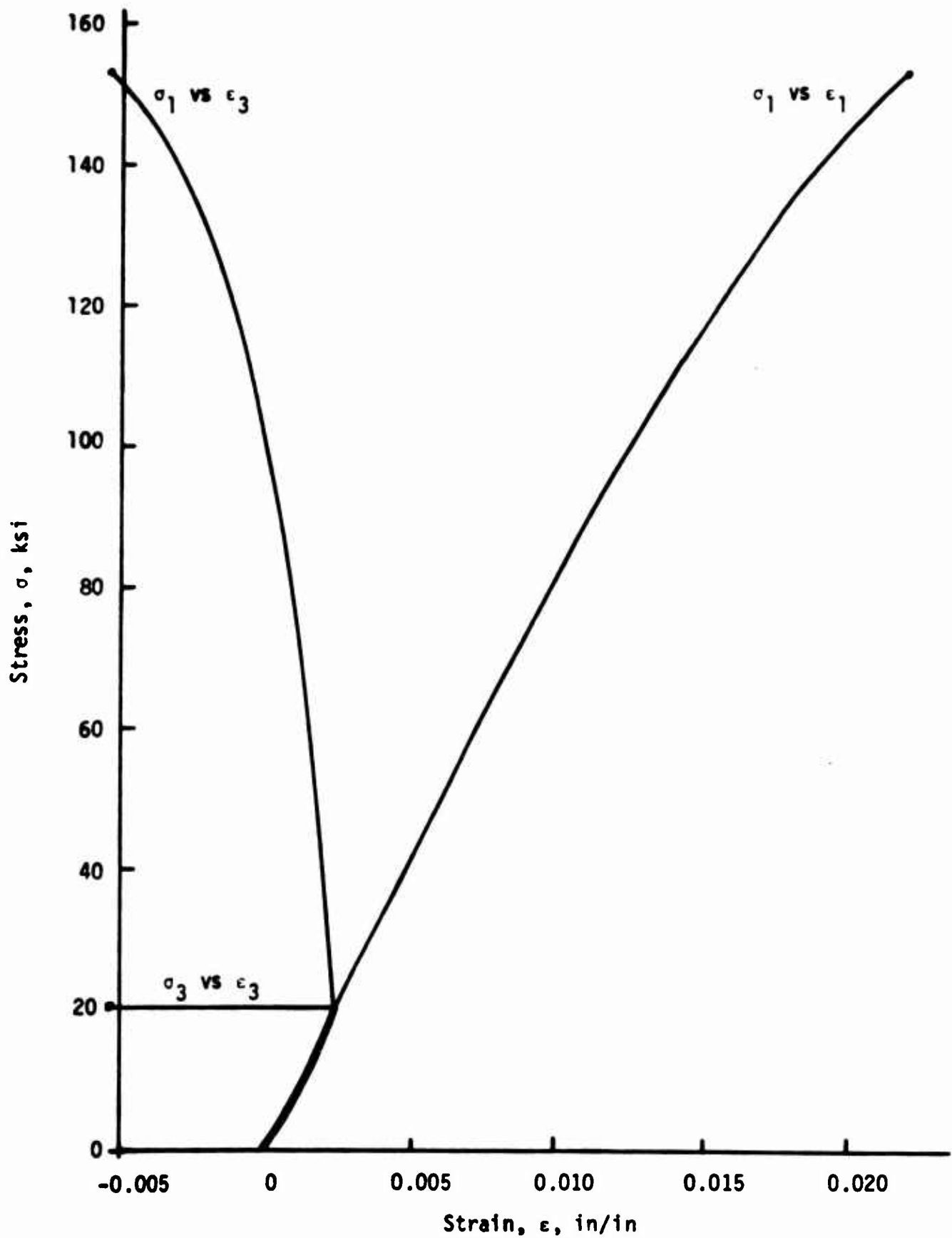


Figure 9. Principal stress-strain curves for Nugget sandstone specimen No. 3, constant confining pressure, $P = 5$ ksi

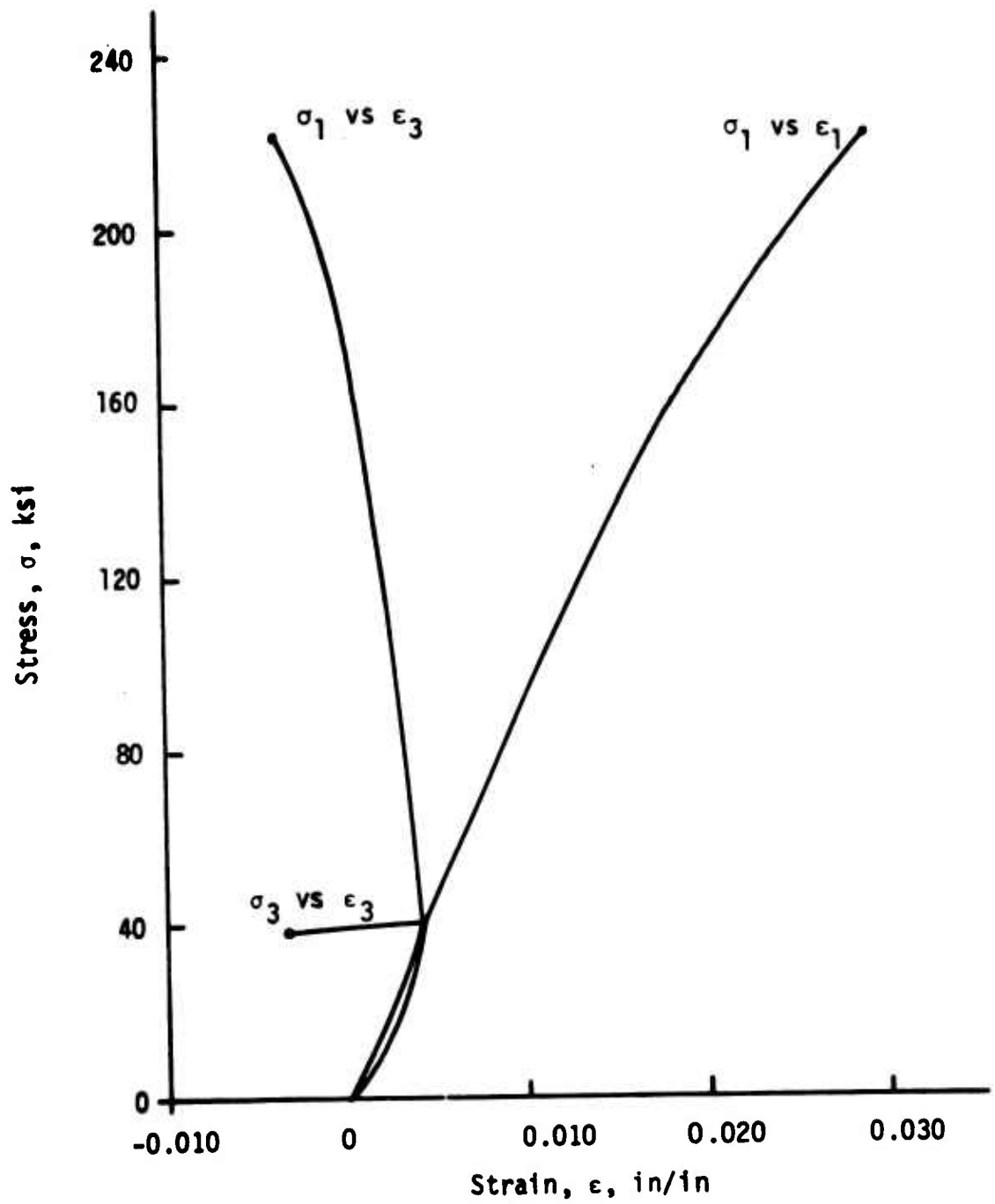


Figure 10. Principal stress-strain curves for Nugget sandstone specimen No. 4, constant confining pressure, $P = 41$ ksi.

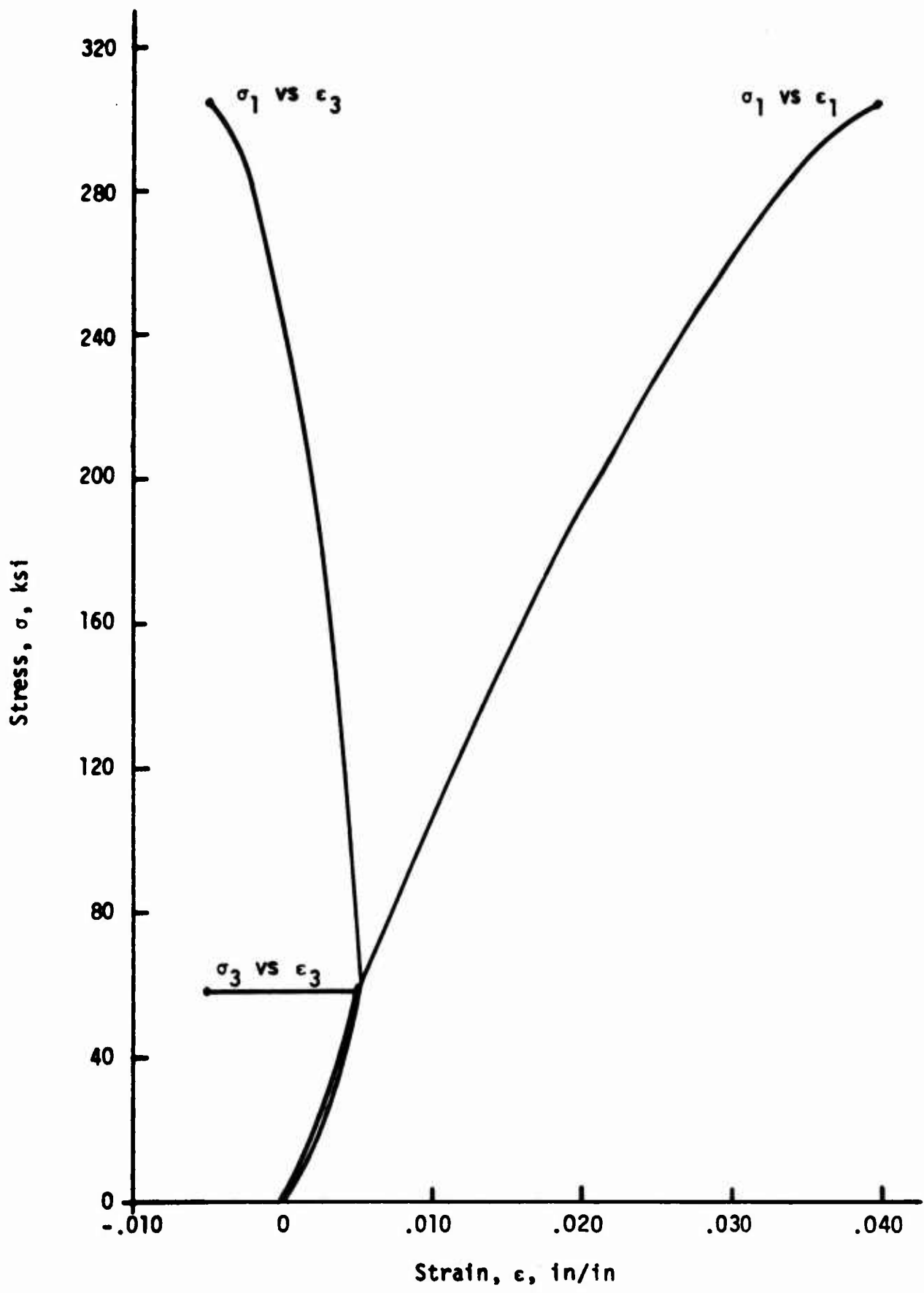


Figure 11. Principal stress-strain curves for Nugget sandstone specimen No. 5, constant confining pressure, $P = 60$ ksi.

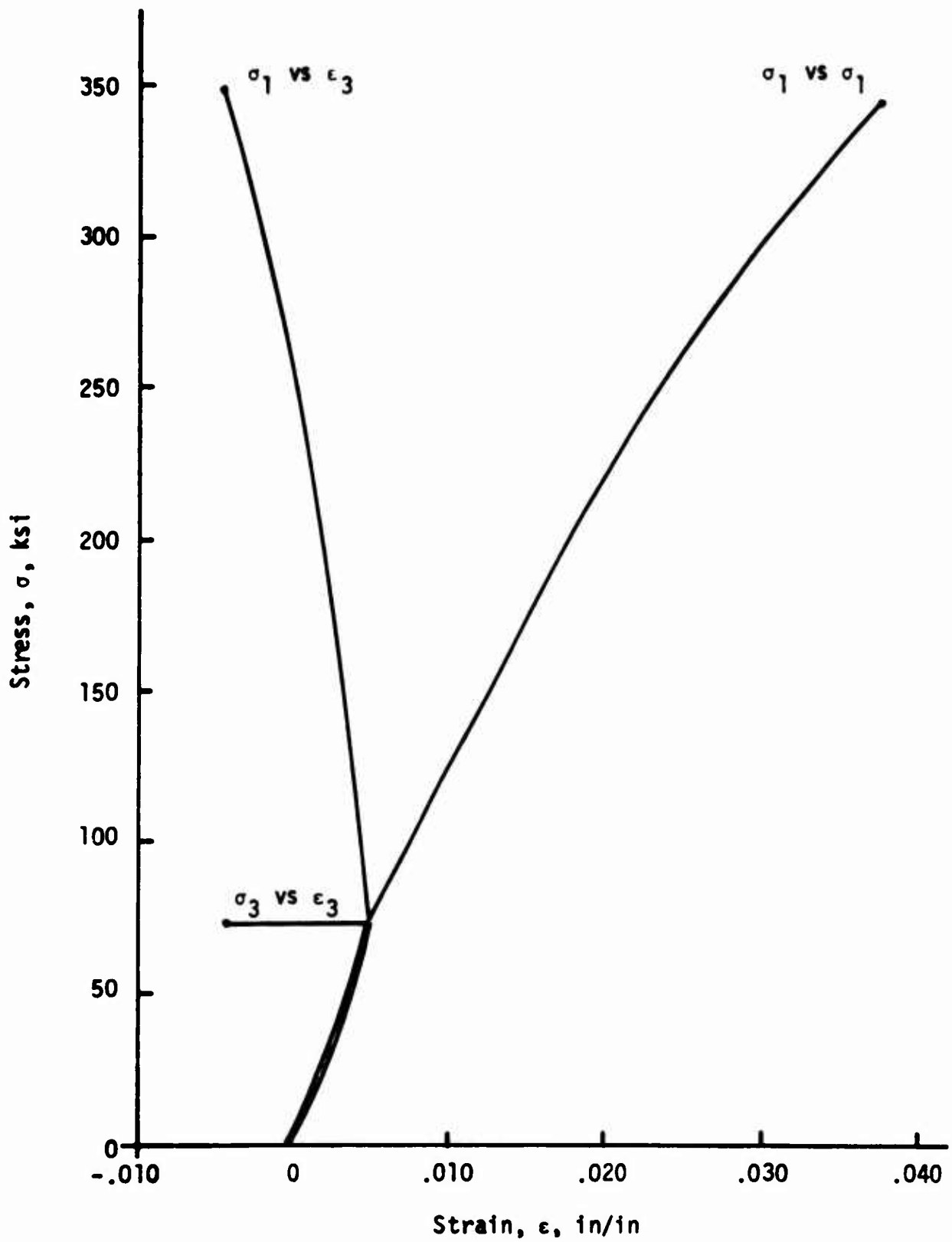


Figure 12. Principal stress-strain curves for Nugget sandstone specimen No. 41, constant confining pressure, $P = 80$ ksi.

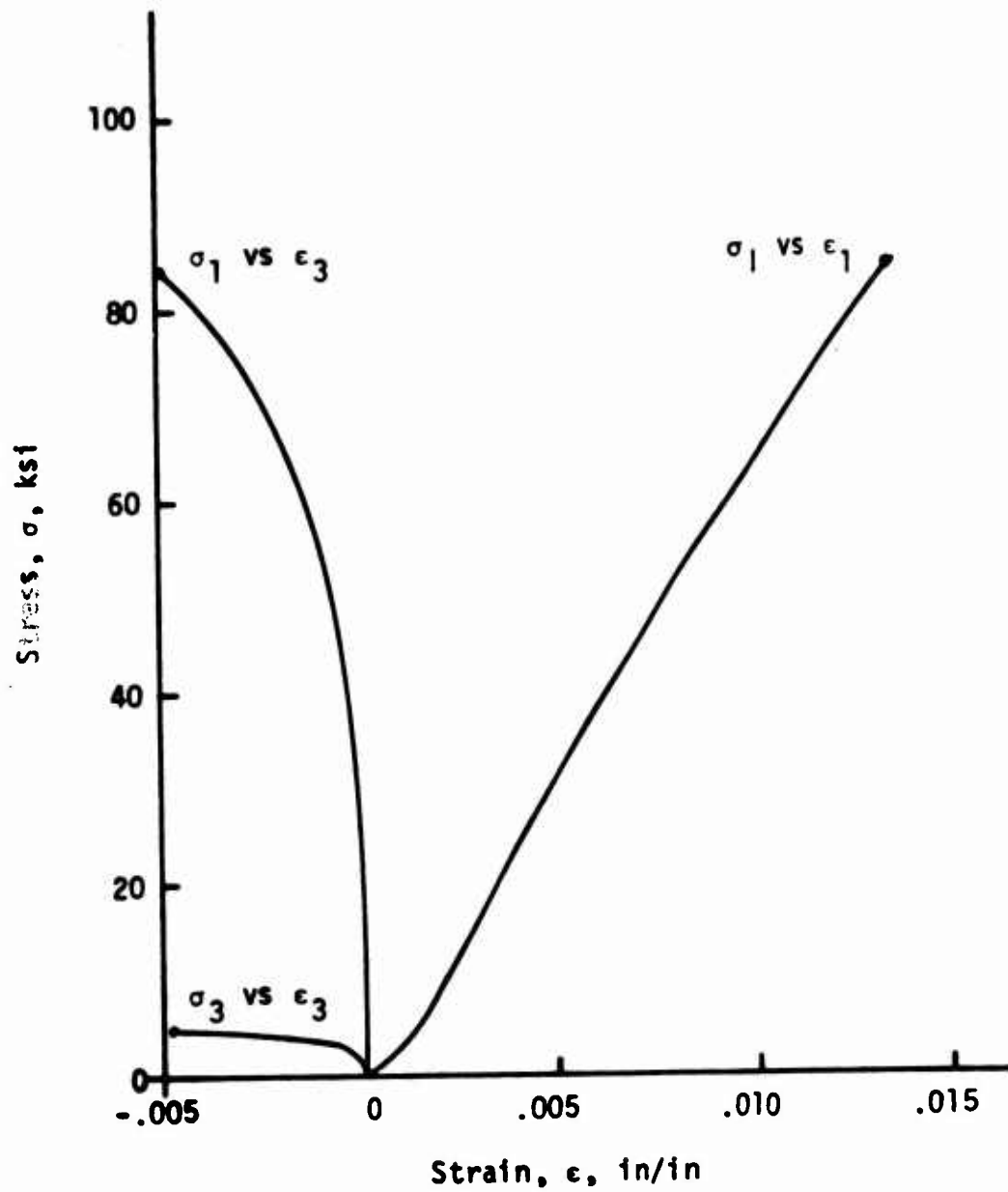


Figure 13. Principal stress-strain curves for Nugget sandstone specimen No. 6 in proportional loading, $\sigma_3/\sigma_1 = 0.056$.

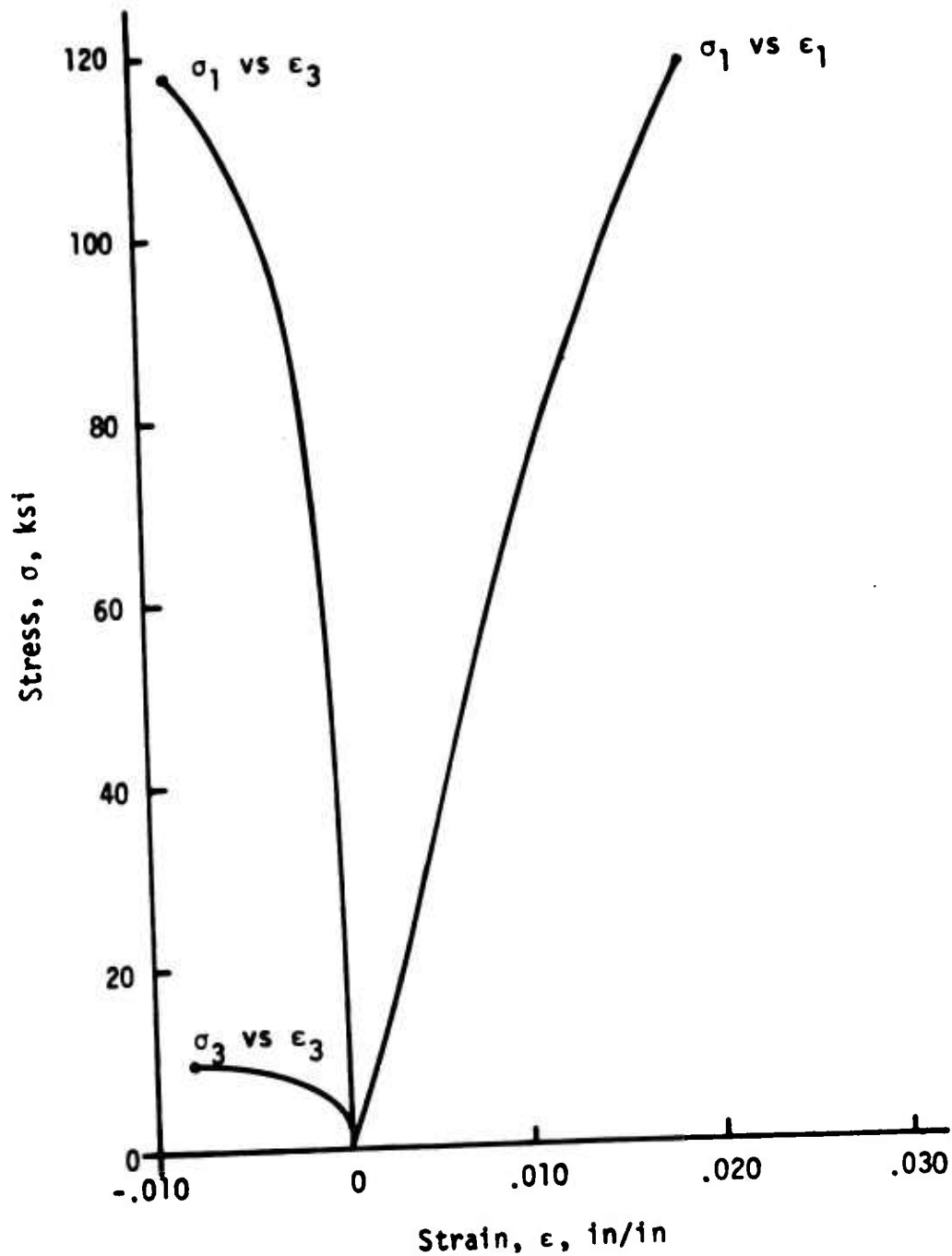


Figure 14 Principal stress-strain curves for Nugget sandstone specimen No. 7 in proportional loading, $\sigma_3/\sigma_1 = 0.084$

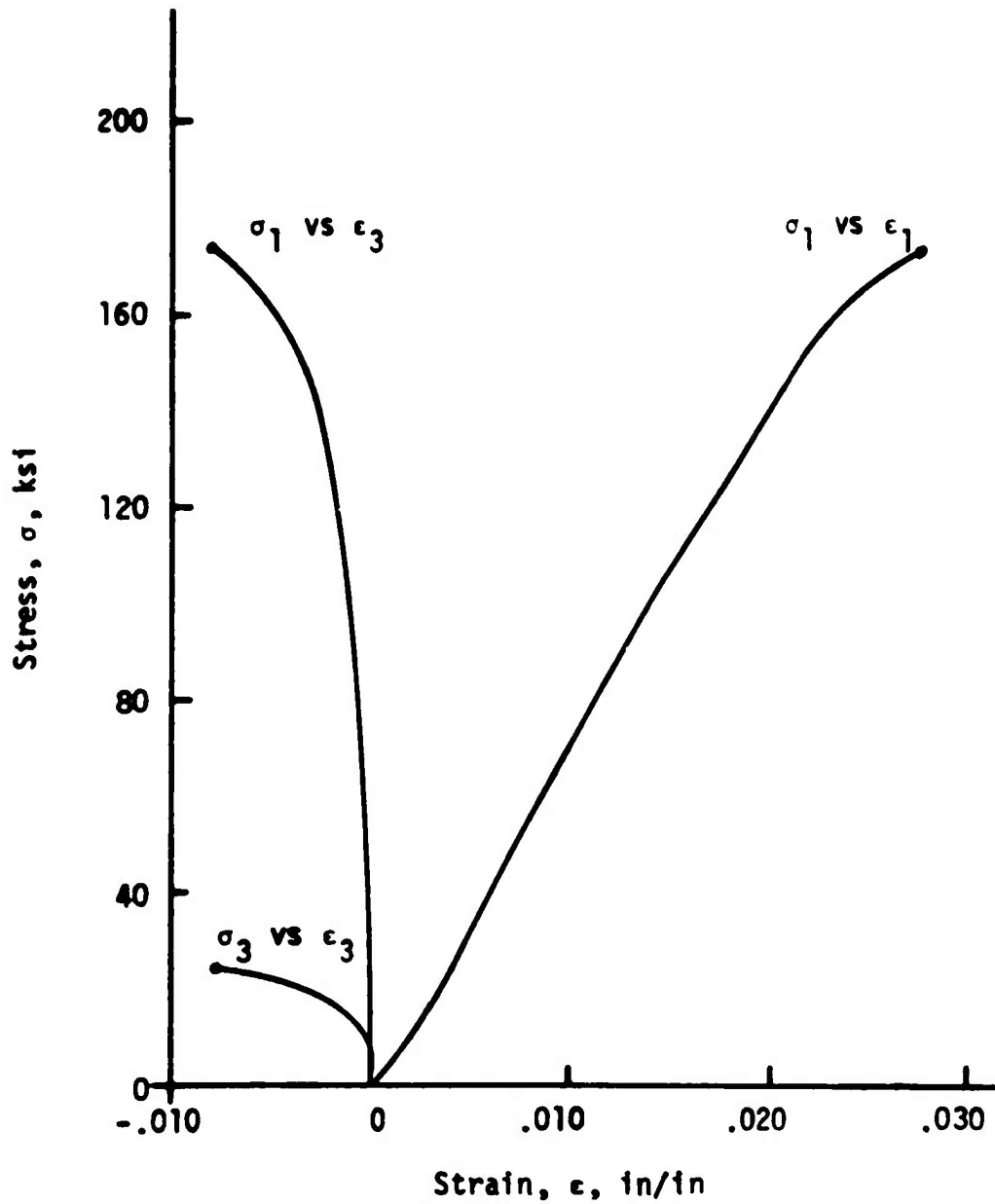


Figure 15. Principal stress-strain curves for Nugget sandstone specimen No. 34 in proportional loading, $\sigma_3/\sigma_1 = 0.142$

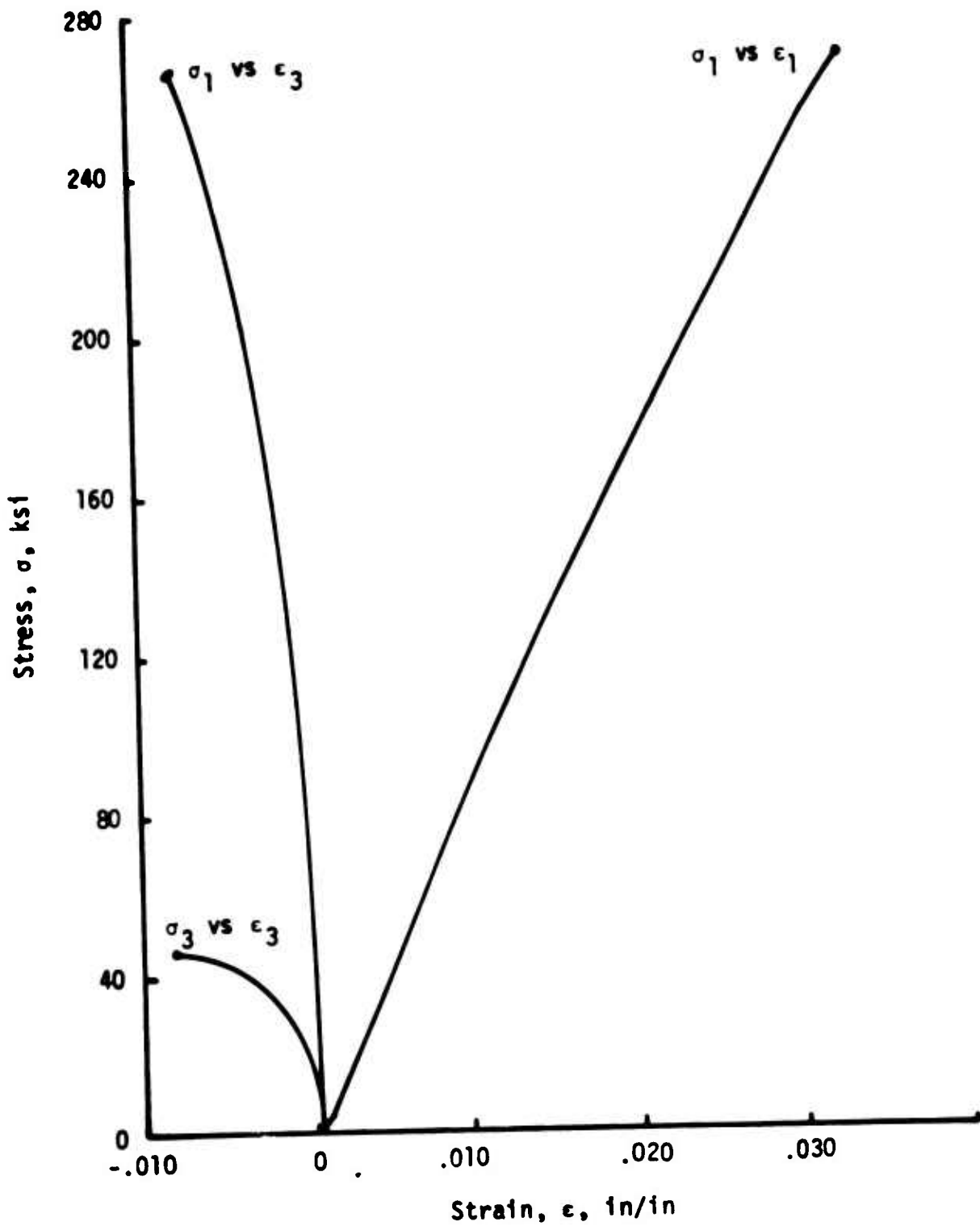


Figure 16. Principal stress-strain curves for Nugget sandstone specimen No. 9 in proportional loading, $\sigma_3/\sigma_1 = 0.177$

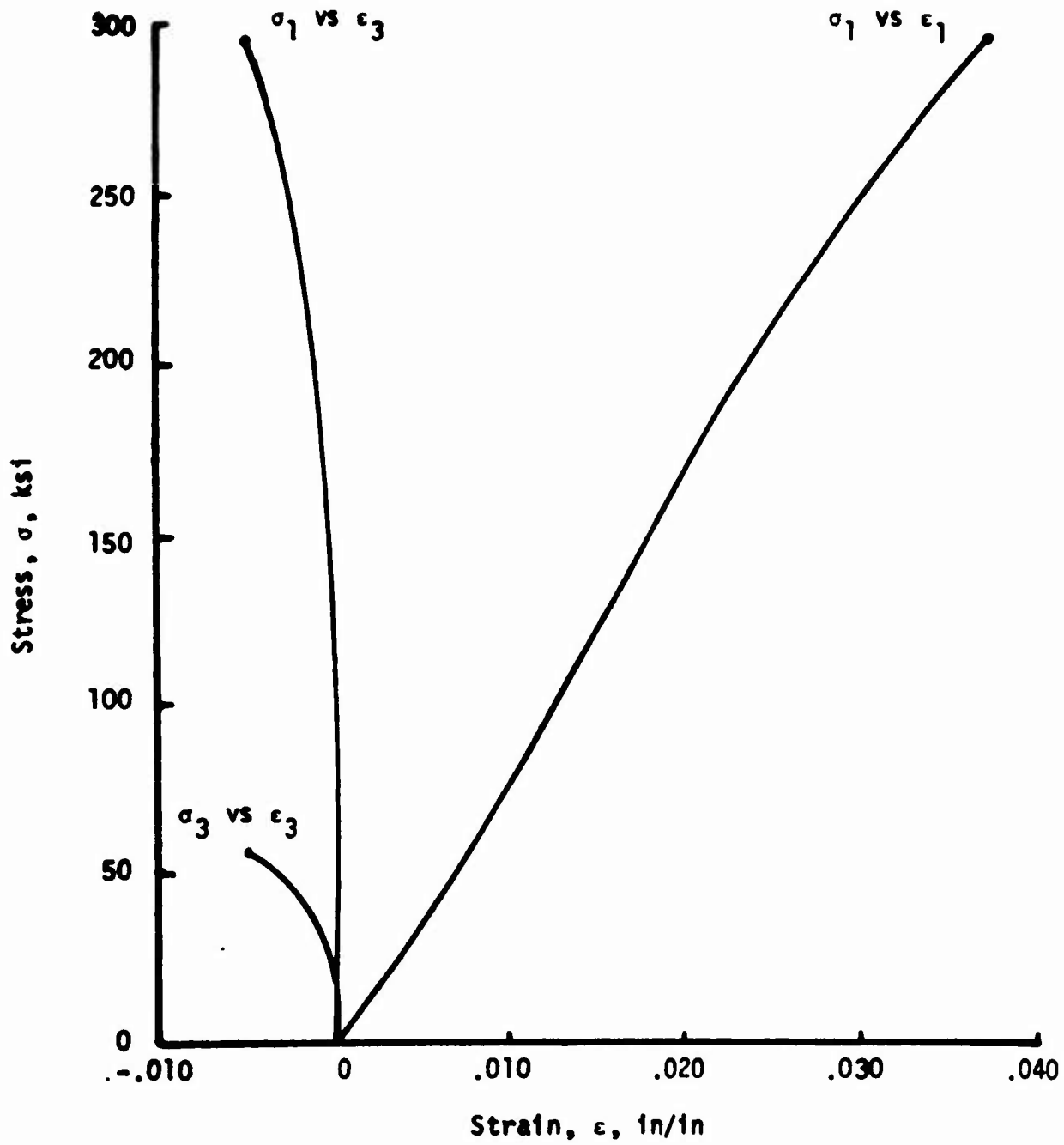


Figure 17. Principal stress-strain curves for Nugget sandstone specimen No. 40 in proportional loading, $\sigma_3/\sigma_1 = 0.190$

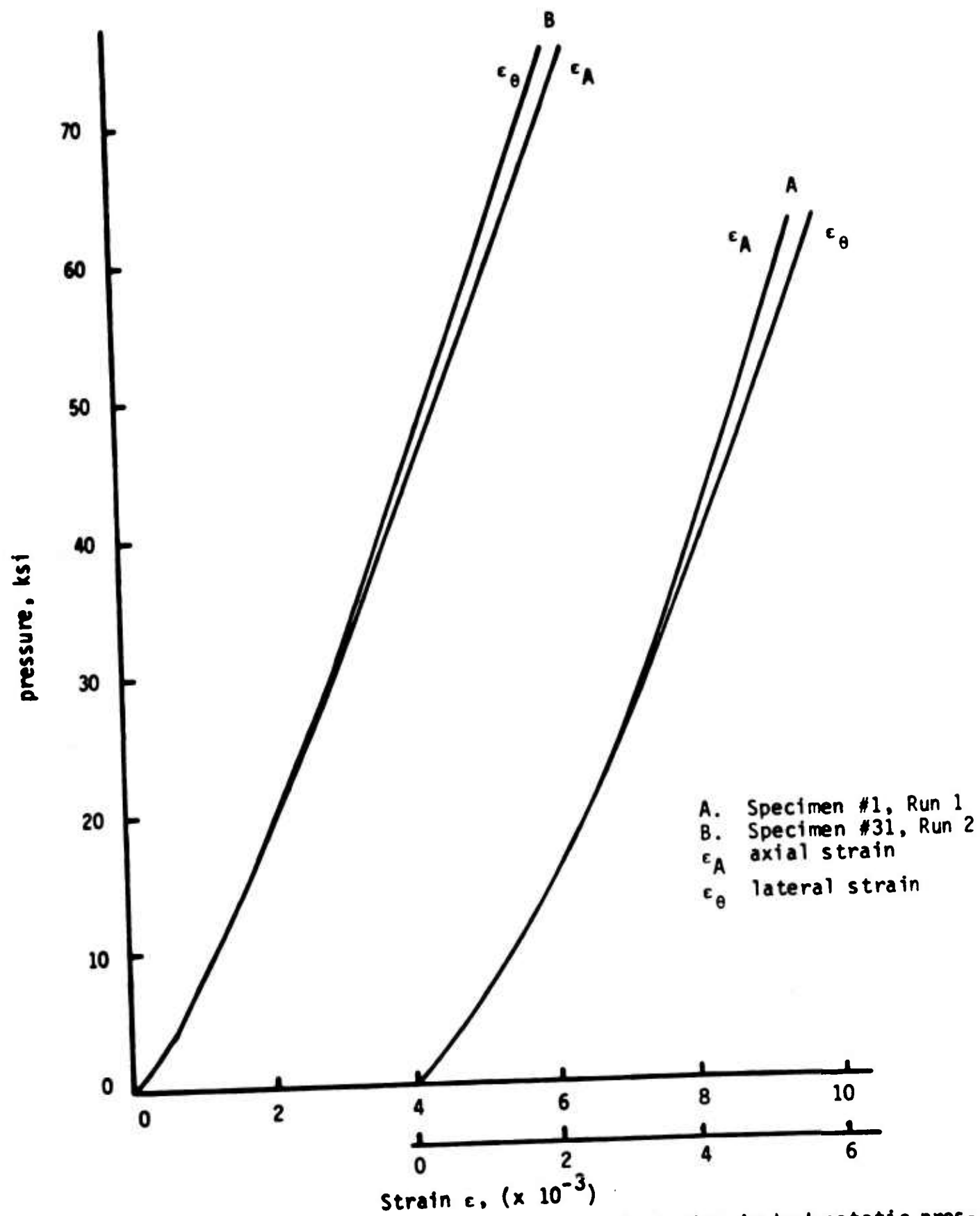


FIGURE 18. Comparison of axial and lateral strains in hydrostatic pressure loading of Nugget sandstone

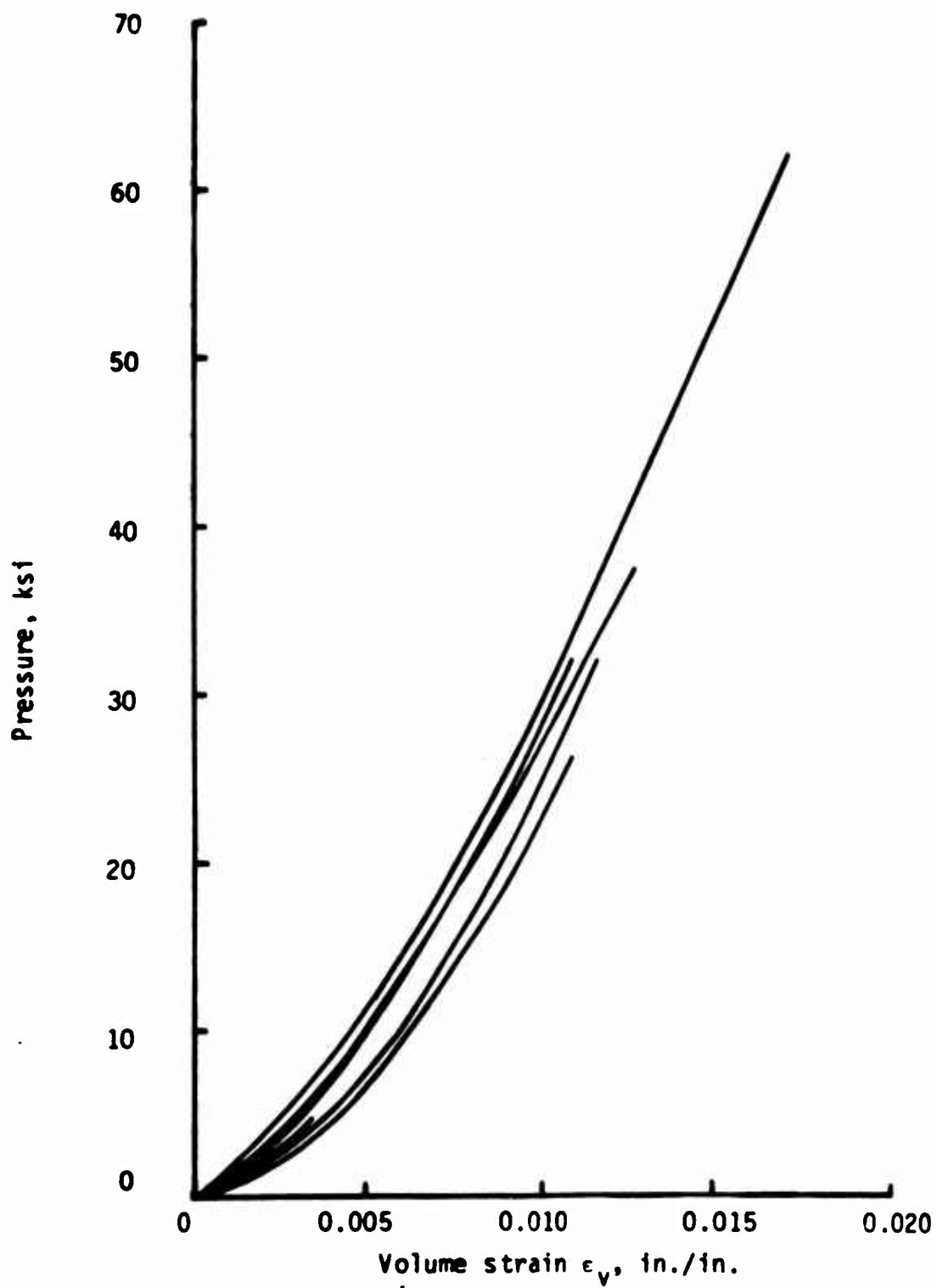


FIGURE 19. Pressure-volume strain curves in hydrostatic pressure loading of five Nugget sandstone specimens

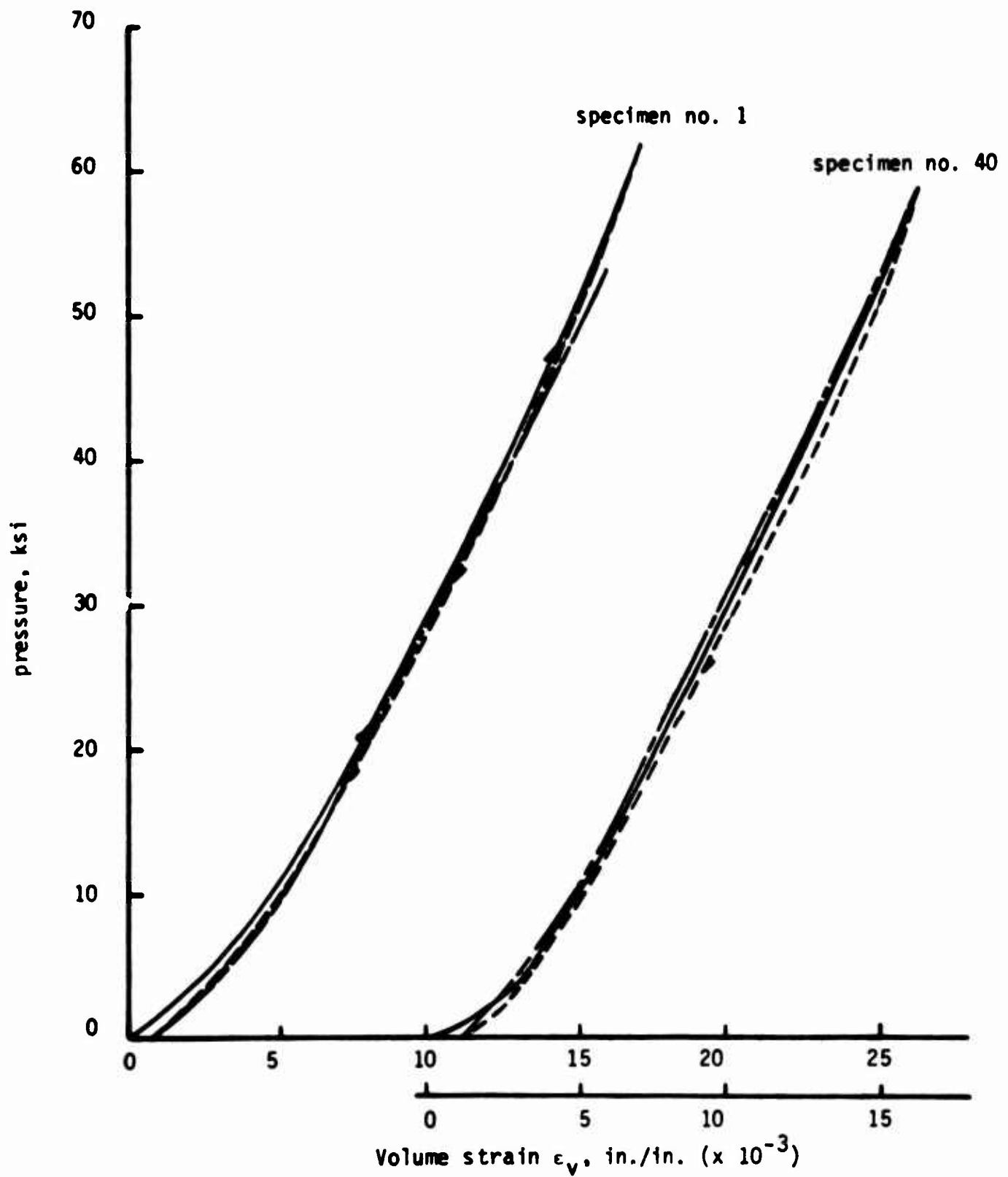


FIGURE 20. Hysteresis in Nugget sandstone under hydrostatic compression loading

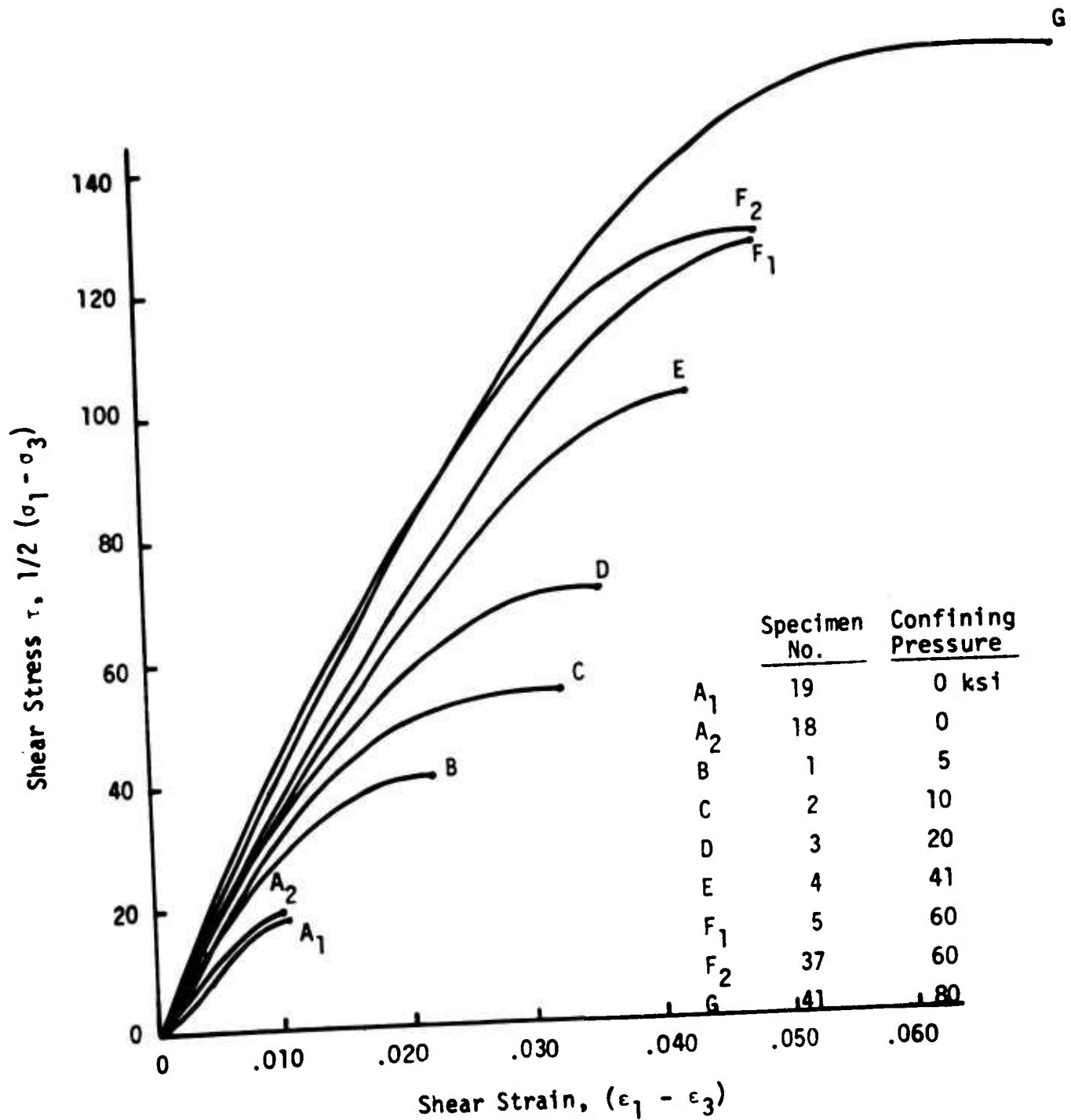


Figure 21. Shear stress-strain curves of Nugget sandstone in constant confining pressure tests

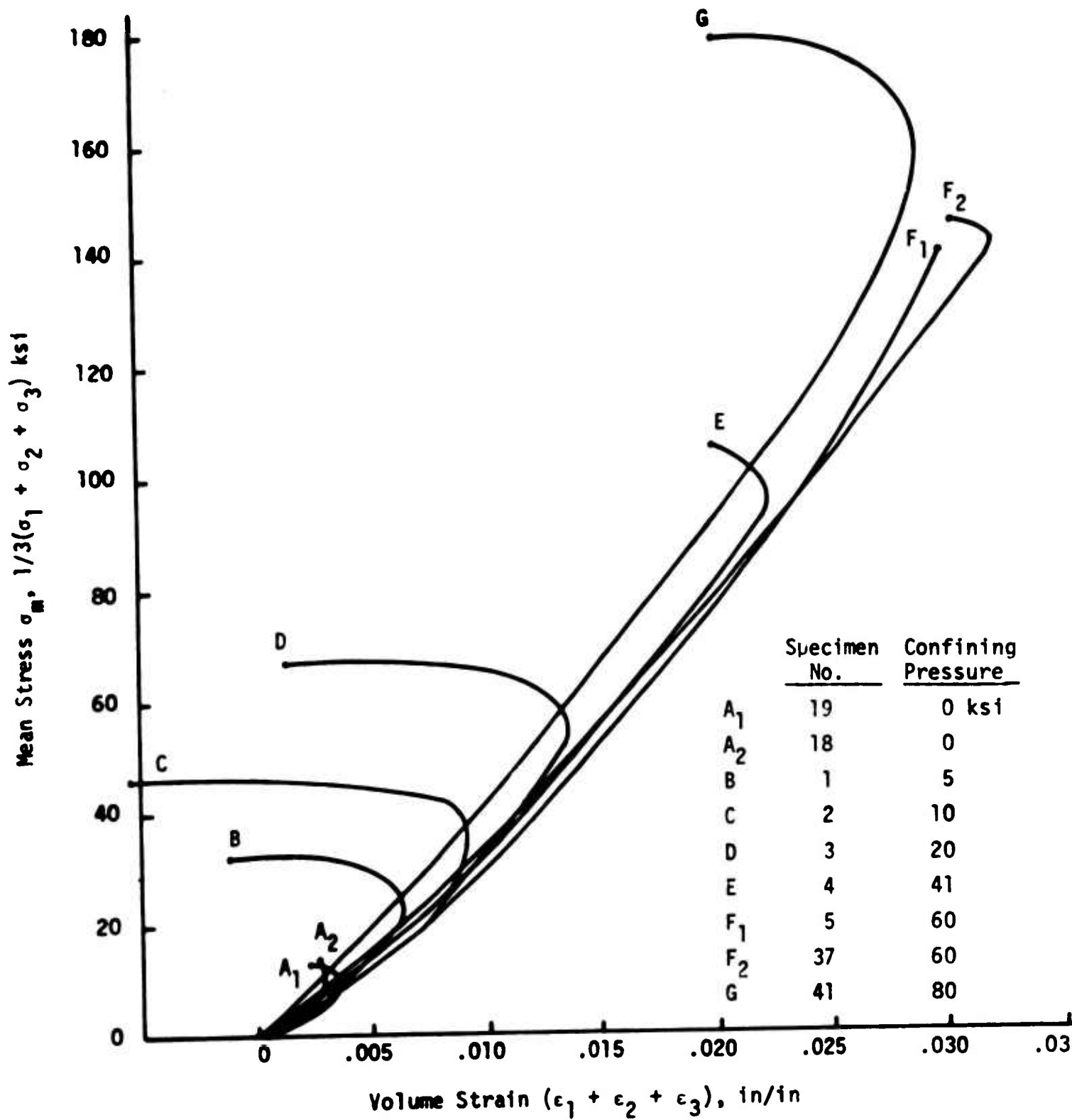


Figure 22. Dilatation stress-strain curves for Nugget sandstone in constant confining pressure tests

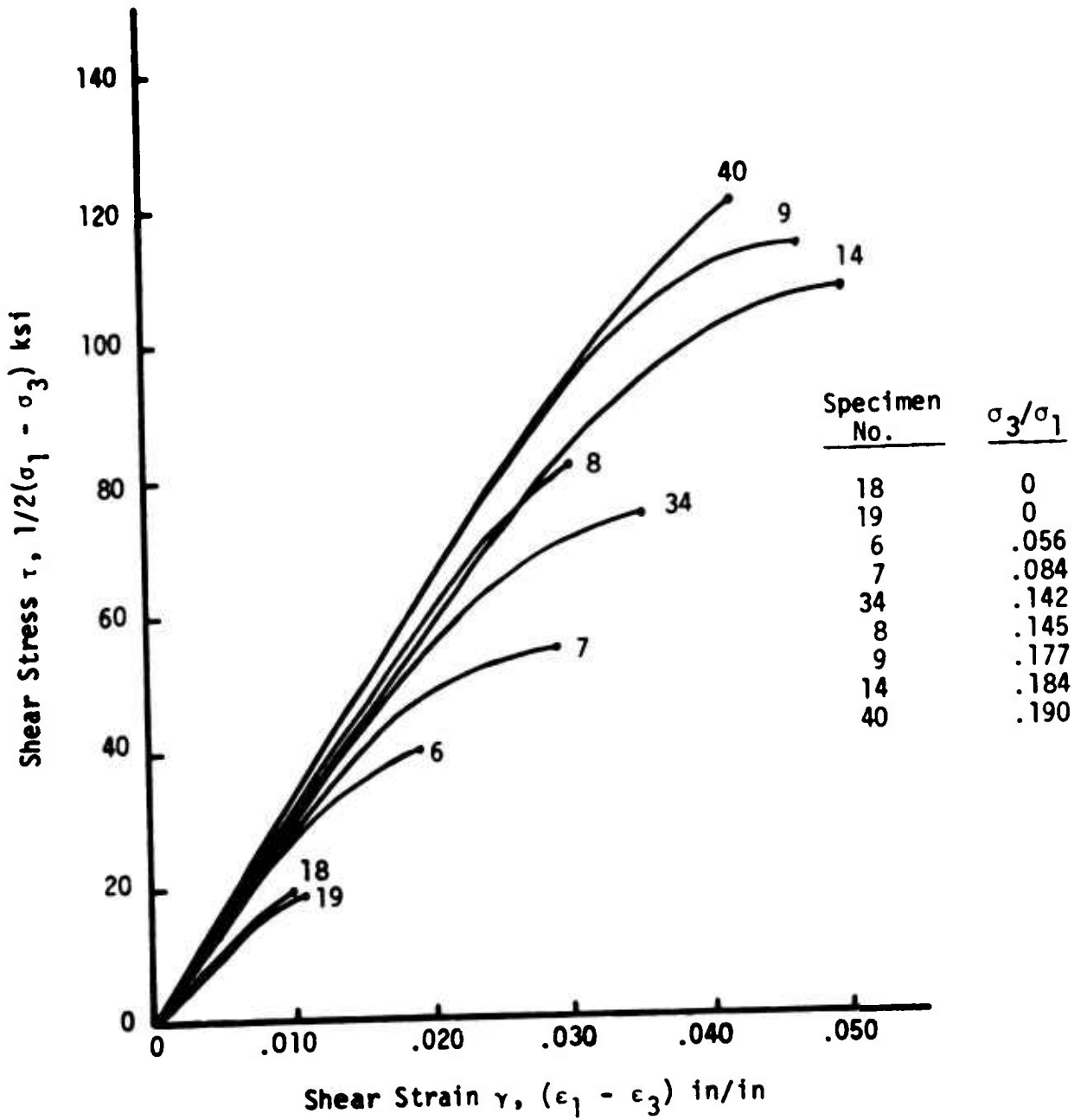


Figure 23. Shear stress-strain curves of Nugget sandstone in proportional loading tests

THIS REPORT HAS BEEN DELIMITED
AND CLEARED FOR PUBLIC RELEASE
UNDER DOD DIRECTIVE 5200.20 AND
NO RESTRICTIONS ARE IMPOSED UPON
ITS USE AND DISCLOSURE.

DISTRIBUTION STATEMENT A

APPROVED FOR PUBLIC RELEASE,
DISTRIBUTION UNLIMITED.

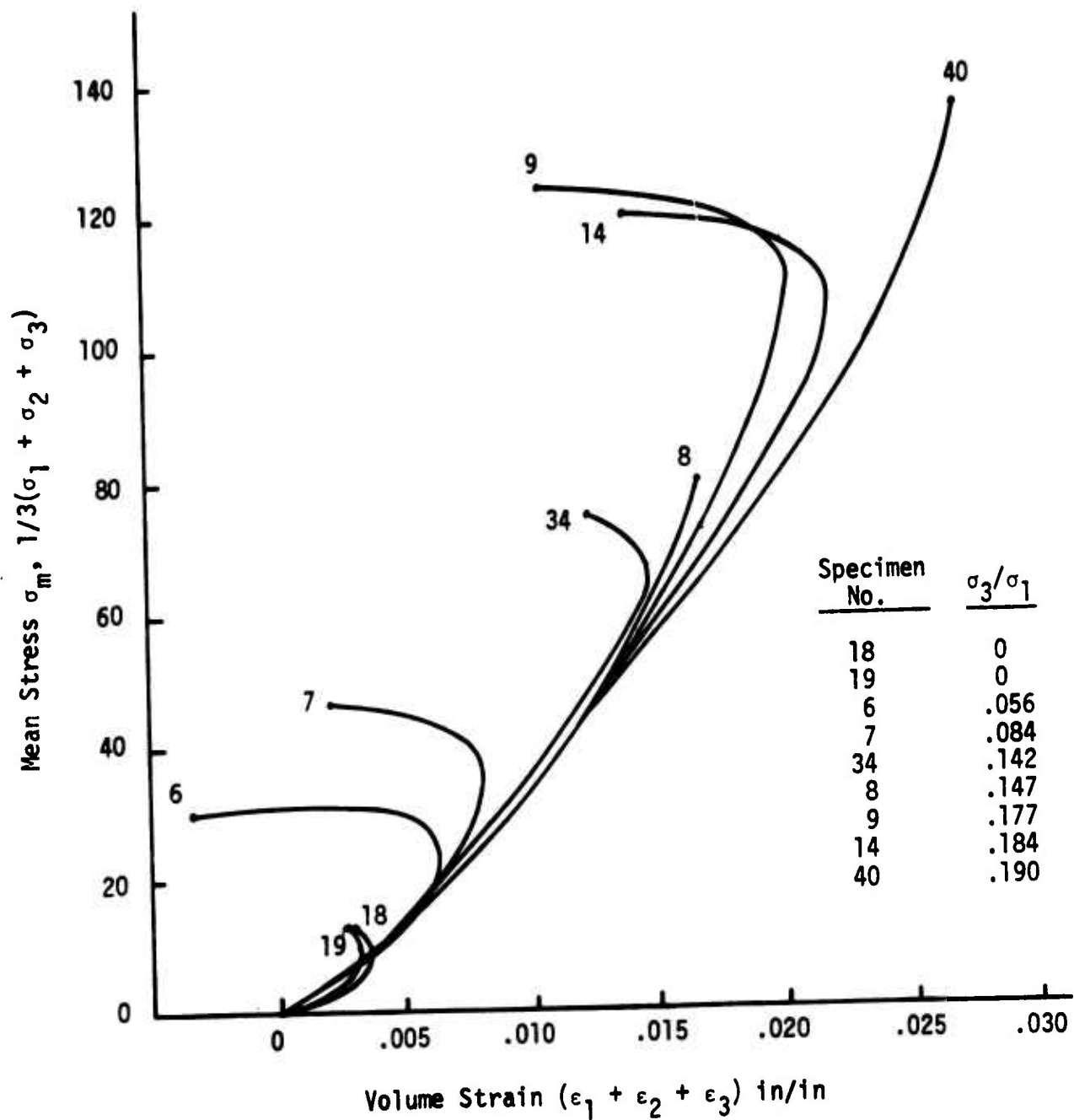


Figure 24. Dilatation stress-strain curves of Nugget sandstone in proportional loading tests

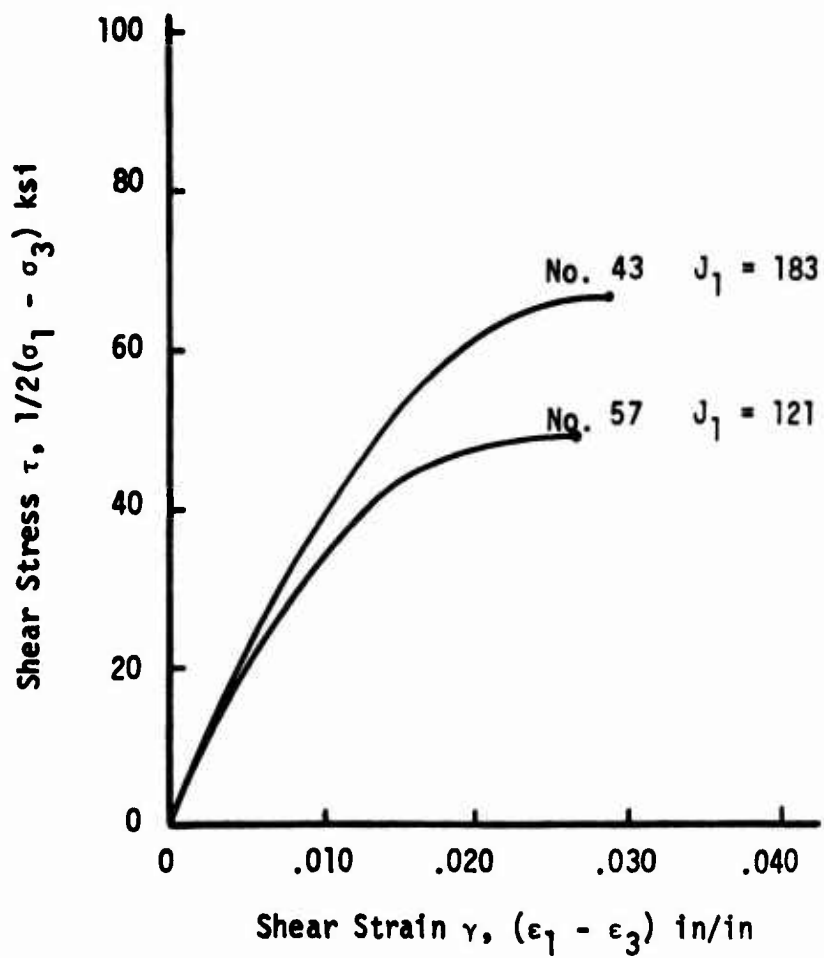


Figure 25. Shear stress-strain curves for Nugget sandstone in constant J_1 tests

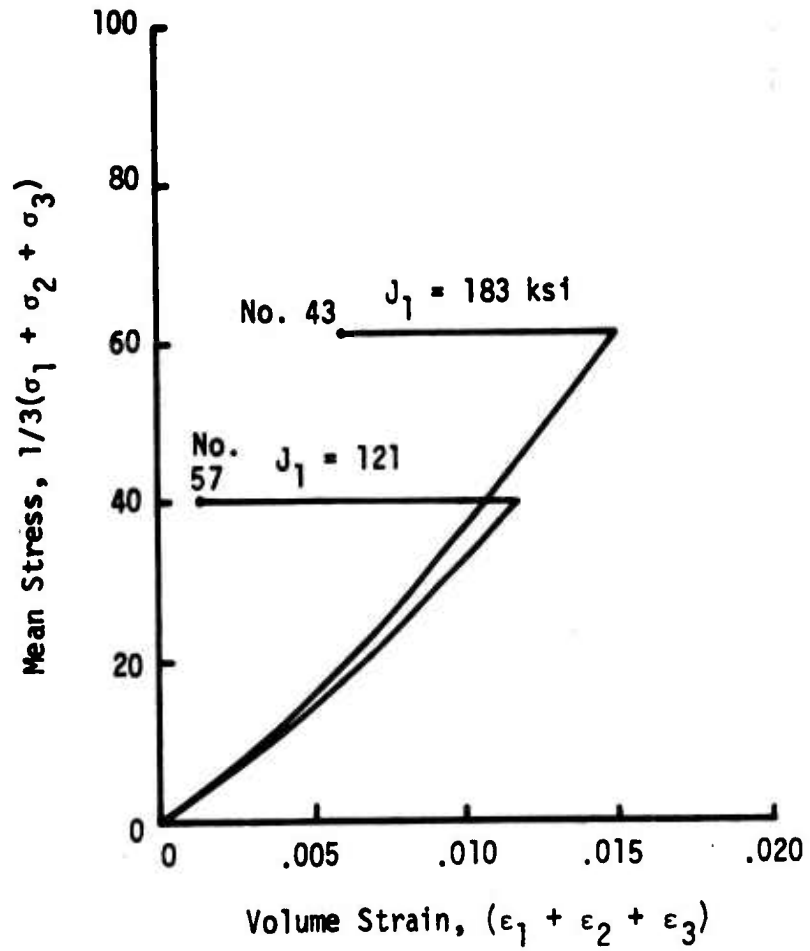


Figure 26. Dilatation stress-strain curves of Nugget sandstone in constant J_1 tests

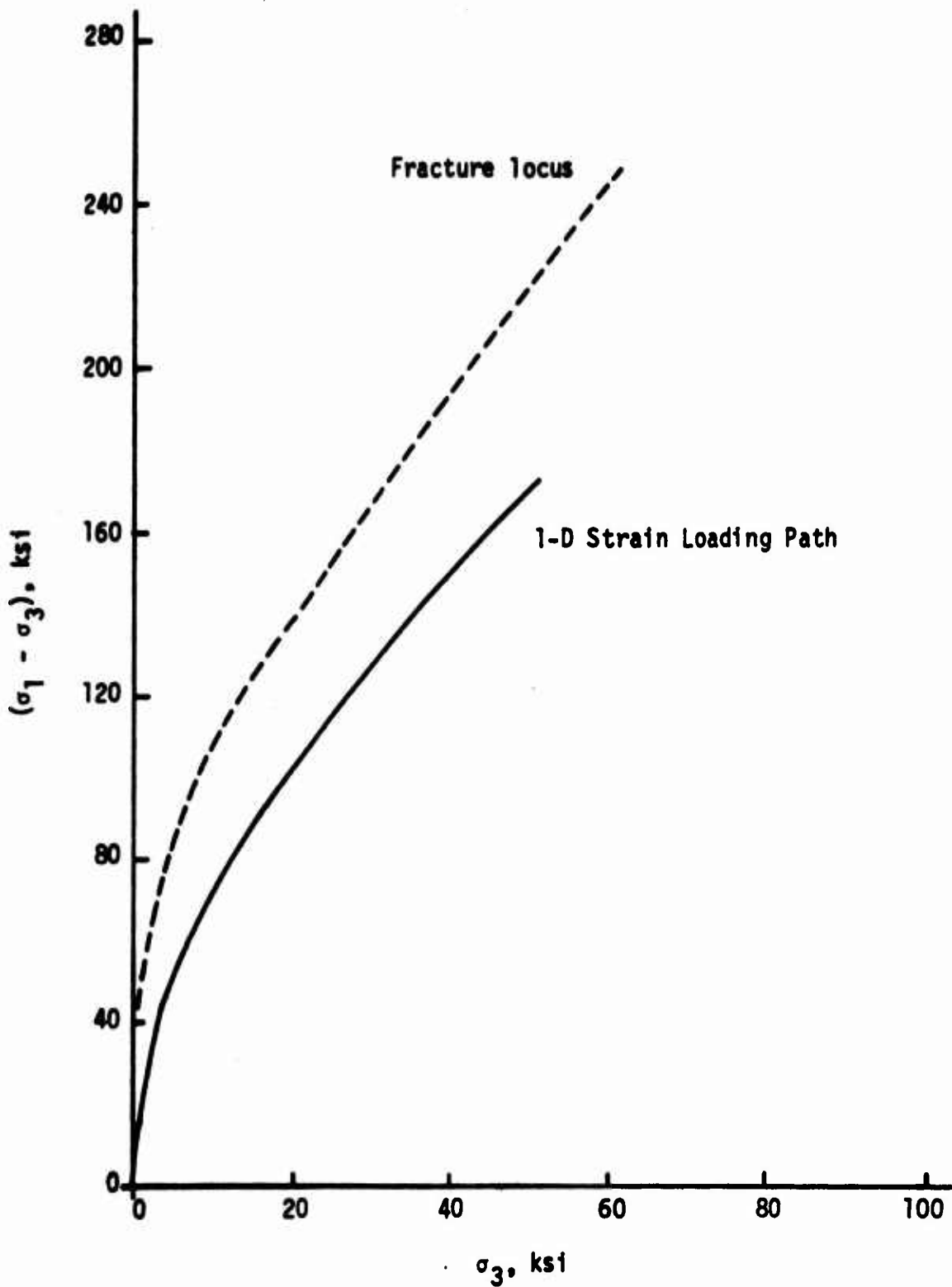


Figure 27. Loading path of one-dimensional strain test of Nugget sandstone specimen No. 42

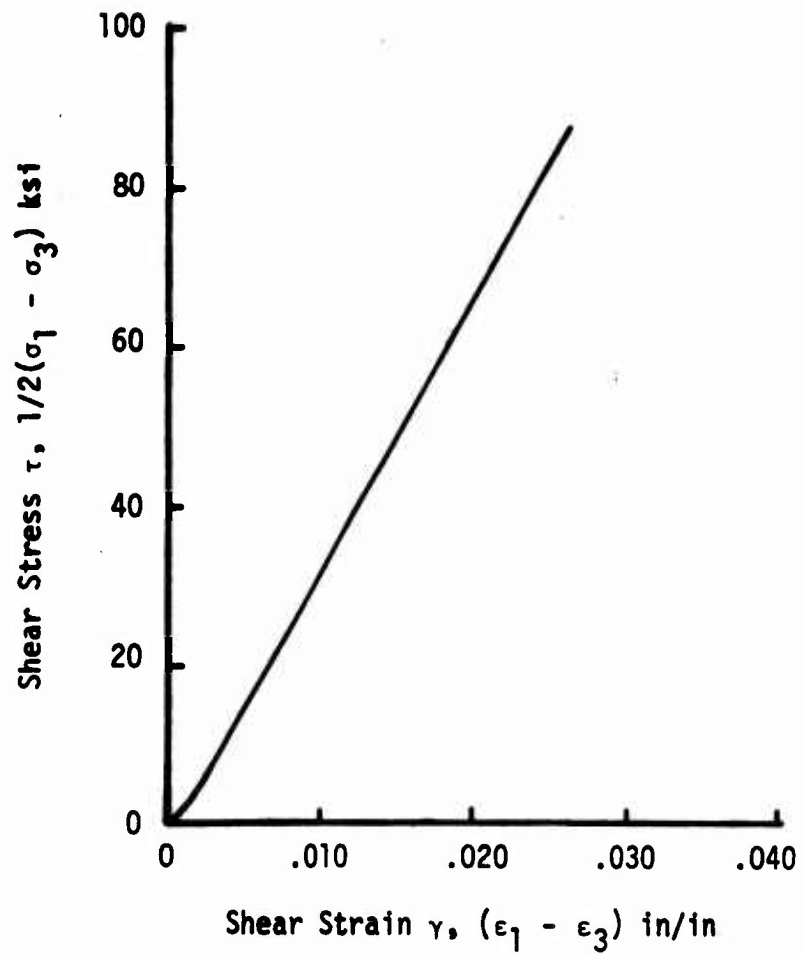


Figure 28. Shear stress-strain curves of Nugget sandstone specimen No. 42 in one-dimensional strain test

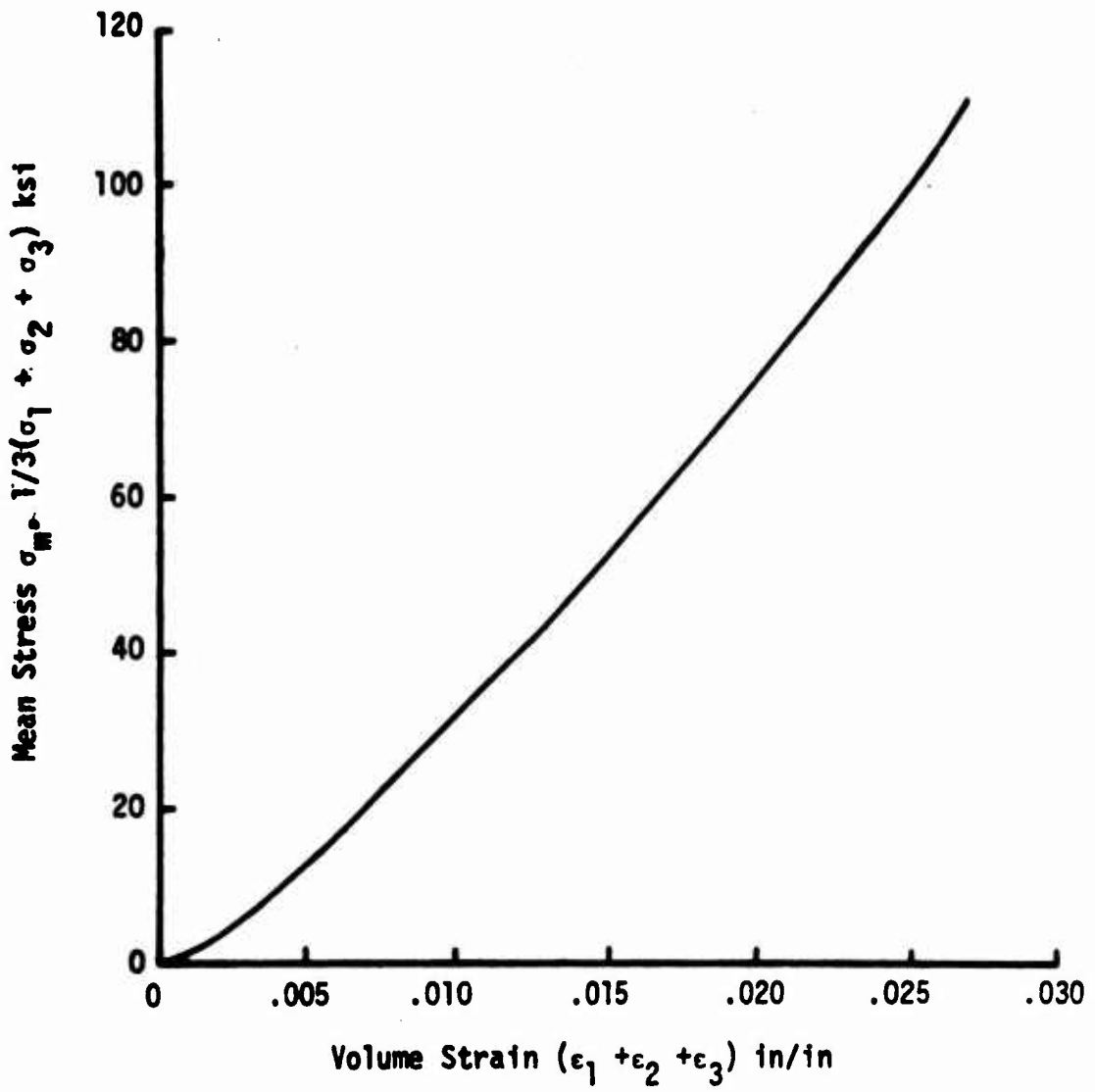


Figure 29. Dilatation stress-strain curve of Nugget sandstone specimen No. 42 in one-dimensional strain test

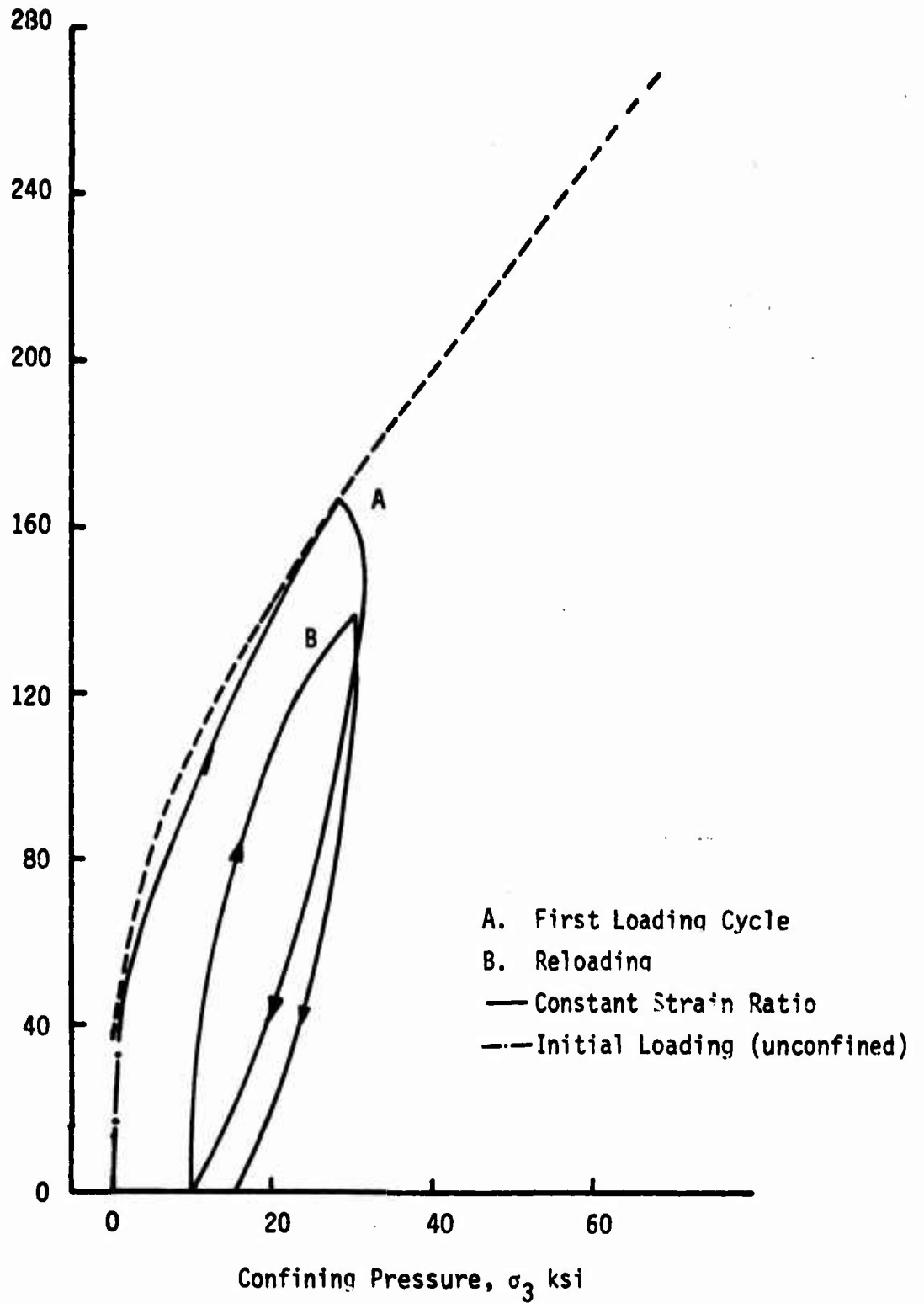


Figure 30. Loading path of Nugget sandstone specimen No. 31 under constant strain ratio loading $\epsilon_3/\epsilon_1 = -.249$

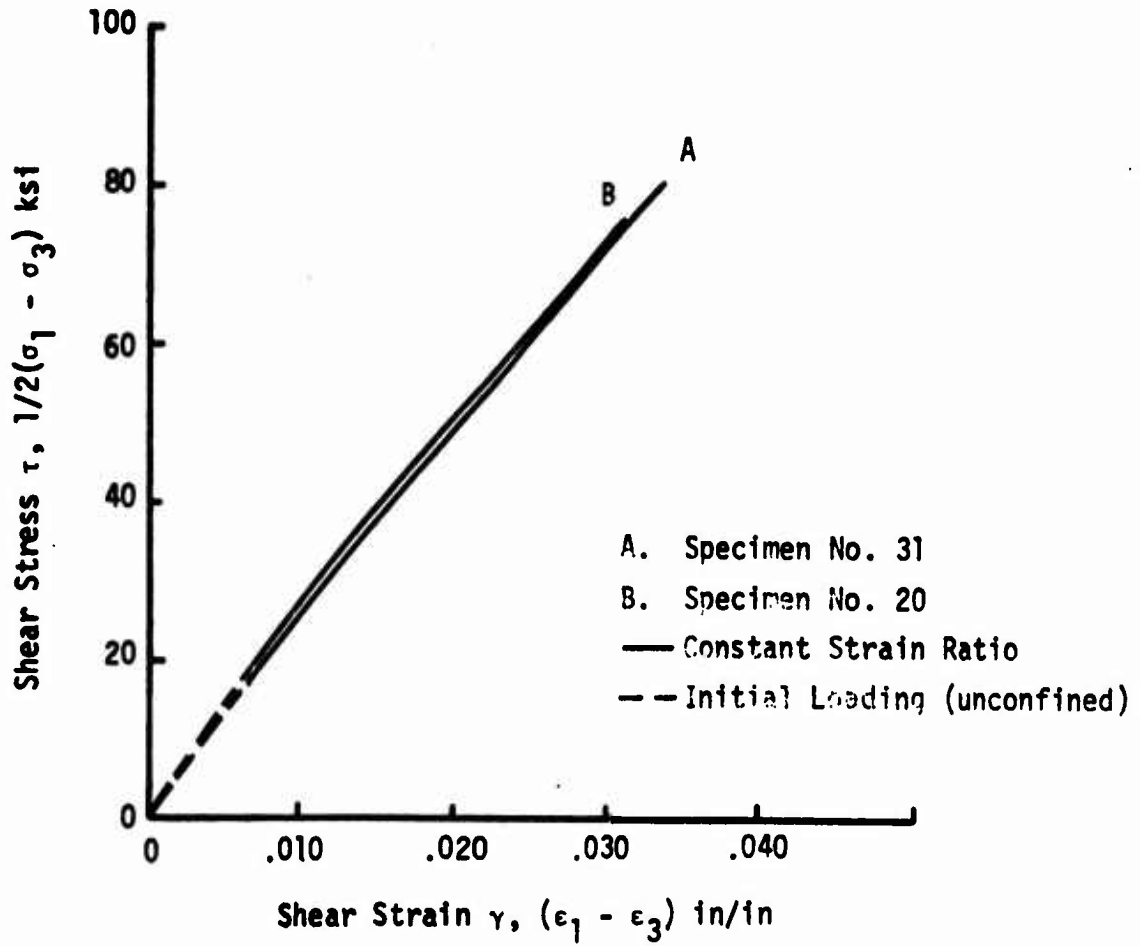


Figure 31. Shear stress-strain curves of Nugget sandstone in proportional strain, $\epsilon_3/\epsilon_1 = -0.249$

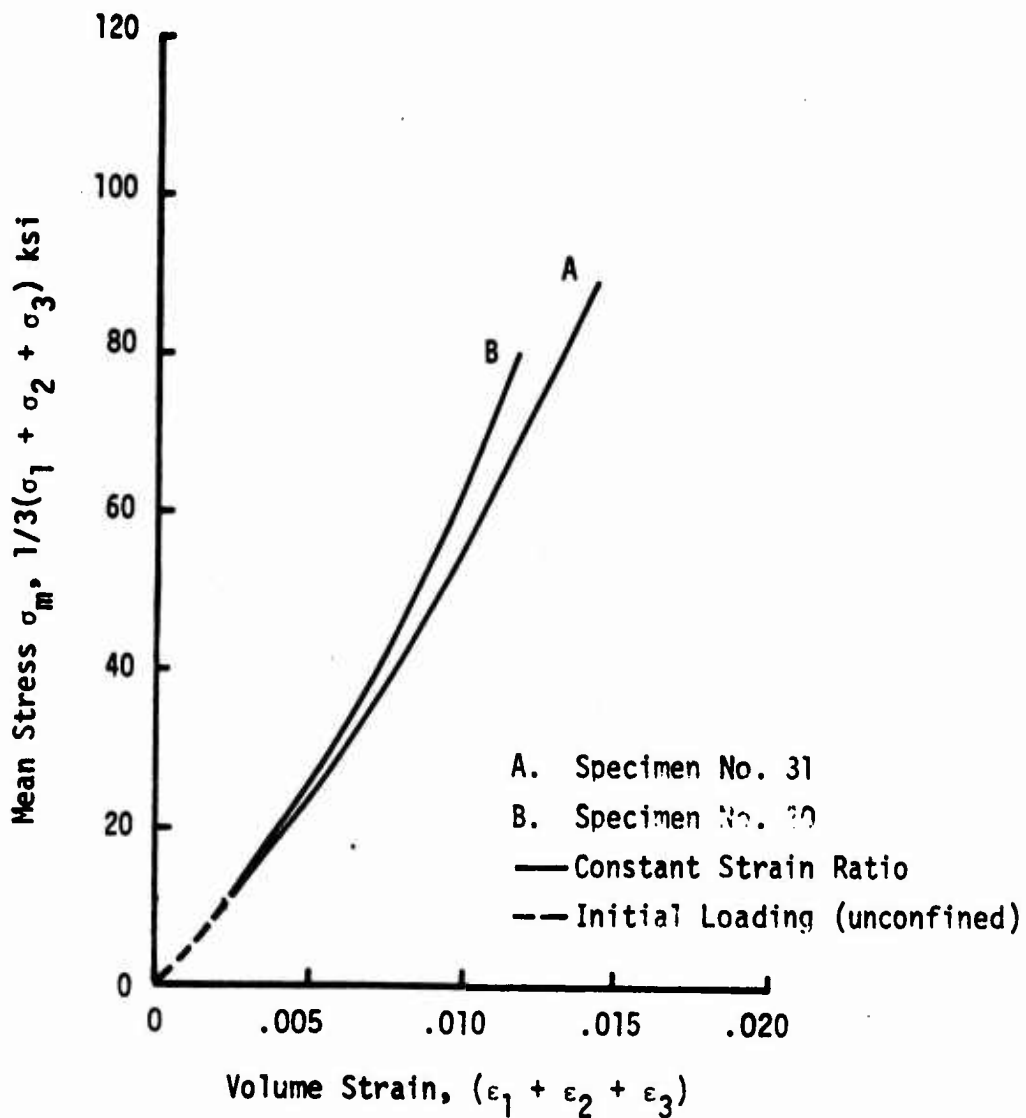


Figure 32. Dilatation stress-strain curves of Nugget sandstone in proportional strain, $\epsilon_3/\epsilon_1 = -0.249$

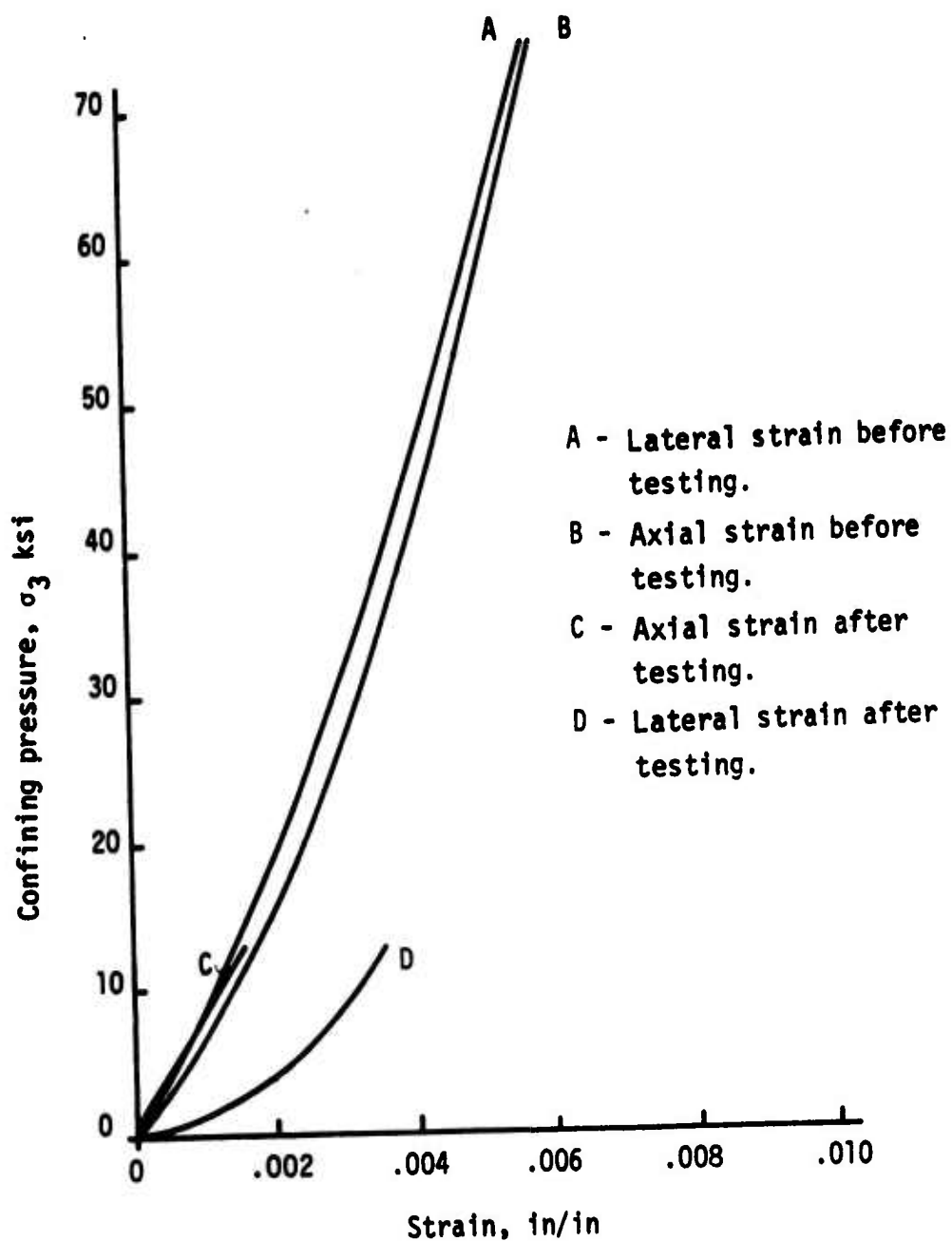


Figure 33. Stress-strain curves in hydrostatic pressure loading of Nugget sandstone specimen No. 31, before and after proportional strain test.

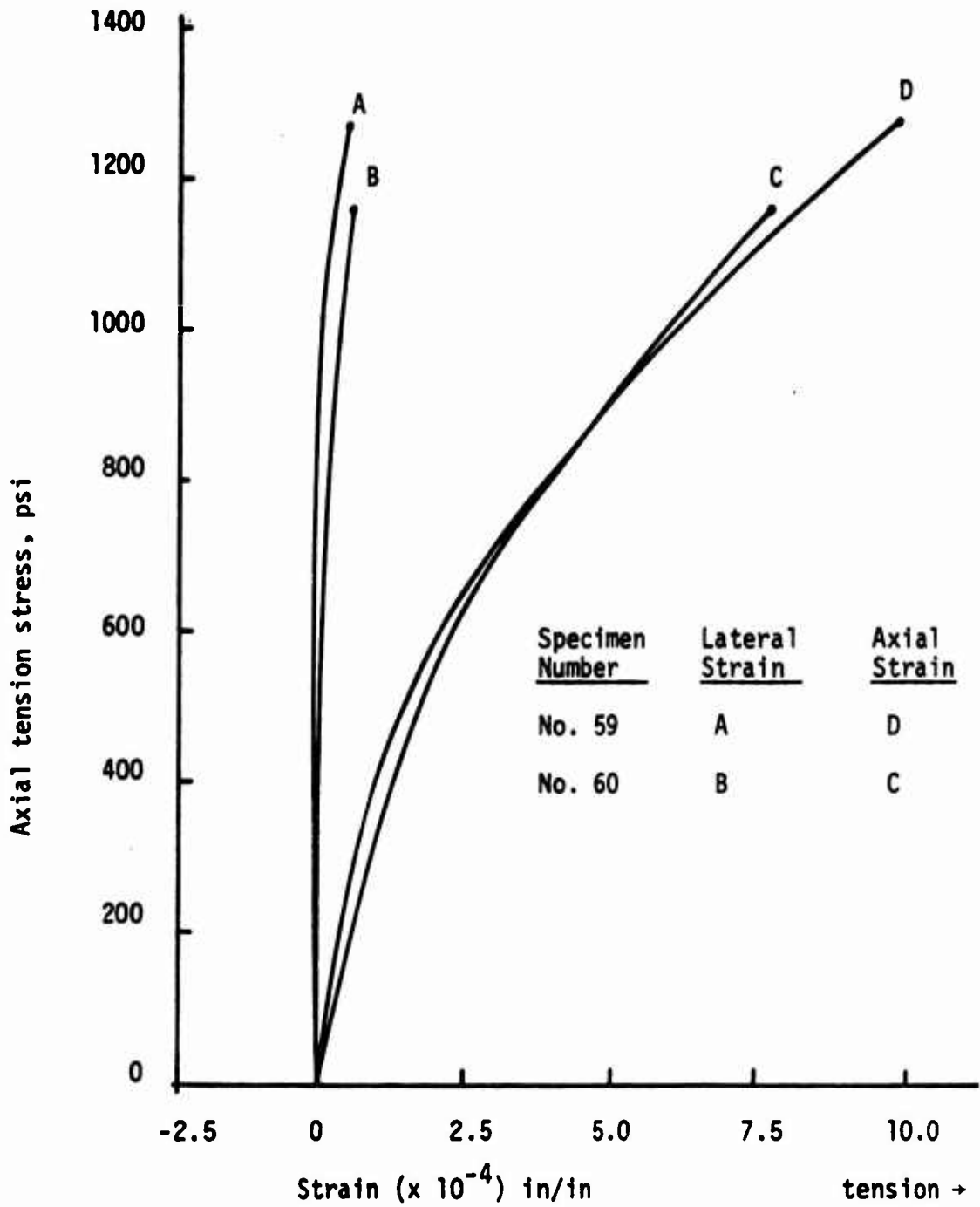


Figure 34. Principal stress-strain curve for tension test of Nugget sandstone specimens.

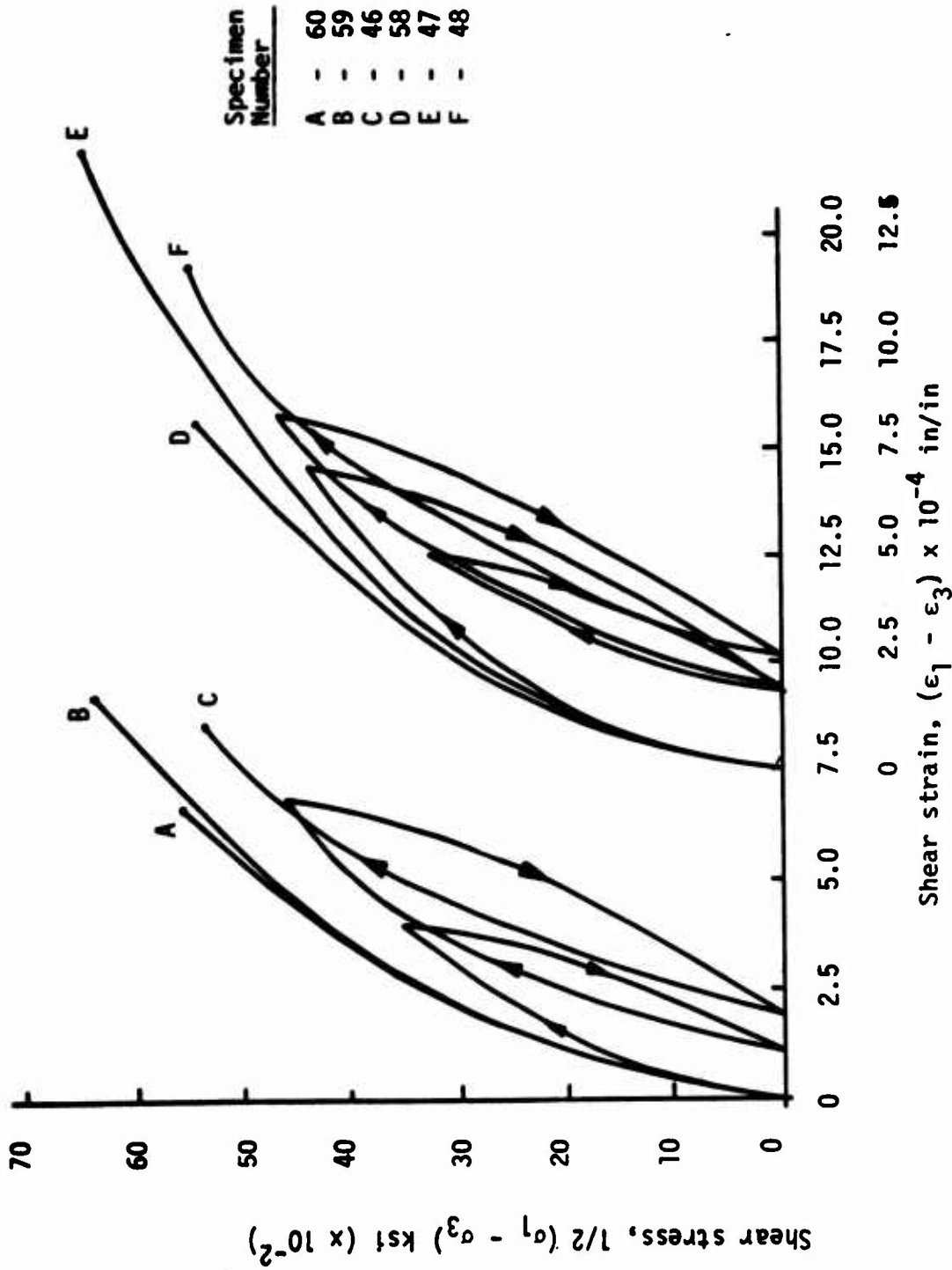


Figure 35. Shear stress-strain curves in unconfined tension tests of Nugget sandstone.

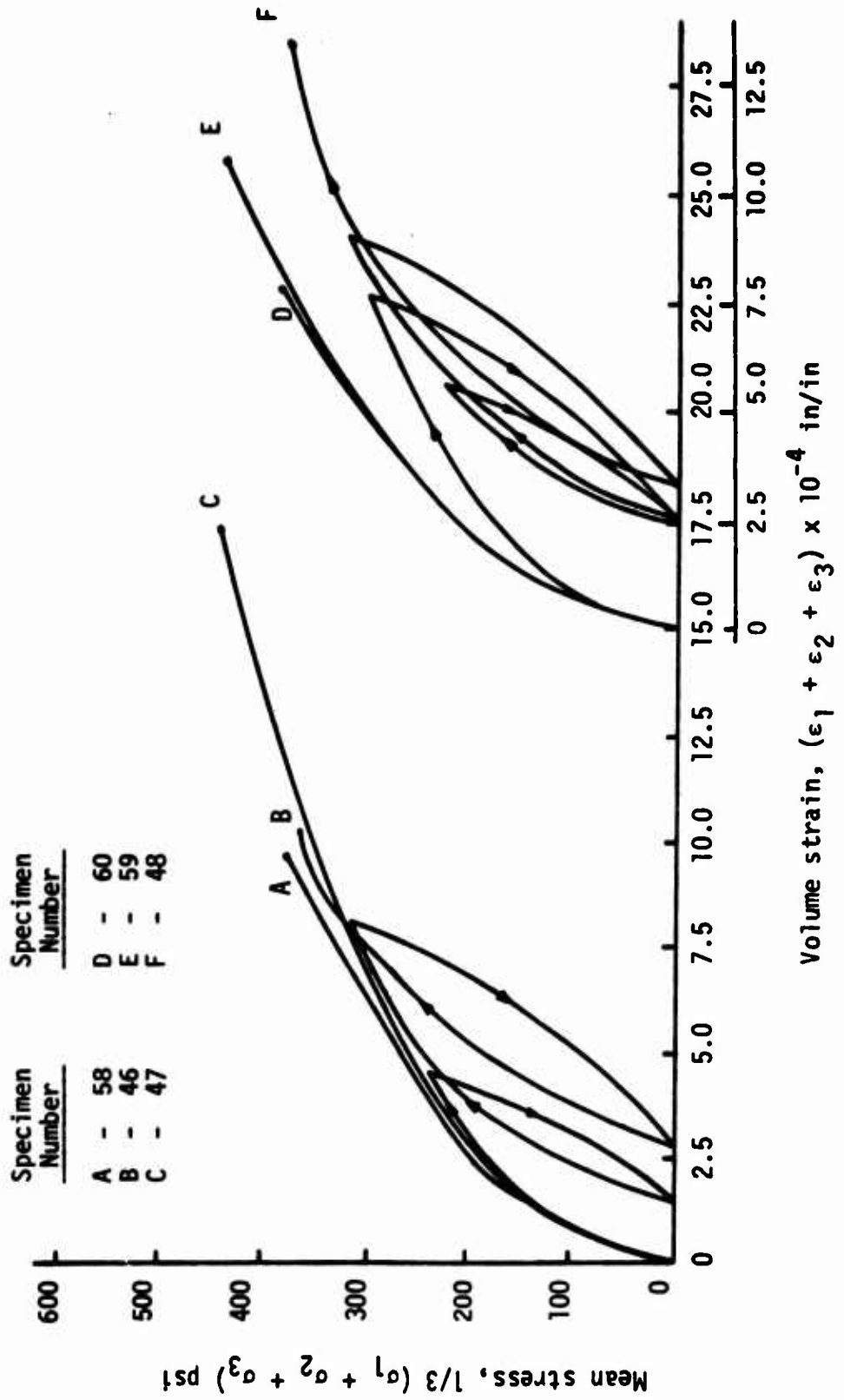


Figure 36. Dilatation stress-strain curves in unconfined tension tests of Nugget sandstone.

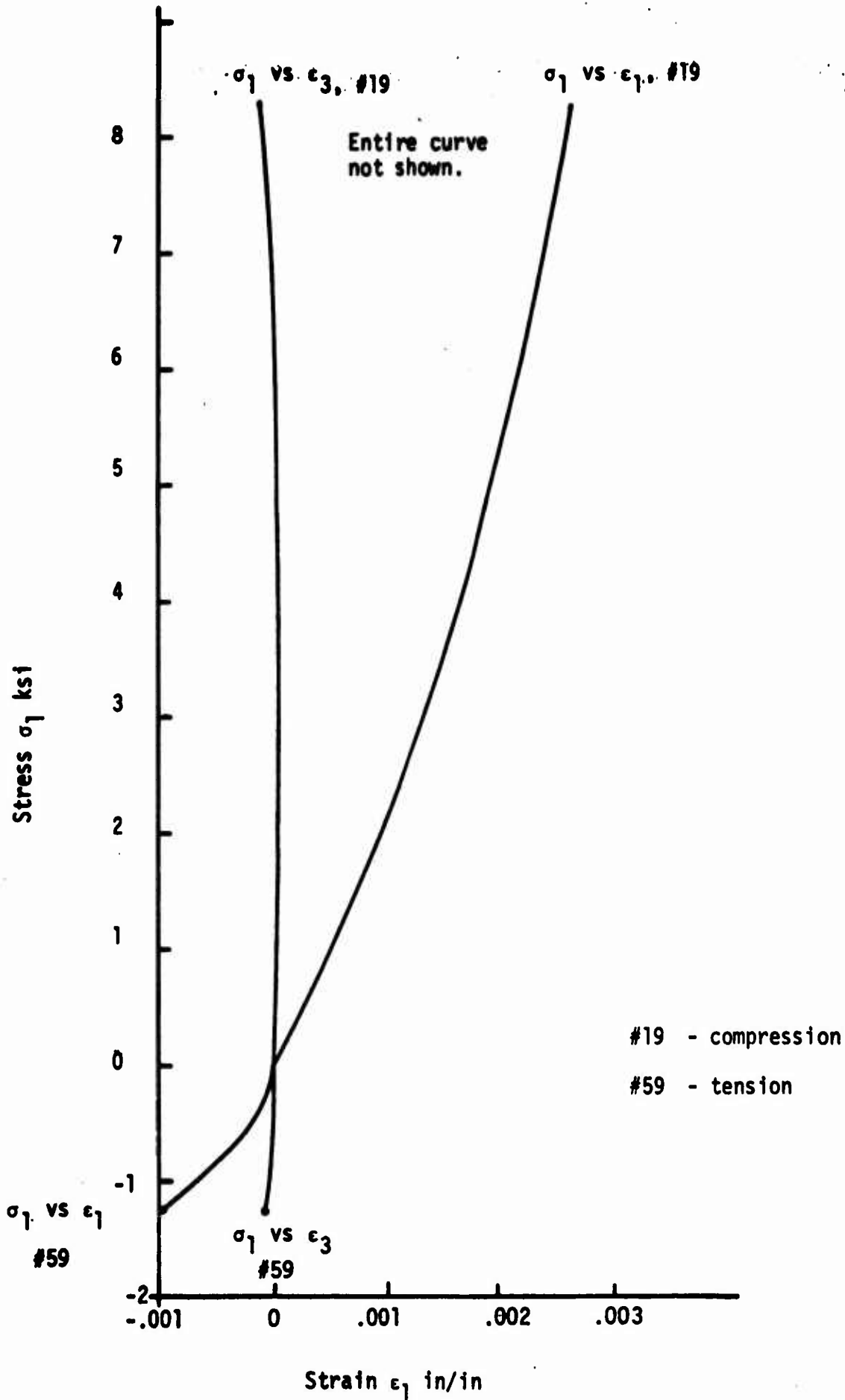


Figure 37. Comparison of principal stress-strain curves of Nugget sandstone in unconfined tension and compression.

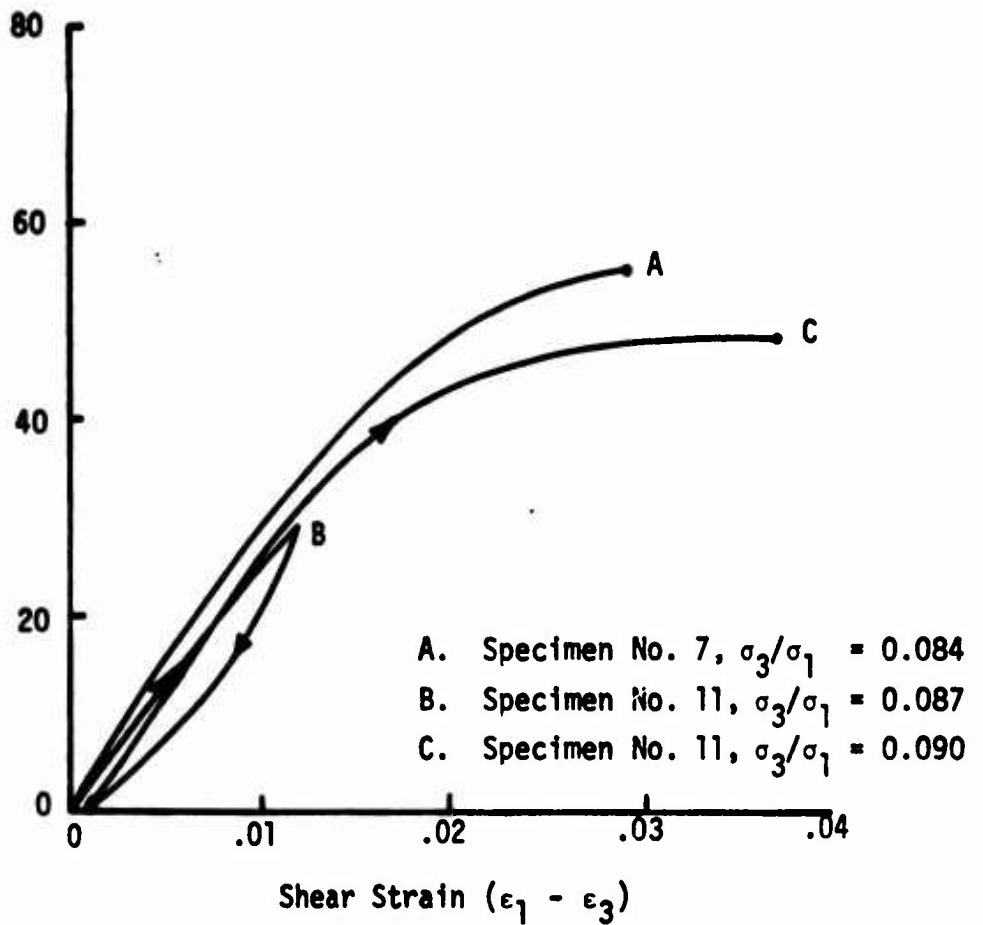


Figure 38. Shear stress-strain curves for constant stress ratio tests of Nugget sandstone specimen No. 11 (cycled) and specimen No. 7

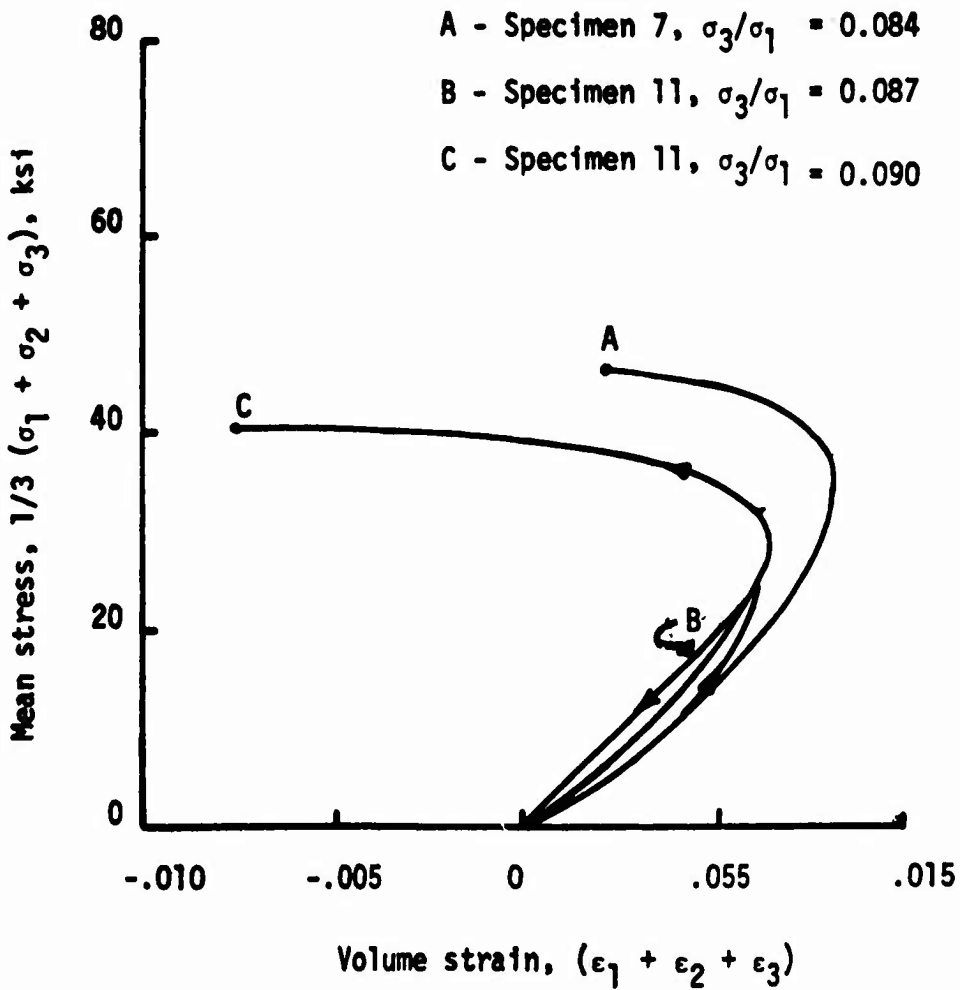


Figure 39. Dilatation stress-strain curves for constant stress ratio tests of Nugget sandstone specimen No. 11 (cycled) and specimen No. 7.

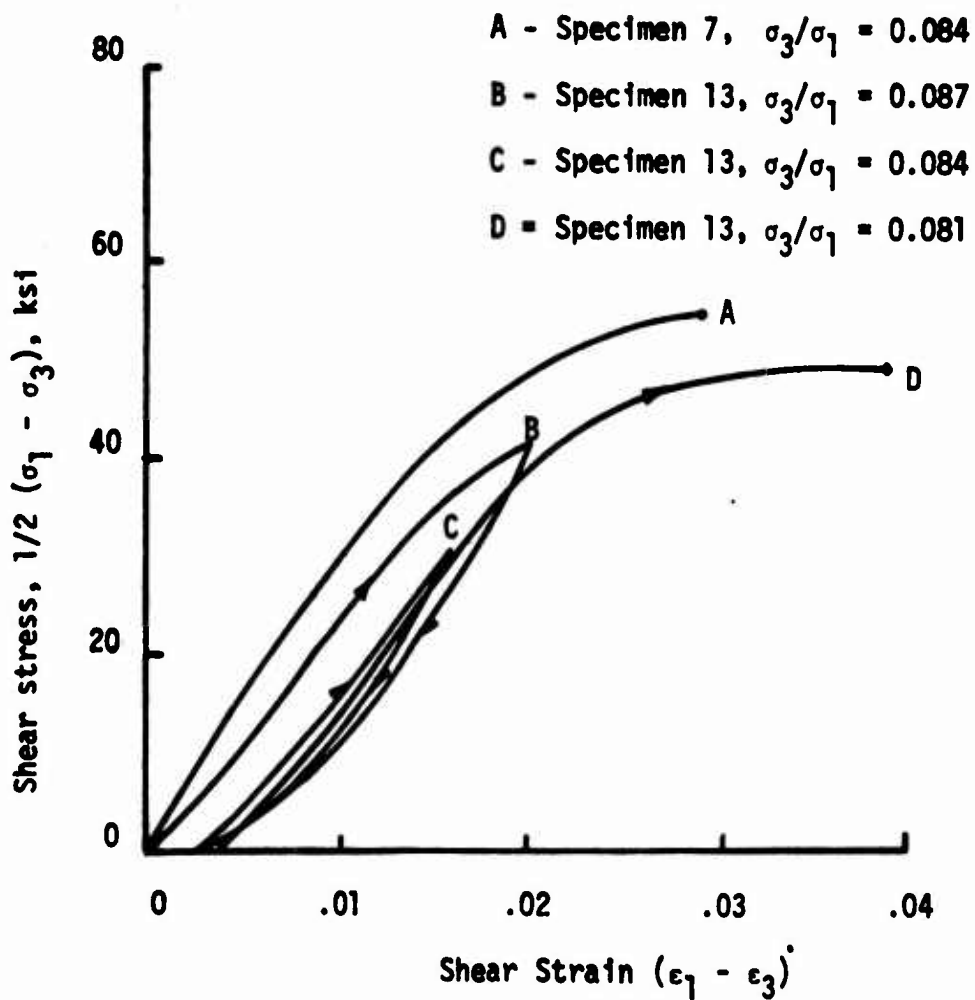


Figure 40. Shear stress-strain curves for constant stress ratio tests of Nugget sandstone specimen No. 13 (cycled) and specimen No. 7.

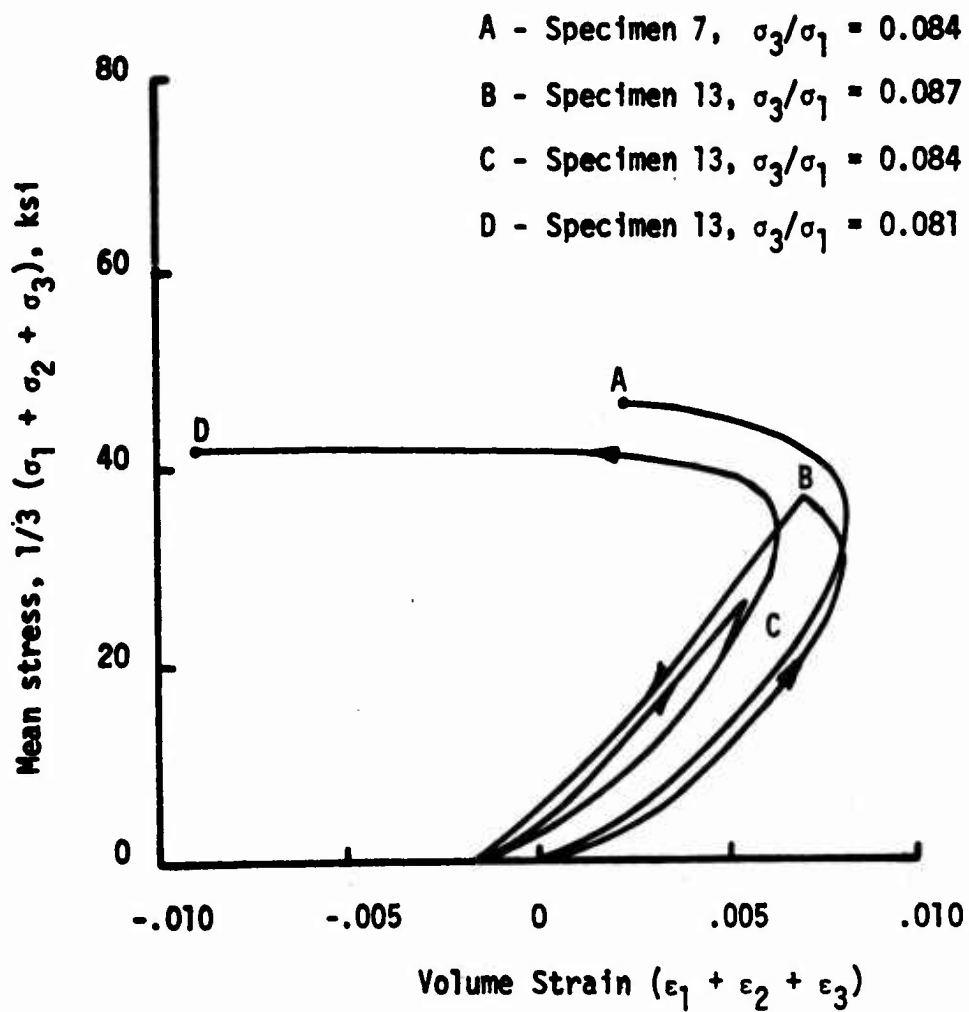


Figure 41. Dilatation stress-strain curves for constant stress ratio test of Nugget sandstone specimen No. 13 (cycled) and specimen No. 7.

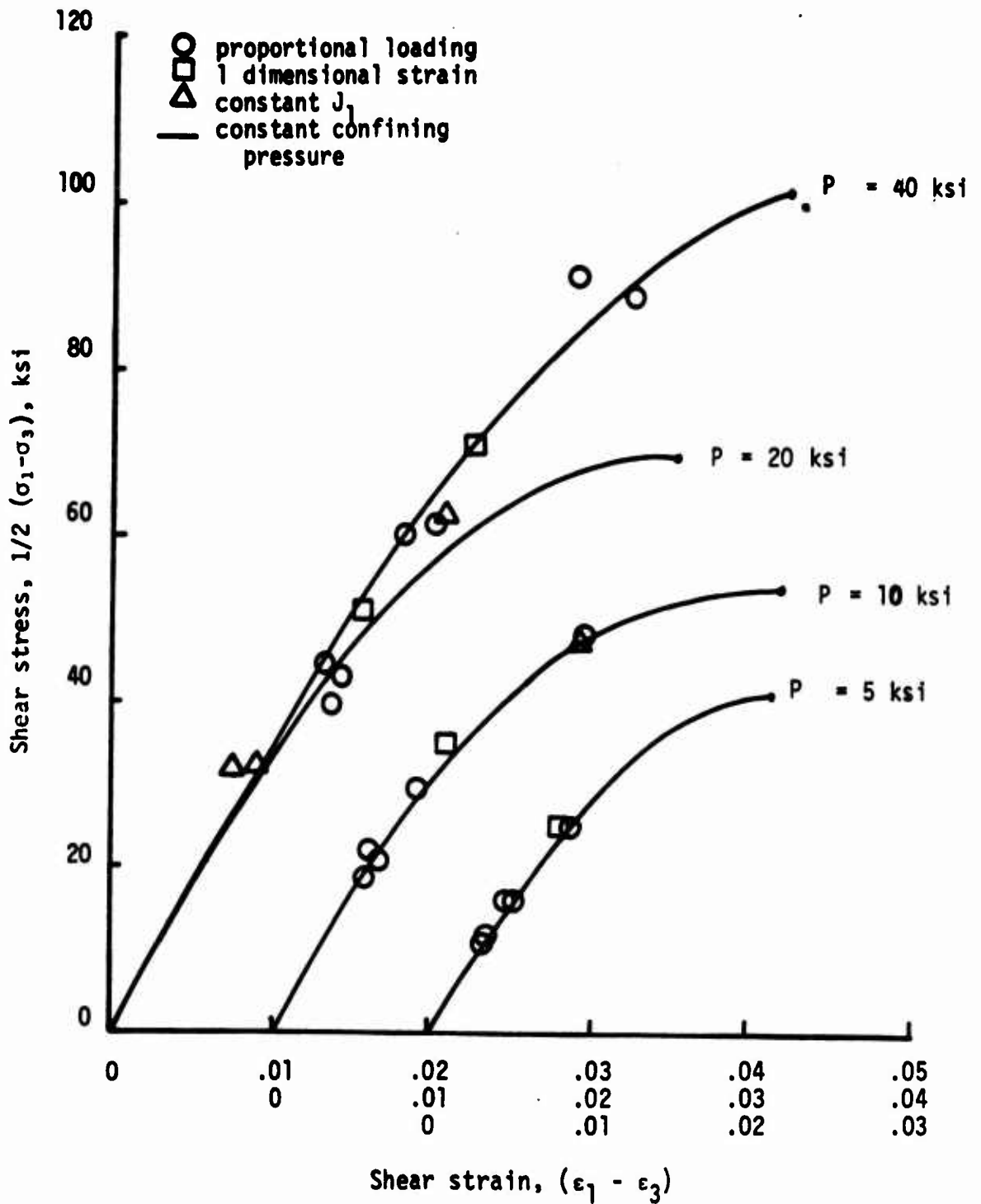


Figure 42. Effect of loading path on shear stress-strain response for Nugget sandstone.

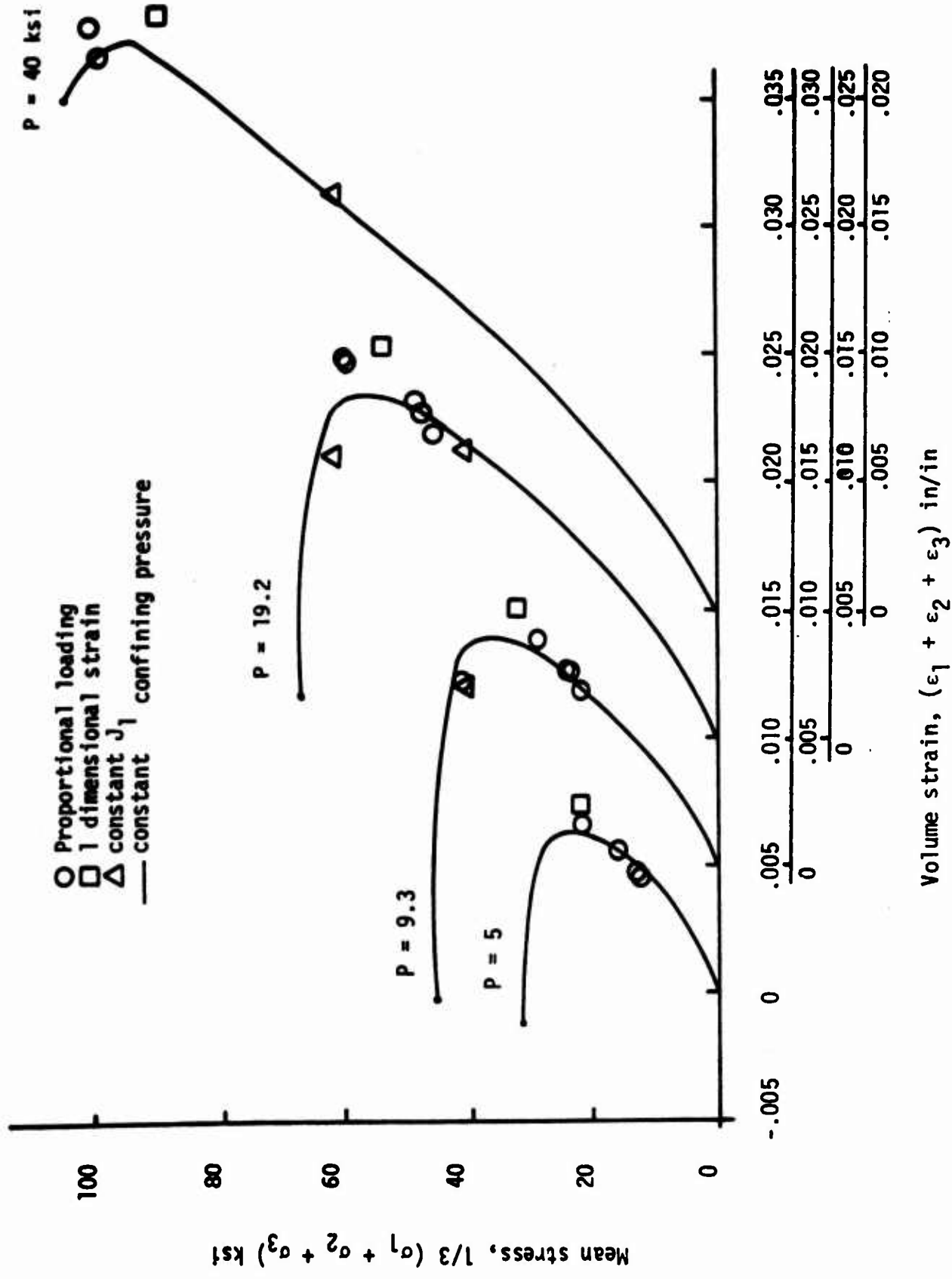


Figure 43. Effect of loading path on dilatational stress-strain response for Nugget sandstone.

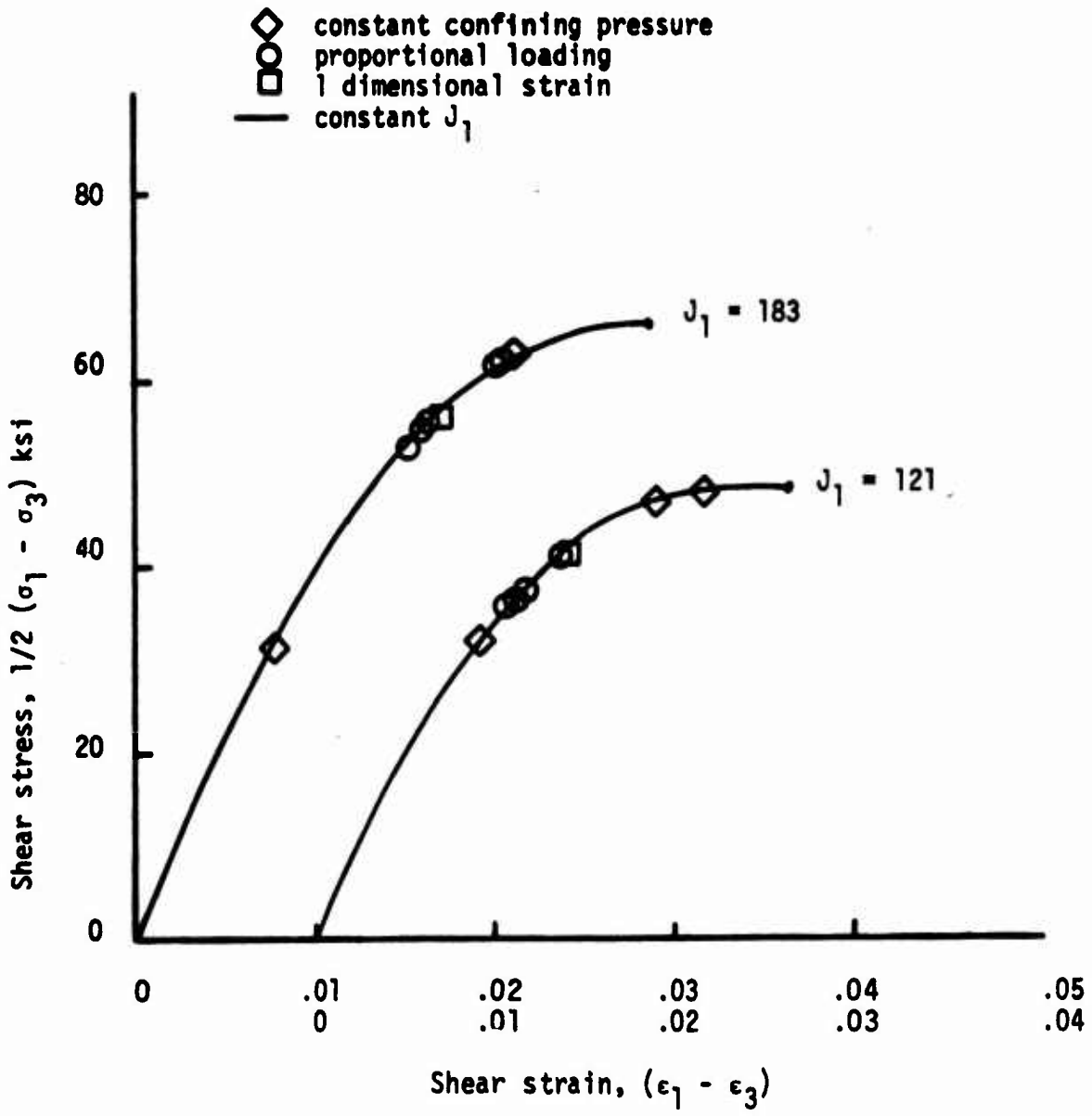


Figure 44. Effect of loading path on shear stress-strain response for Nugget sandstone.

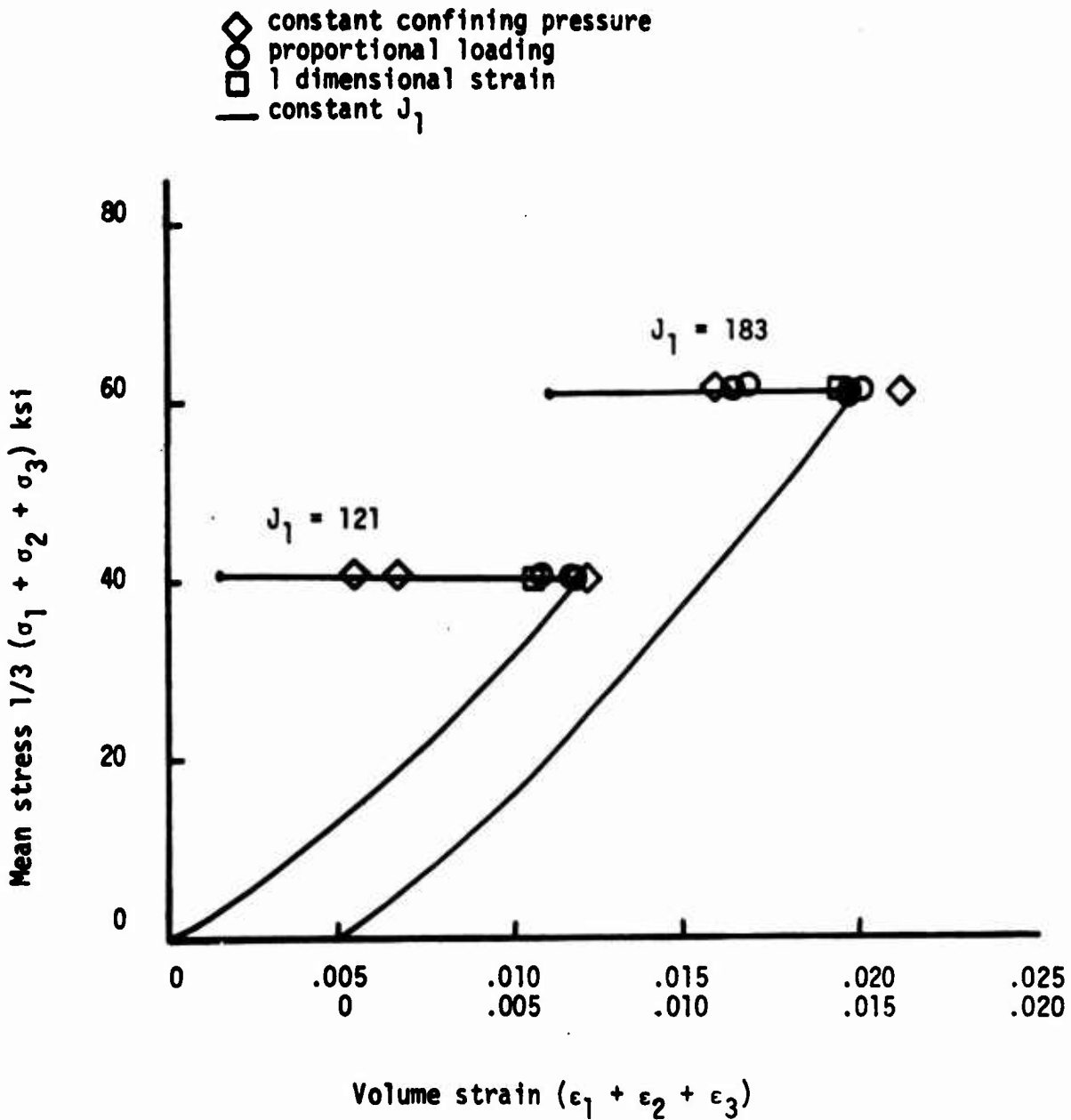


Figure 45. Effect of loading path on dilatational stress-strain response for Nugget sandstone.

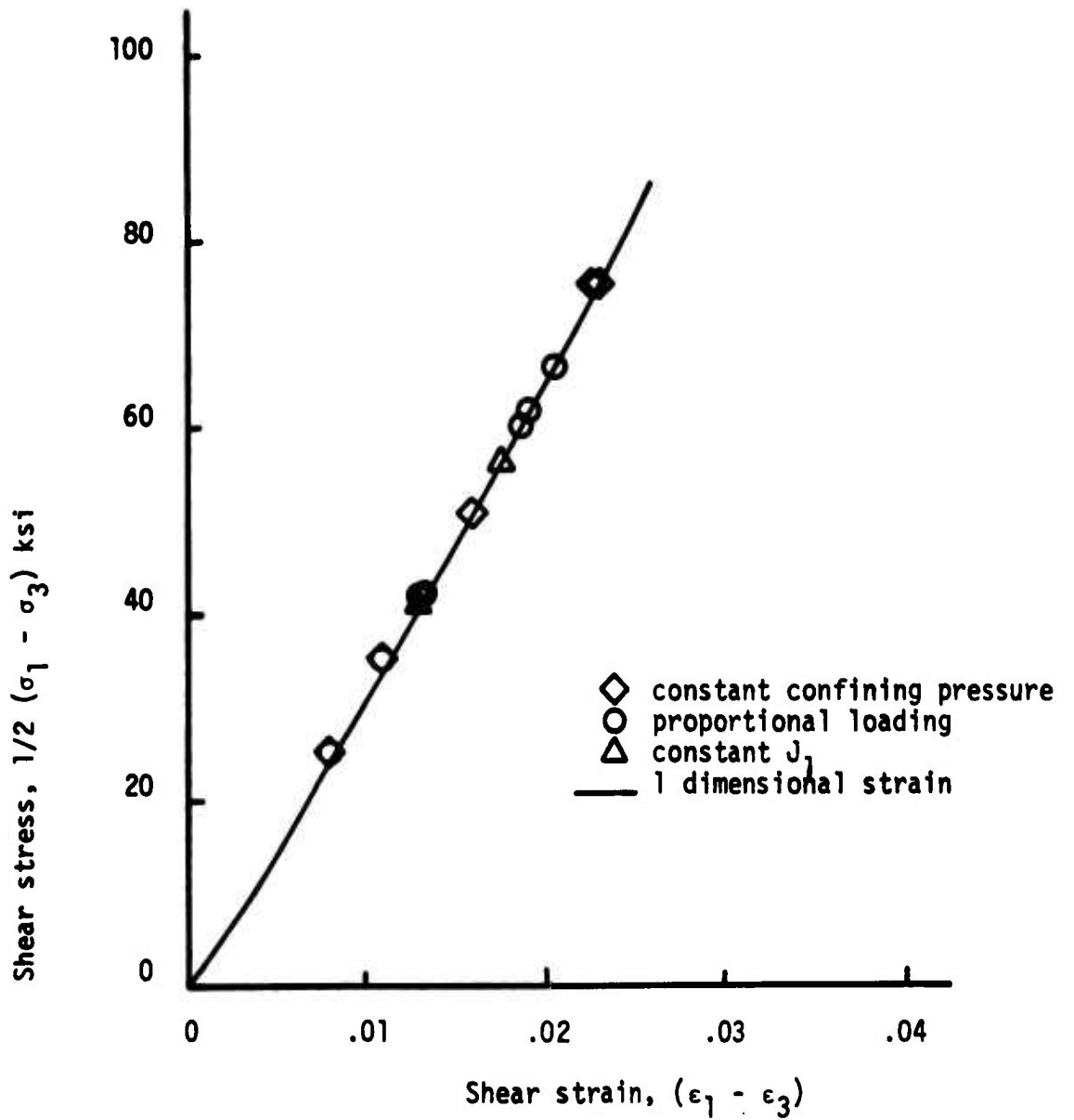


Figure 46. Effect of loading path on shear stress-strain response for Nugget sandstone.

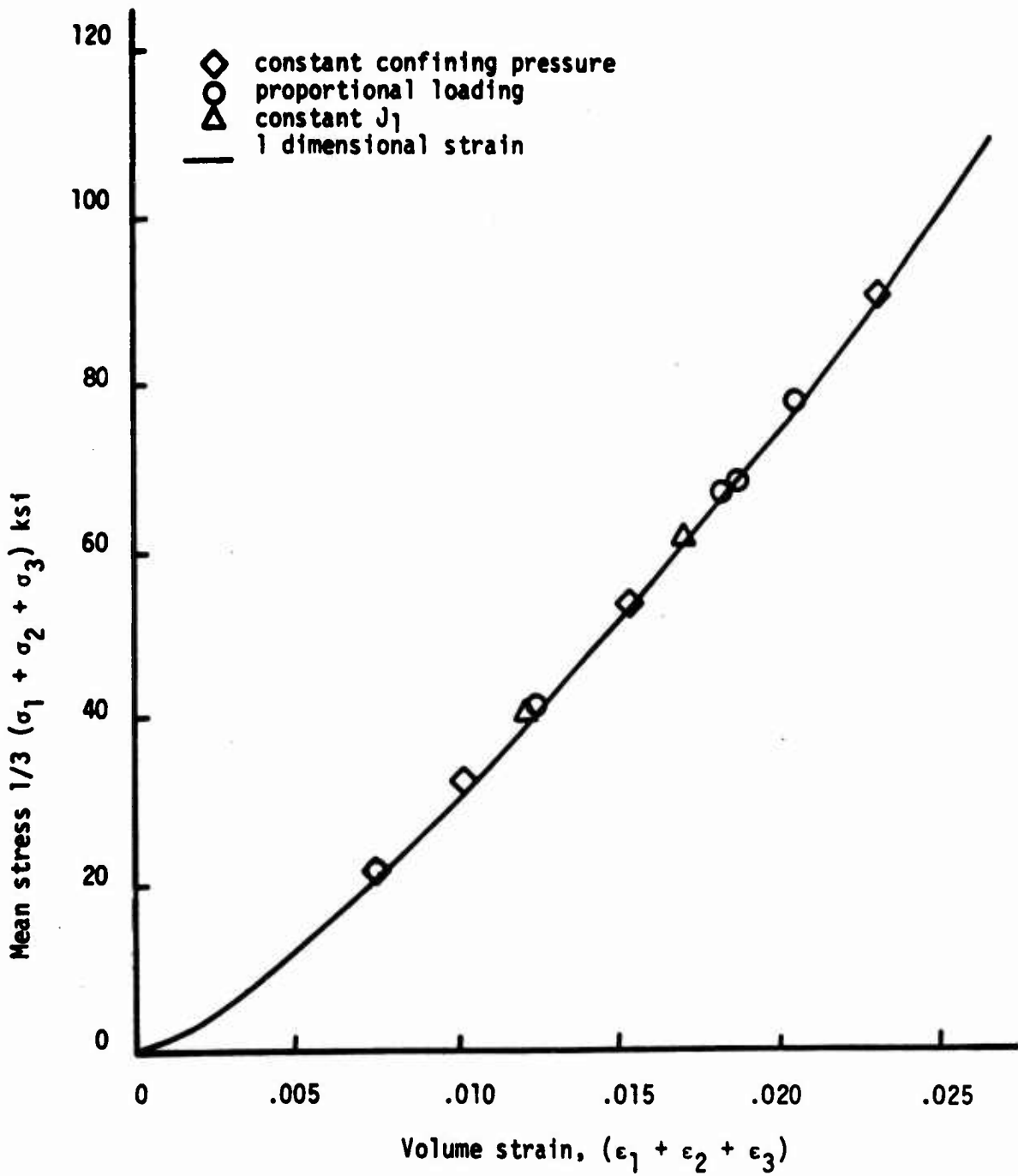


Figure 47. Effect of loading path on dilatational stress-strain response for Nugget sandstone.

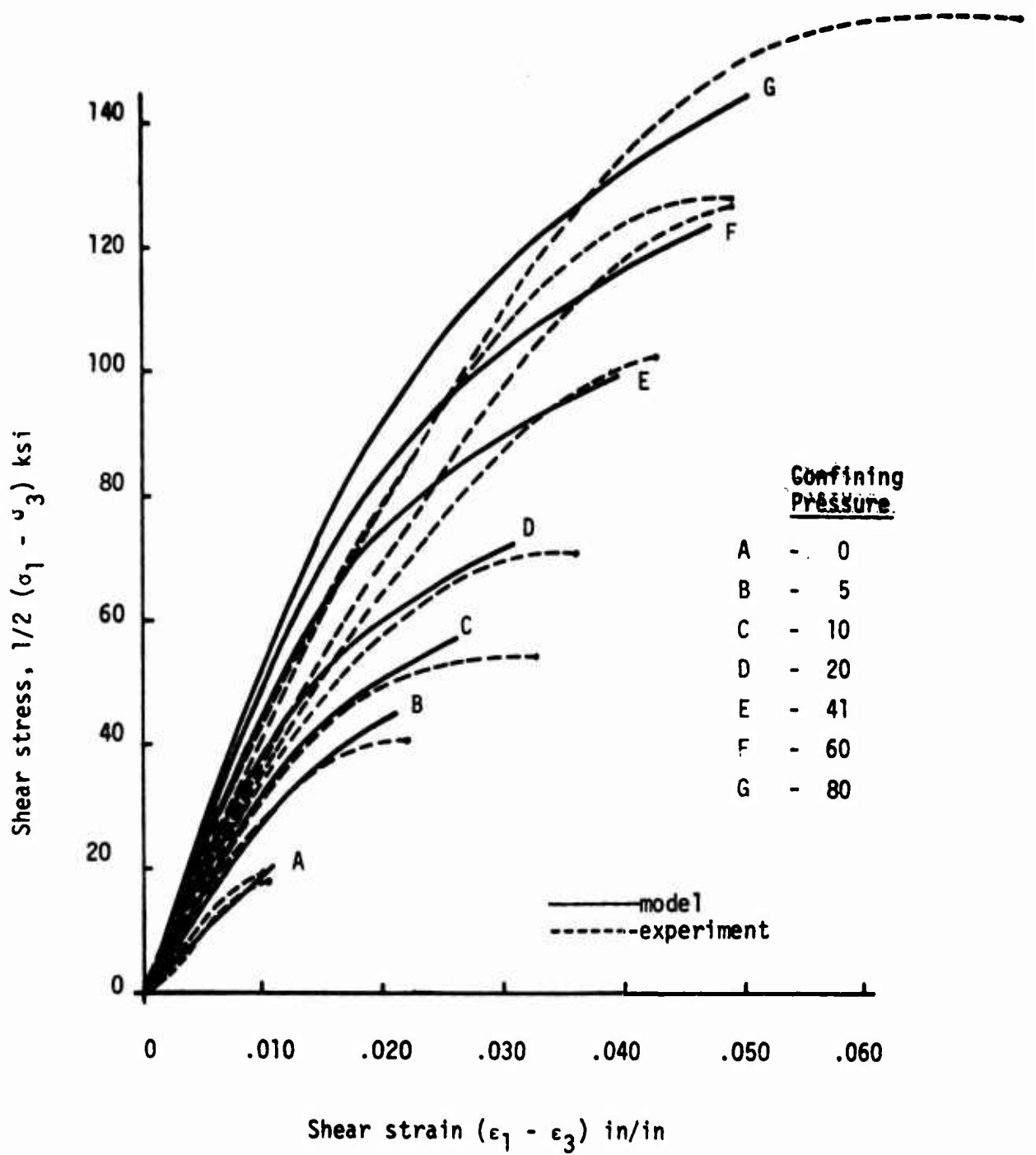


Figure 48. Comparison of model and experiment; constant confining pressure tests of Nugget sandstone.

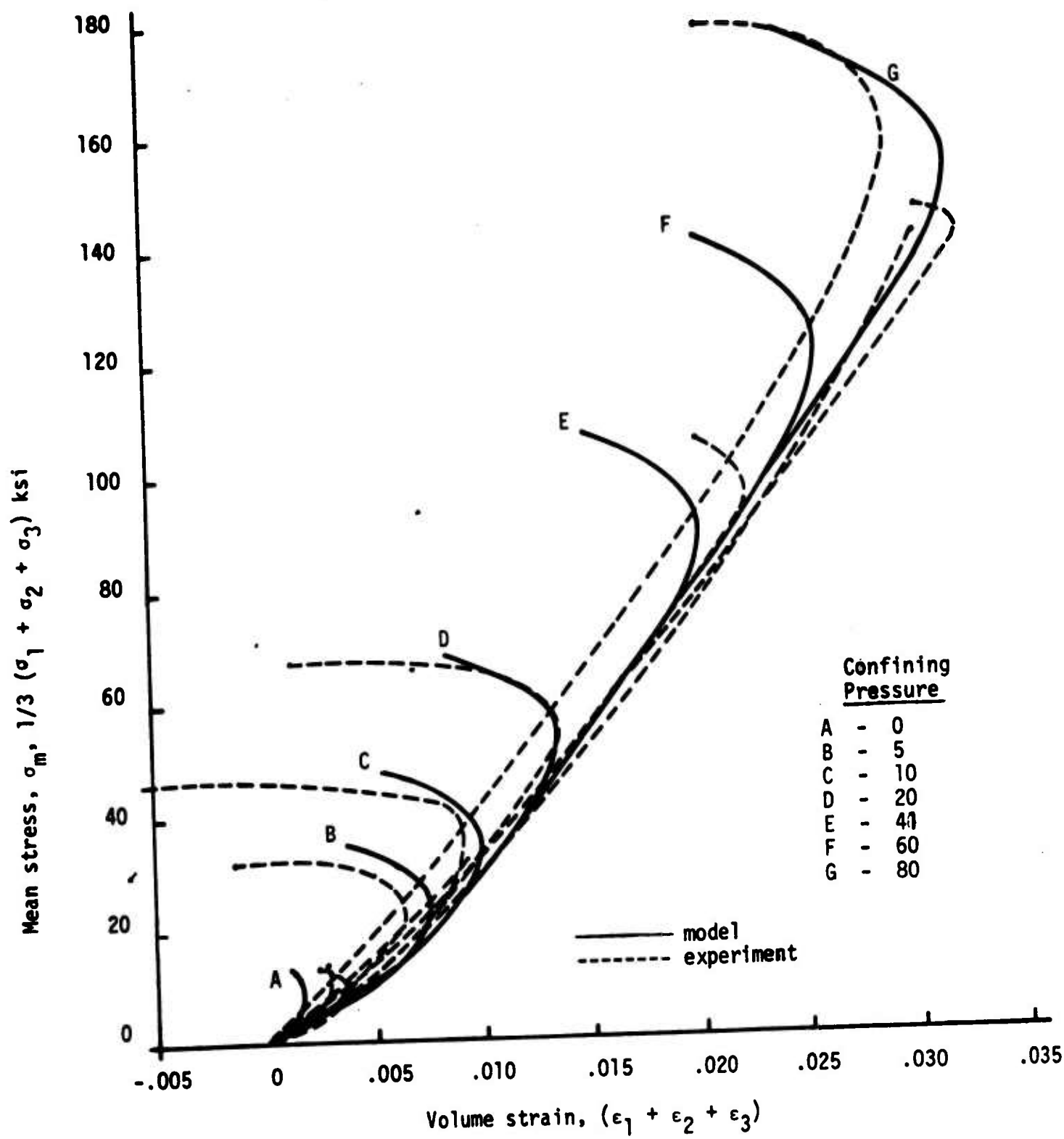


Figure 49. Comparison of model and experiment; constant confining pressure tests of Nugget sandstone.

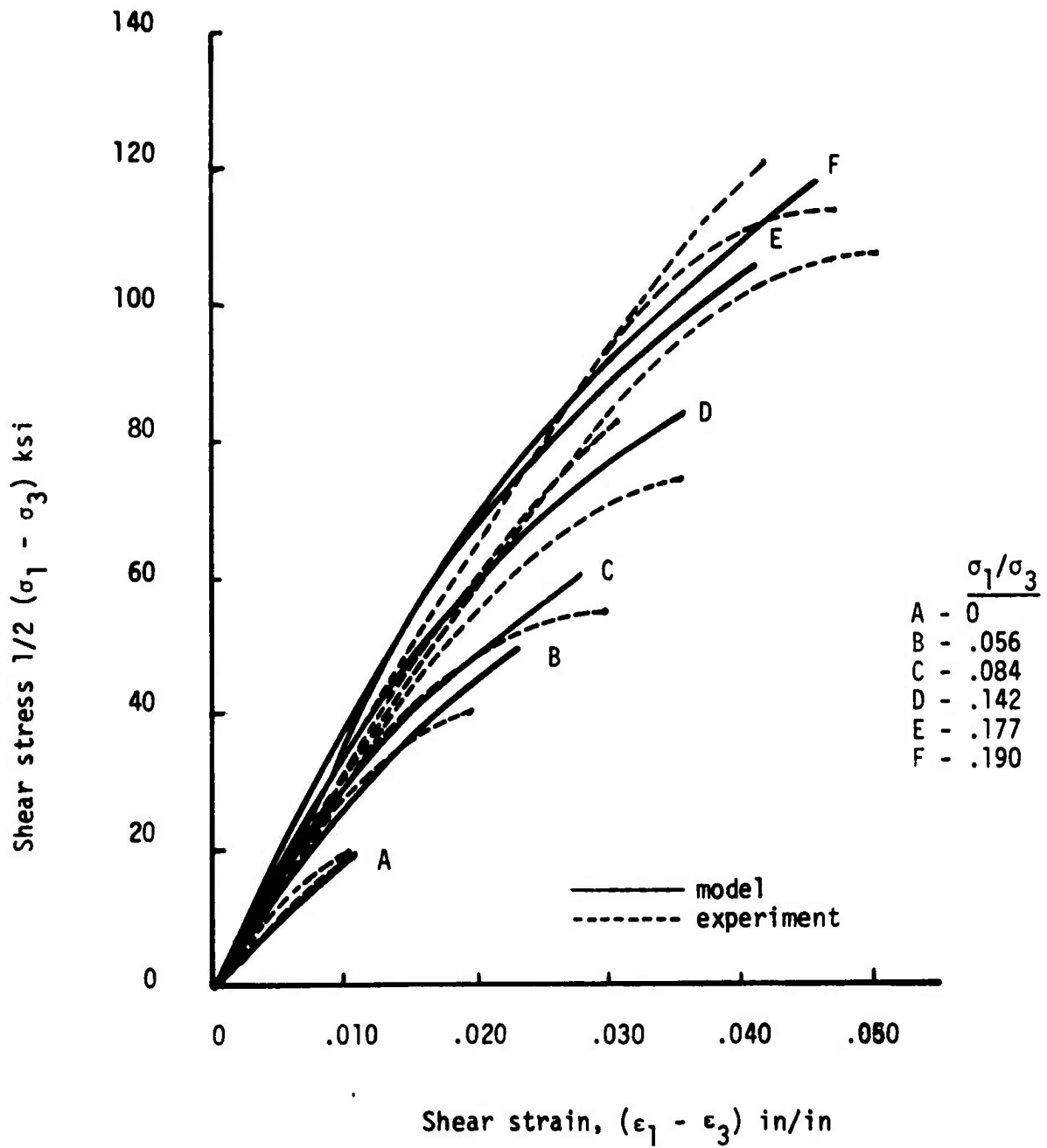


Figure 50. Comparison of model and experiment; proportional stress loading of Nugget sandstone.

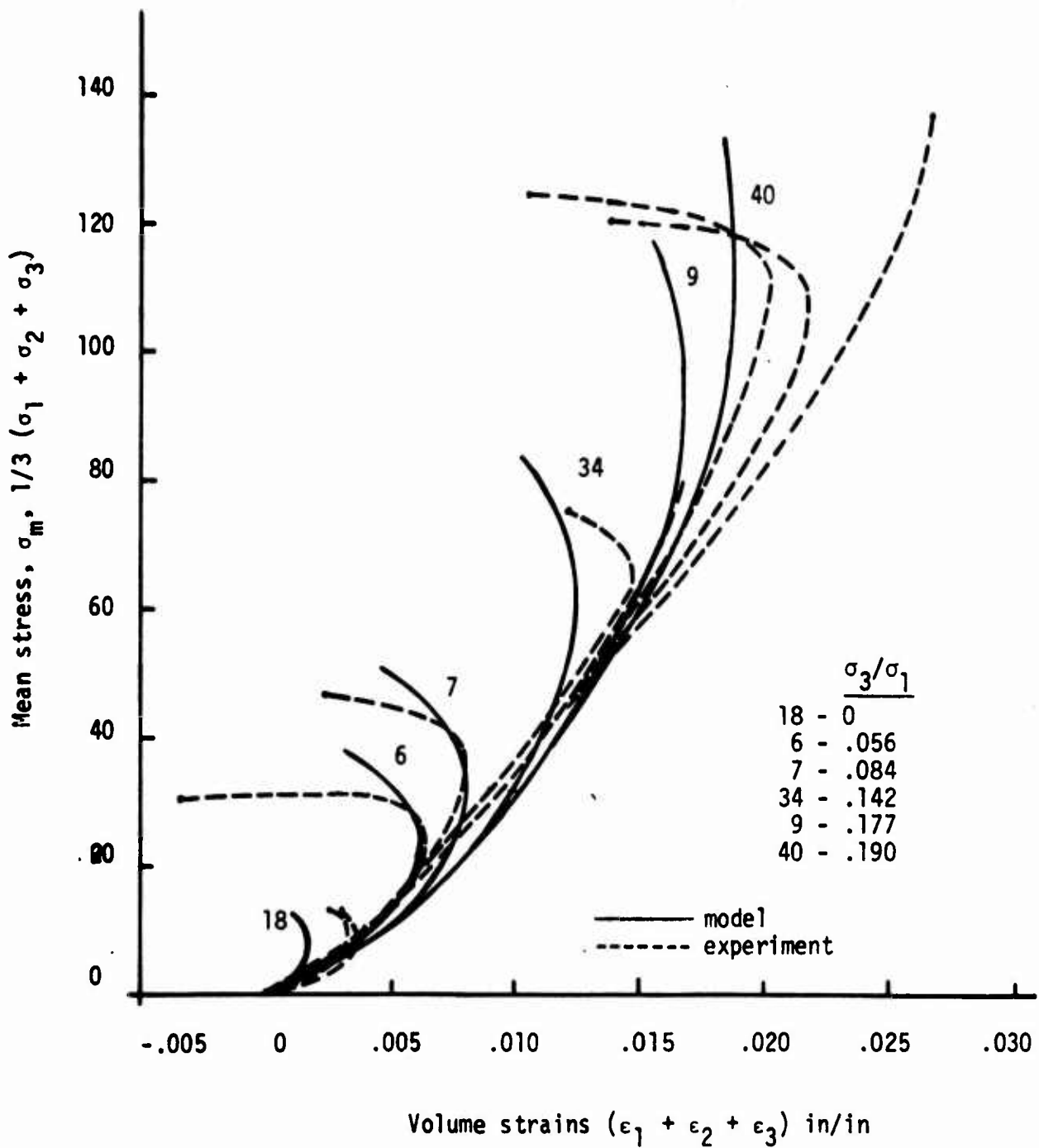


Figure 51. Comparison of model and experiment; proportional stress loading of Nugget sandstone.

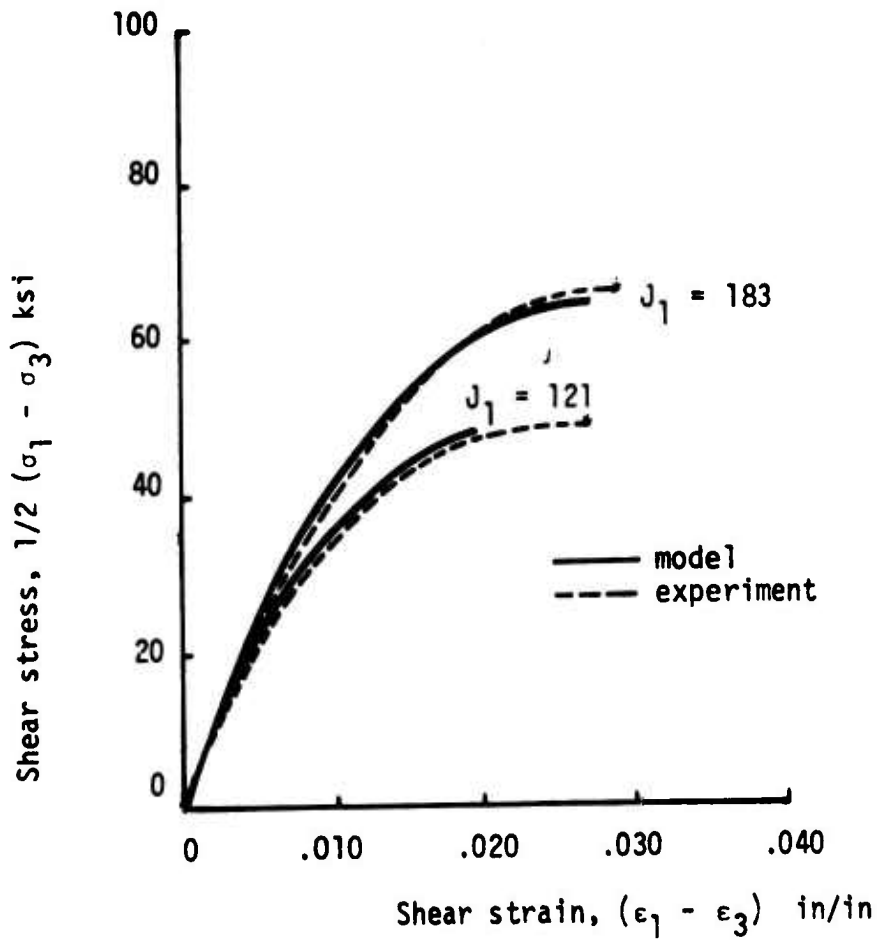


Figure 52. Comparison of model and experiment; constant J_1 loading of Nugget sandstone.

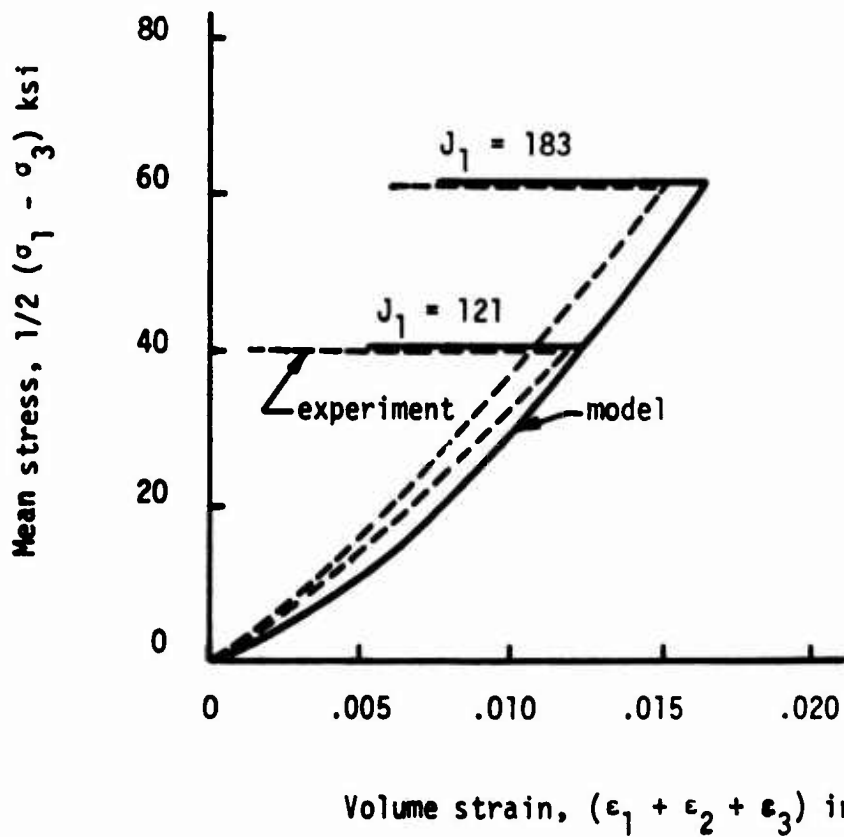


Figure 53. Comparison of model and experiment; constant J_1 loading of Nugget sandstone.

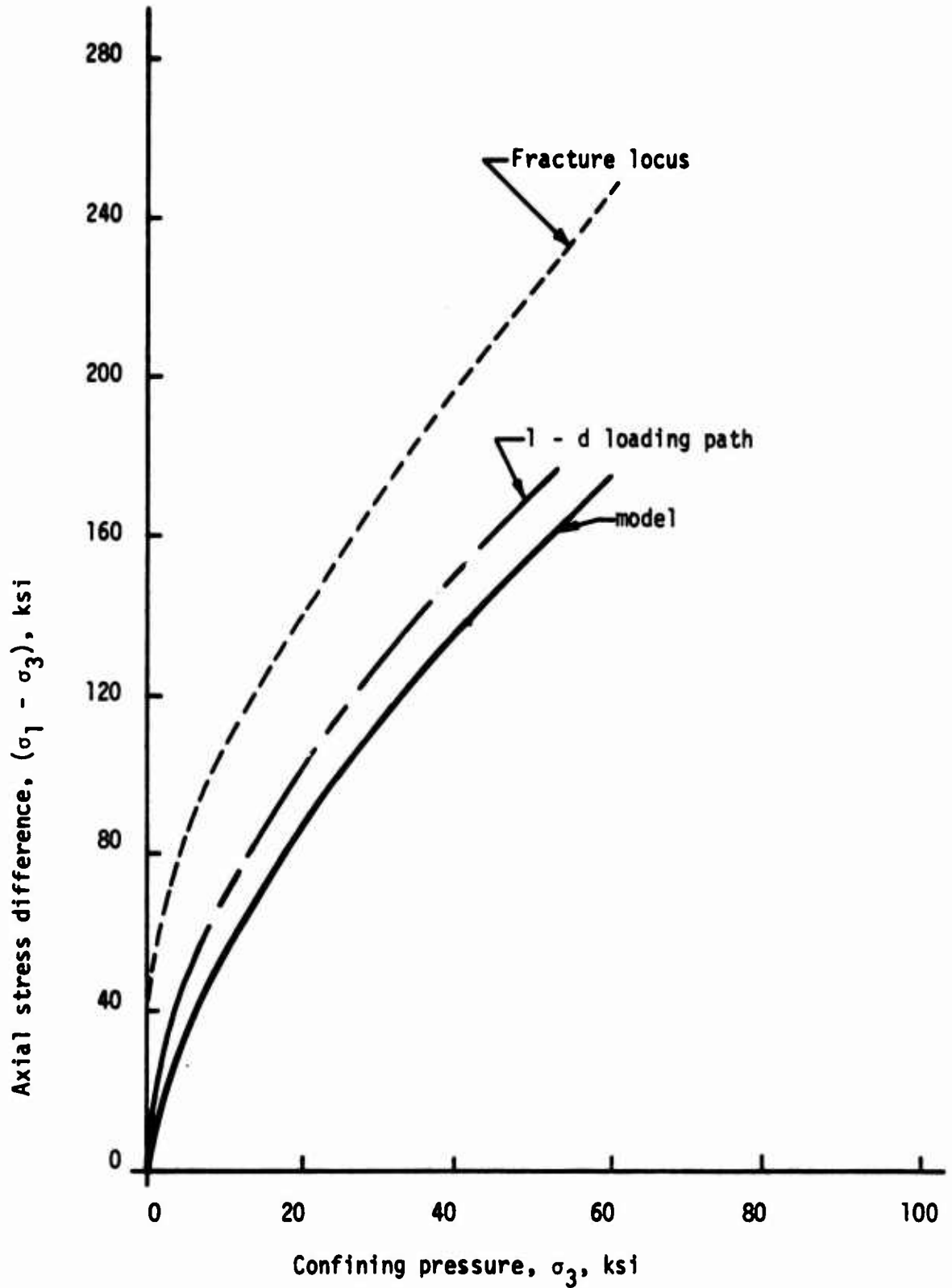


Figure 54. Comparison of model and experiment; one-dimensional strain loading of Nugget sandstone.

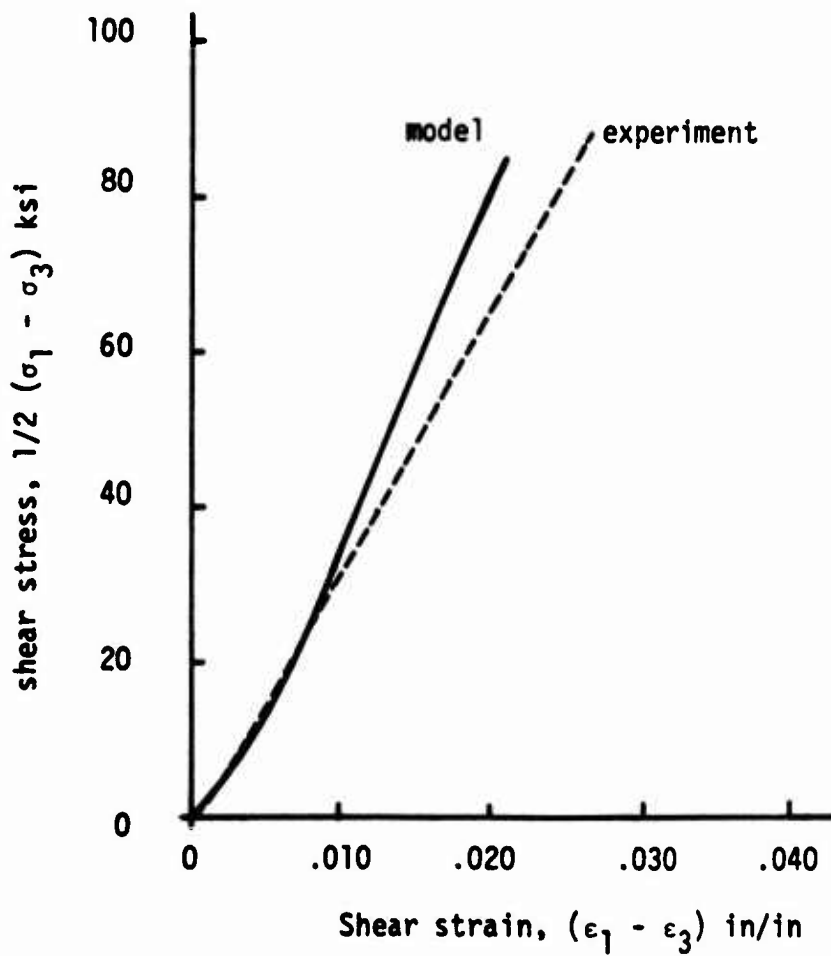


Figure 55. Comparison of model and experiment; one-dimensional strain loading of Nugget sandstone.

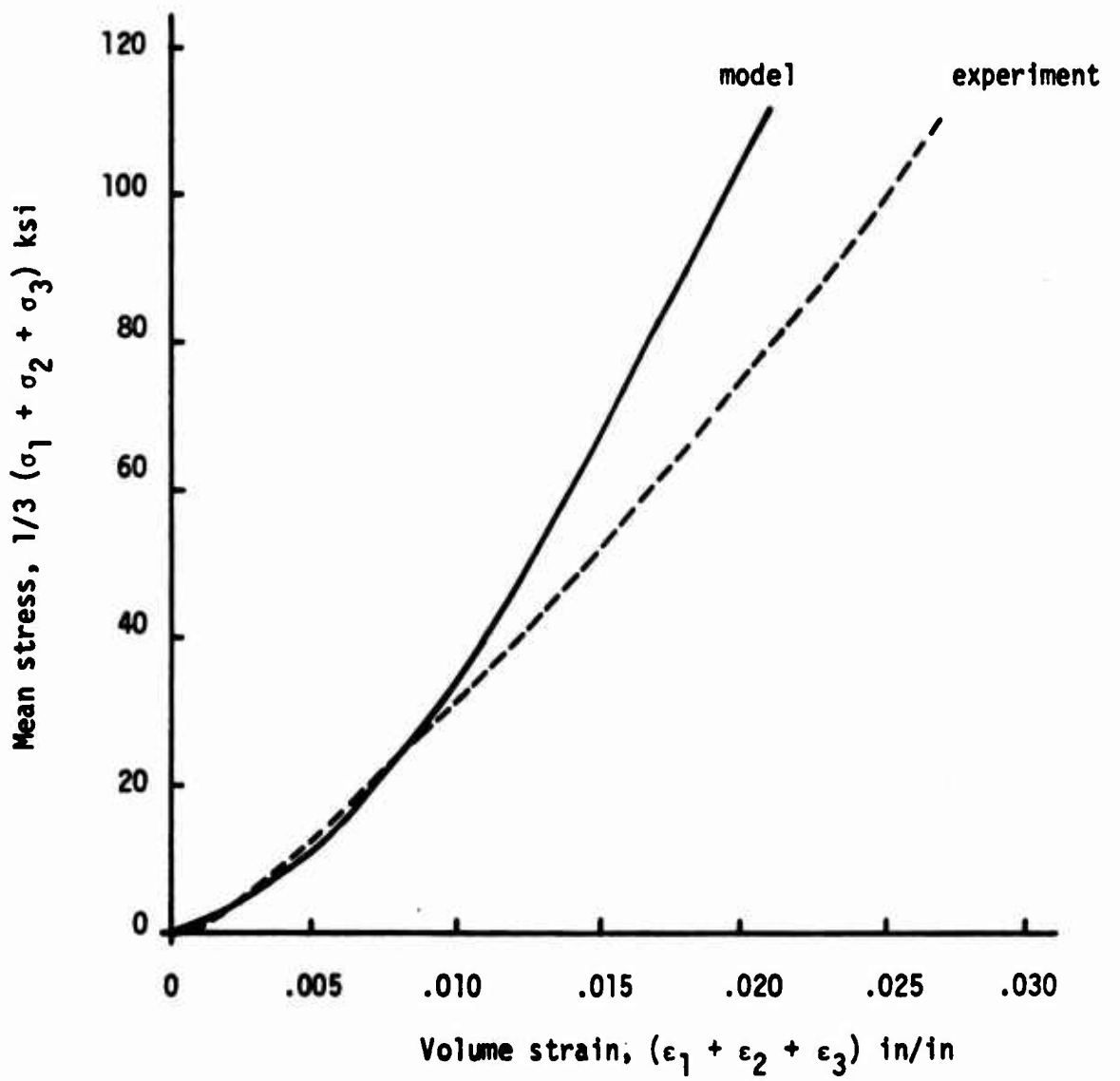


Figure 56. Comparison of model and experiment; one-dimensional strain loading of Nugget sandstone.

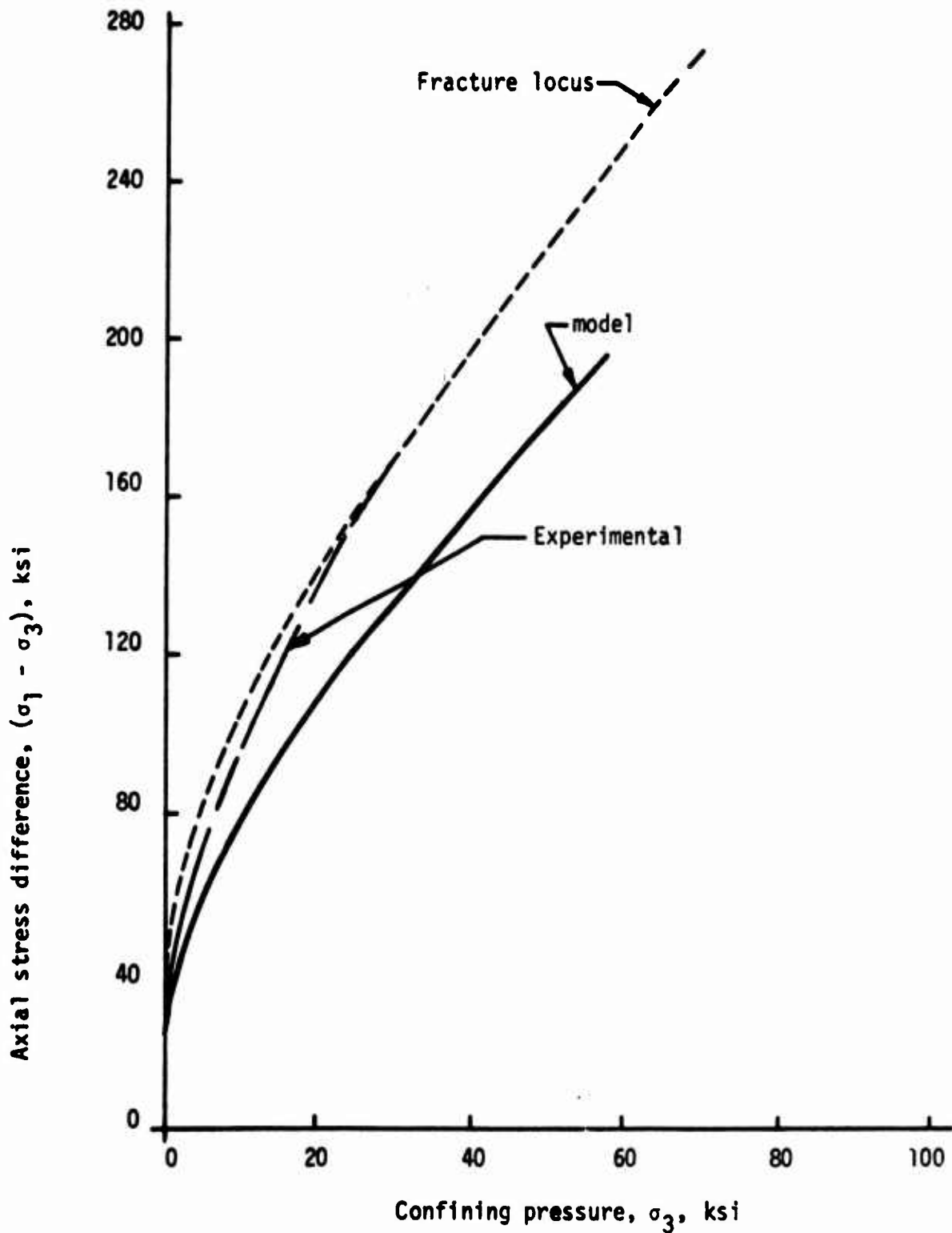


Figure 57. Comparison of model and experiment; proportional strain ($\epsilon_3/\epsilon_1 = -0.249$) loading of Nugget sandstone.

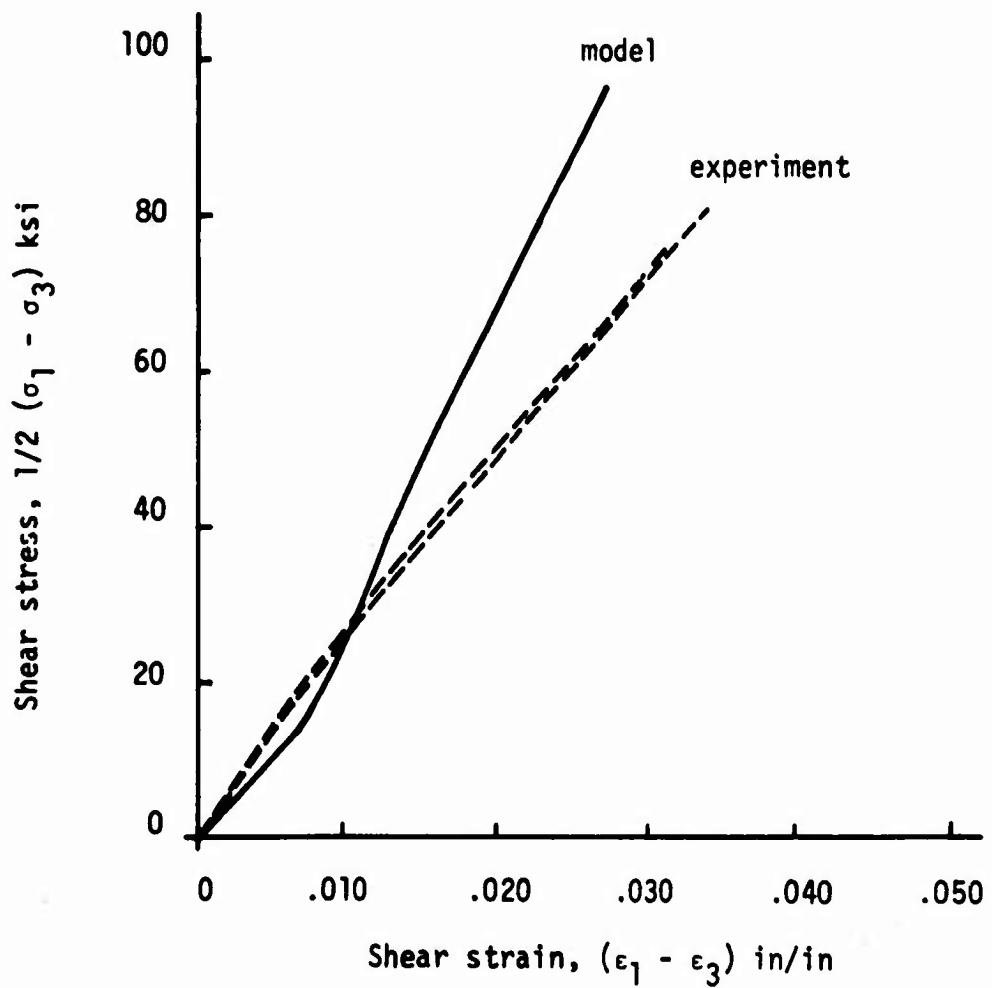


Figure 58. Comparison of model and experiment; proportional strain ($\epsilon_3/\epsilon_1 = -0.249$) loading of Nugget sandstone.

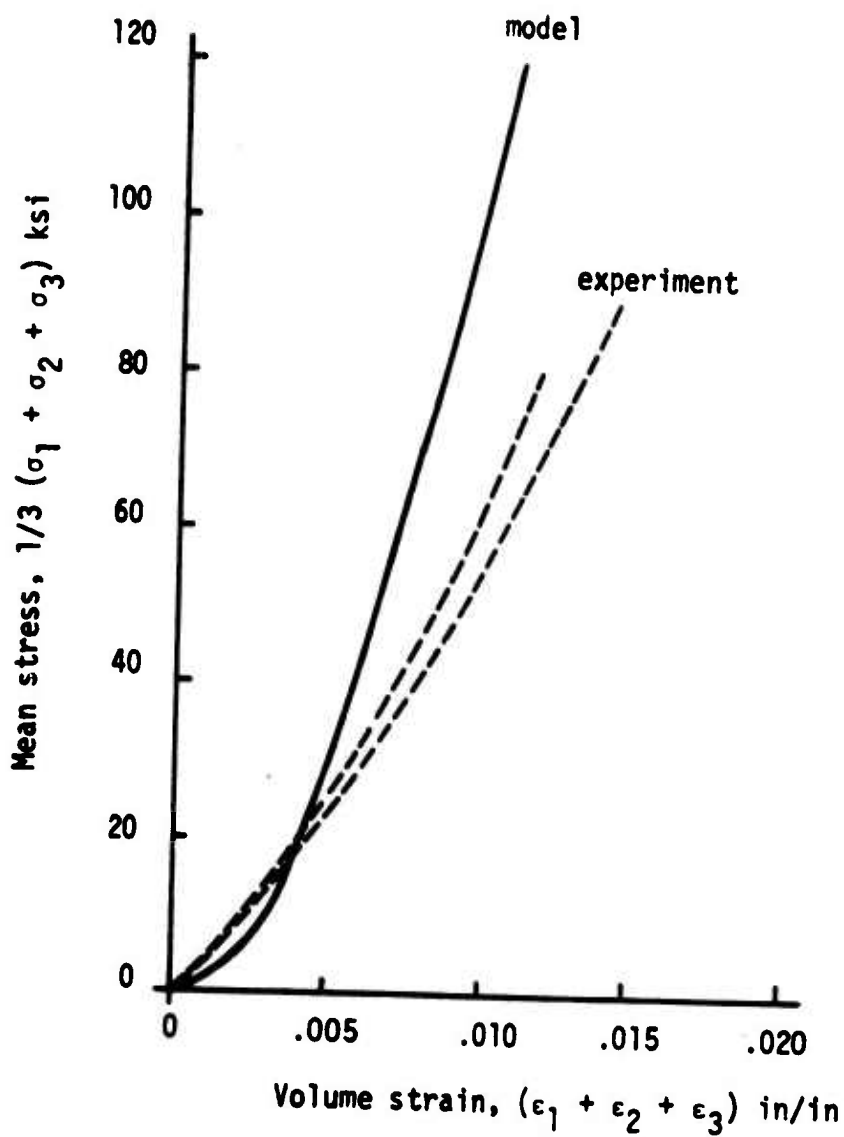


Figure 59. Comparison of model and experiment; proportional strain ($\epsilon_3/\epsilon_1 = -0.249$) loading of Nugget sandstone.

REFERENCES

1. Brown, W. S. and Swanson, S. R., "Influence of Load Path and State of Stress on Failure Strength and Stress-Strain Properties of Rocks," Air Force Weapons Laboratory Technical Report No. AFWL-TR-70-53, Kirtland Air Force Base, New Mexico, January 1971.
2. Brown, W. S. and Swanson, S. R., "Constitutive Equations for Westerly Granite and Cedar City Tonalite for a Variety of Loading Conditions," University of Utah Final Report DASA-2473, March 1970.
3. Brown, W. S., Swanson, S. R., and Wawersik, W. R., "Influence of Dynamic Loading, Biaxial Loading, and Pre-Fracturing on the Stress-Strain and Fracture Characteristics of Rocks," University of Utah Final Report to Defense Atomic Support Agency, March 1971 (in review).
4. Swanson, S. R. and Brown, W. S., "An Observation of Loading Path Independence of Fracture in Rock," submitted to Int. J. Rock Mech Min. Sci., 1970.
5. Brace, W. F., Paulding, B. W. and Scholz, C., "Dilatancy in the Fracture of Crystalline Rocks," J. Geophys. Res., 71, 3939-3953, 1966.
6. Walsh, J. B., "The Effect of Cracks on the Compressibility of Rock," J. Geophys. Res., 70, 381-389, 1965.
7. Wawersik, W. R., "Detailed Analysis of Rock Failure in Laboratory Compression Tests," Ph.D. thesis, University of Minnesota, 1968.
8. Walsh, J. B., "The Effect of Cracks on the Uniaxial Compression of Rocks," J. Geophys. Res., 70, 399-411, 1965.
9. Walsh, J. B., "The Effect of Cracks in Rocks on Poisson's Ratio," J. Geophys. Res., 70, 5249-5257, 1965.
10. Brady, B. T., "A Mechanical Equation of State for Brittle Rock, Part I--The Pre-Failure Behavior of Brittle Rock," Int. J. Rock Mech. Min. Sci., 7, 385-421, 1970.
11. Brace, W. F., Discussion of "Transition from Elastic to Plastic States of Rocks under Triaxial Compression," by S. Serata, Proc. 4th Sym. on Rock Mechanics, Penn. State Univ., Univ. Park, Pennsylvania, 73-82, 1961.
12. Swanson, S. R., "Representation of the Post-Fracture Mechanical Behavior of Nugget Sandstone," Terra Tek, Inc., Technical Report TR 71-13, 1971. Salt Lake City, Utah.

UNCLASSIFIED

Security Classification

DOCUMENT CONTROL DATA - R & D

(Security classification of title, body of abstract and indexing annotation must be entered when the overall report is classified)

1. ORIGINATING ACTIVITY (Corporate author) University of Utah College of Engineering Salt Lake City, Utah 84112	2a. REPORT SECURITY CLASSIFICATION UNCLASSIFIED
	2b. GROUP

3. REPORT TITLE
STRESS-STRAIN AND FRACTURE PROPERTIES OF NUGGET SANDSTONE

4. DESCRIPTIVE NOTES (Type of report and inclusive dates)
November 1968 through July 1971

5. AUTHOR(S) (First name, middle initial, last name)
Wayne S. Brown and Stephen R. Swanson

6. REPORT DATE October 1971	7a. TOTAL NO. OF PAGES 96	7b. NO. OF REFS 12
--------------------------------	------------------------------	-----------------------

8a. CONTRACT OR GRANT NO. F29601-68-C-0071 b. PROJECT NO. 5710 c. Subtask SB144 d.	8b. ORIGINATOR'S REPORT NUMBER(S) AFWL-TR-71-54
	8c. OTHER REPORT NO(S) (Any other numbers that may be assigned this report) UTEC ME 71-058

10. DISTRIBUTION STATEMENT
Distribution limited to US Government agencies only because of test and evaluation (1 Sep 71). Other requests for this document must be referred to AFWL (DEV).

11. SUPPLEMENTARY NOTES	12. SPONSORING MILITARY ACTIVITY AFWL (DEV) Kirtland AFB, NM 87117
-------------------------	--

13. ABSTRACT (Distribution Limitation Statement B)
Experimental measurements of the stress-strain and fracture properties of laboratory specimens of Nugget sandstone are described. A servo-controlled triaxial compression testing apparatus was employed which permitted simultaneous control of the lateral and axial stresses. Results are given for a variety of stress path conditions including: unconfined compression and tension, constant confining pressure, proportional stress, constant mean stress, one-dimensional strain, and proportional strain tests. In general, Nugget sandstone was found to be reasonably isotropic and to exhibit considerable inelastic behavior including hysteresis and dilatancy. A plasticity model was formulated which is capable of representing the stress-strain characteristics of the sandstone reasonably well over a variety of stress path conditions.

KEY WORDS	LINK A		LINK B		LINK C	
	ROLE	WT	ROLE	WT	ROLE	WT
Rock mechanics Nugget sandstone Servo-controlled triaxial test Fracture properties Material properties Civil engineering						